

UNIVERSITÀ DEGLI STUDI DI NAPOLI “FEDERICO II”

Dipartimento di Ingegneria Chimica, dei Materiali

e della Produzione Industriale



Dottorato di ricerca in Ingegneria Chimica

XXVII CICLO

**Cell motility and proliferation in 2D and 3D
substrata. Applications to chemotaxis,
wound healing and collective migration.**

Scientific Committee

Prof. Stefano Guido

Prof. Sergio Caserta

Prof. Pietro Formisano

Candidate

Flora Ascione

Anno Accademico 2014/2015

L'importante è non smettere di interrogarsi.

La curiosità ha una precisa ragione per l'esistenza.

(Albert Einstein)

TABLE OF CONTENTS

CHAPTER 1

CELL DYNAMICS, STATE OF THE ART 3

1. ABSTRACT.....	3
2. MOTIVATION.....	3
3. BACKGROUND.....	5
3.1. Single cell migration.....	5
3.2. Cell proliferation.....	9
3.3. Collective cell dynamics.....	11
3.4. Collective dynamics in cell sheets.....	16
3.5. Dynamic evolution of cell clusters.....	17
3.6. Live cell imaging.....	21
3.7. Random migration assays.....	22
3.8. Chemotaxis assays.....	23
3.9. Wound healing assays.....	28
4. AIM OF THE WORK.....	39

CHAPTER 2

INVESTIGATION OF CELL DYNAMICS IN VITRO BY TIME LAPSE MICROSCOPY AND IMAGE ANALYSIS..... 40

1. INTRODUCTION.....	40
2. MATERIALS AND METHODS.....	43
2.1. Cell culture.....	43
2.2. Chemotaxis chamber.....	43
2.3. Time Lapse Microscopy workstation.....	44
2.4. Experimental methods.....	45
2.5. Image analysis.....	45
3. RESULTS AND DISCUSSION.....	45
4. CONCLUSIONS.....	48

CHAPTER 3

COMPARISON BETWEEN FIBROBLAST WOUND HEALING AND CELL RANDOM MIGRATION ASSAYS IN VITRO 50

1. INTRODUCTION.....	50
2. MATERIALS AND METHODS.....	54
2.1. Cell cultures.....	54
2.2. Time-lapse microscopy.....	54
2.3. Experimental methods.....	55
2.4. Image analysis.....	55
2.5. Data analysis.....	55
2.6. Statistical analysis.....	56
3. RESULTS AND DISCUSSION.....	57
4. CONCLUSIONS.....	67

CHAPTER 4

THE WOUND HEALING ASSAY REVISITED: A TRANSPORT PHENOMENA APPROACH..... 70

1. INTRODUCTION.....	70
2. MATERIALS AND METHODS.....	74

2.1.	Cell cultures.....	74
2.2.	Time Lapse Microscopy.....	74
2.3.	WH assays.....	75
2.4.	Image analysis.....	75
3.	RESULTS AND DISCUSSION.....	76
4.	CONCLUSION.....	87
CHAPTER 5		
DYNAMICS OF MONOLAYER FORMATION IN T84 EPITHELIAL CELLS.....		88
1.	INTRODUCTION.....	88
2.	MATERIALS AND METHODS.....	89
2.1.	Cell cultures.....	89
2.2.	Experimental methods.....	90
2.3.	Image analysis.....	90
3.	RESULTS AND DISCUSSION.....	91
4.	CONCLUSIONS.....	101
CHAPTER 6		
FROM SINGLE CELLS TO CELL AGGREGATES CHEMOTAXIS.....		103
1.	INTRODUCTION.....	103
2.	MATERIALS AND METHODS.....	104
2.1.	Cell cultures and cell spheroids preparation.....	104
2.2.	Chemotaxis chamber.....	105
2.3.	Sample preparation.....	105
2.4.	Imaging by time-lapse microscopy.....	106
3.	RESULTS AND DISCUSSION.....	106
CHAPTER 7		
CONCLUSIONS.....		110
BIBLIOGRAPHY.....		112
APPENDIX..... a		
1.	PUBBLICATIONS.....	a
2.	CONFERENCES.....	a

Chapter 1

Cell dynamics, state of the art

1. Abstract

A wide range of physiological and pathological processes, such as inflammation, tissue regeneration, angiogenesis, tumour growth and invasion, are strongly linked to cell proliferation and migration mechanisms that govern the dynamic evolution of both individual cells and cell aggregates. The complex mechanisms governing cell dynamic behavior have yet to be completely clarified. A detailed analysis of these processes requires a rigorous approach to quantitatively analyze cell dynamics and measure cell movement and proliferation indices. This work is addressed to investigate the dynamic evolution of cells, from single to collective cell dynamic behavior, in a quantitative way. Our methodological approach is based on live cell imaging *in vitro*, coupled to several cell migration assays, and image analysis techniques. Live cell imaging based on *in vitro* time-lapse microscopy is a powerful analytical tool that allows direct visualization of biological systems during their dynamic evolution. In order to maintain cell viability, the sample is kept in a controlled air, constant temperature environment. The experimental data are used to model cell dynamic evolution using mathematical equations based on the transport phenomena approach.

2. Motivation

A wide range of biological processes are strongly dependent on cell proliferation and migration mechanisms [1] that govern the dynamic evolution of individual cells and cell aggregates [2-4]. Cell proliferation and migration play a key role in both physiological and pathological processes, including embryogenesis, tissue repair, immune responses, and tumour growth and invasion. For example, during embryogenesis large groups of cells migrate collectively as sheets to form the three layers of the resulting embryo and then grow and differentiate to form various tissues and organs [5]. Subsequently, cells migrate from various epithelial layers to target locations throughout the developing embryo where they differentiate and form various tissues and organs. Analogous migration mechanisms occur in the adult where, skin and intestine are renewed continuously from precursors that migrate up from the basal layer and the crypts, respectively.

Migration and proliferation also play a pivotal role in physiological as well as pathological processes occurring in the adult organism. In the inflammatory response (Figure 1.1.A) leukocytes migrate out of the blood vessels into the tissues, reaching the area of insult, where they mediate phagocytic and immune functions [6]. Cell growth and migration are also relevant in tissue repair (Figure 1.1.B), where two cell sheets dynamically evolve to close the wound space [7]. Tumour development is accompanied by the formation of blood vessels (angiogenesis) (Figure 1.1.C) which arise from proliferation and migration of their endothelial cells [8, 9]. In metastatic cancer (Figure 1.1.D), some tumour cells showing a malignant phenotype escape from the primary tumour and invade adjacent tissues where they proliferate forming secondary tumours [10]. Finally, the dynamic evolution of cells is essential in technological applications such as tissue engineering [11].

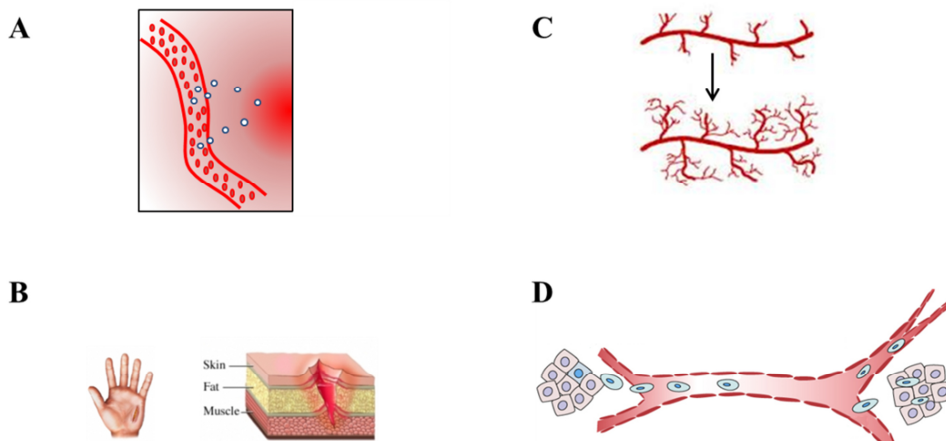


Figure 1.1: (A) Inflammation; (B) tissue repair; (C) angiogenesis; (D) tumour progression.

Most of these biological phenomena are governed by chemotaxis mechanism [12, 13], i.e., the directional movement of cells along a chemical concentration gradient [14, 15].

The complex mechanisms governing cell dynamic behavior are still far from full comprehension [16, 17]. A detailed analysis of these processes requires a rigorous approach to quantitatively measure cell movement and proliferation indices. For this reason, the development of such analyses is nowadays within the core business of Chemical Engineering [18], which can contribute to the building of mathematical models, based on the transport phenomena approach, useful to describe and predict the mechanisms driving cell dynamics [19].

3. Background

3.1. Single cell migration

Single cell migration has been studied extensively over many decades, leading to a well-established model of cell motility at the individual cell level.

Many types of cells, including amoebae, leucocytes, epithelial cells and neurite growth cells, migrate by crawling across a solid substrates [20]. Cell migration occurs following the so called cell motility cycle, which is characterized by a well-known sequence of steps [21], based on polarized intracellular signaling which leads to protrusion of the plasma membrane at the leading edge of the cell, integrin-mediated adhesion to the substrate of cell migration, actomyosin contraction of the cell body and detachment of the trailing edge, which moves the cell forward [16, 22] (Figure 1.2). This process requires a complex signaling pathways and regulatory network [23]. In fact, cell movement involves the spatio-temporal control and integration of a number of processes, including the transduction of chemical (growth factors and other chemotactic cues) and mechanical signals from the environment, intracellular biochemical responses, and translation of the intra- and extracellular signals into a mechanical response [24, 25]. Individual cells detect extracellular chemical and mechanical signals via membrane receptors, and this initiates signal transduction cascades that produce intracellular signals. These signals control the motile machinery of the cell and thereby determine the spatial localization of contact sites with the substrate and the sites of force generation needed to produce directed motion.

Extension of the leading edge: This process is regulated by the actin and microtubule cytoskeleton and by the formation of cell protrusions in the direction of migration. As a consequence, the cell acquires a front and a backside. Protrusive structures at the leading edge of motile cells are highly dynamic and contain dense arrays of actin filaments [26]. Protrusive structures are lamellipodia and filopodia, both containing filamentous actin, as well as structural and signalling proteins (Rho family of GTPases, ERK/MAP kinases and other regulatory molecules); they lead to dynamic interactions with the extracellular matrix [23, 27-29]. However, they have strikingly different designs of the actin polymerization machinery and are regulated by different signaling pathways [30]. Lamellipodia are thin sheets of cytoplasm containing networks of actin filaments forming a branched network. They are composed of diagonal networks of actin filaments [31], and withdrawal terminates with the formation of actin bundles parallel to the cell edge.

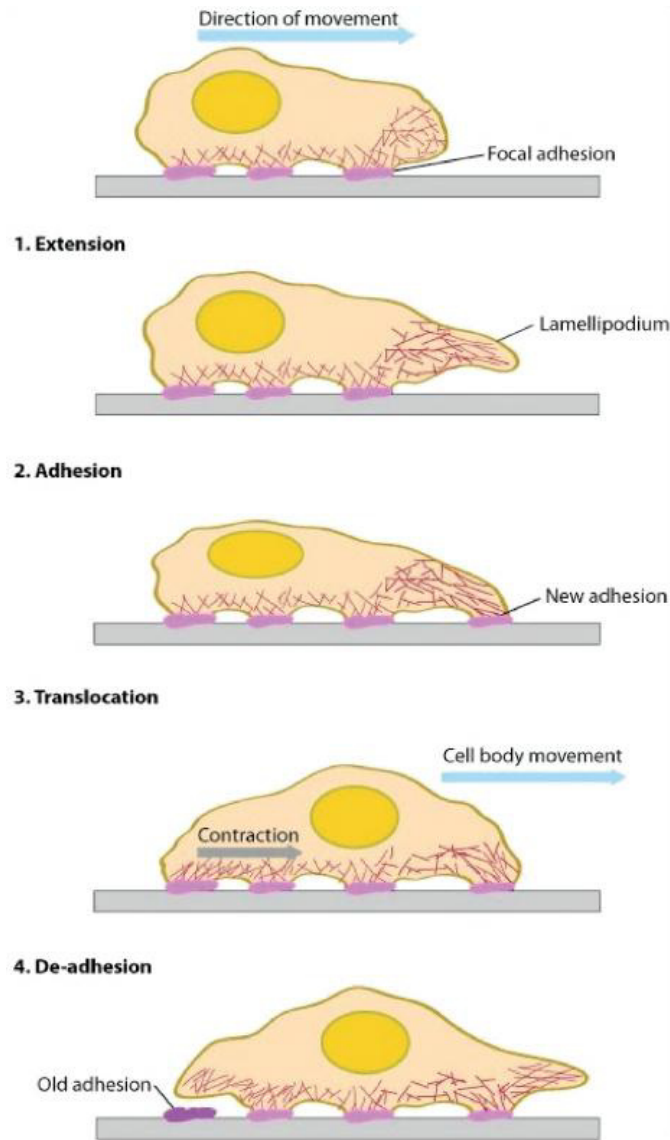


Figure 1.2: Steps of cell migration [21].

The current model for lamellipodial dynamics [32] suggests that treadmilling of the branched actin filament array consists of repeated cycles of dendritic nucleation, elongation, capping, and depolymerization of filaments. Dendritic nucleation is mediated by the Arp2/3 complex, which is activated by members of WASP family [33]. In filopodia, which are thin cellular processes, actin filaments are long, parallel, and organized into tight bundles [33, 34]. The actin filaments are held together in the bundle by cross-linking proteins such as fimbrin [24]. Analysis of cellular localization of known actin cross-linking proteins in mouse melanoma B16F1 cells showed that fascin was specifically localized along the entire length of all filopodia, whereas other actin cross-linkers were not [35]. Moreover, a kinetic and structural

investigation of filopodial initiation in the same cells revealed that filopodial bundles doesn't arise by a specific nucleation event, but are formed by gradual reorganization of the lamellipodial dendritic network in a process that involves elongation of a subset of lamellipodial filaments, self-segregation of these filaments into filopodial precursors, and initiation of bundling at the tips of the precursors [36].

Adhesion to the matrix: Within newly formed protrusions, novel cell adhesions have to be established to attach the cell to the underlying ECM. These adhesions are transient and depending on the cell type, substratum and migration profile; their turnover can be very high. Adhesions initiate as small so-called focal complexes, which are mainly localized at the cell leading edge. These newly formed adhesions stabilize the lamellipodium and attach the protrusion to the ECM. In tightly adhering and non-motile or slowly migrating cells these focal complexes mature into focal adhesions. Depending from the cell type and ECM substrate, focal contact assembly and migration can be regulated by different integrins. These are a family of heterodimeric transmembrane adhesion receptors that support adhesion to the ECM (or other cells) by linking matrix components outside the cell to actin filaments inside the cell. Next to this adhering function, integrins are known for their 'inside-out signalling' via activation by cytoplasmic signals [1, 23].

Focalized proteolysis: The engagement of integrins and other adhesion receptors leads to the recruitment of surface proteolytic enzymes, that become concentrated near substrate binding sites. Matrix metalloproteinases (MMPs) anchored to plasma membrane, called membrane-type MMPs (MT-MMPs), play pivotal roles for ECM remodeling [37]. In close proximity to the cell surface proteases degrade ECM structural proteins, such as collagen, fibronectin and laminins, mediating the chemical and physical modification of the extracellular microenvironment to provide the space required for cell expansion and migration [38]. Pericellular proteolysis is spatio-temporally regulated through enzyme processing, enzyme internalization and the inactivation of the catalytic site by protease-specific inhibitors, including the tissue inhibitor of metalloproteinases (TIMPs) [39]. In close proximity to the cell surface proteases degrade ECM components and cleave pre-matrix metalloproteinases (MMPs) to create active soluble MMPs, known for their protein cleavage activities. Soluble proteases can directly bind to integrins and similarly, membrane-type matrix metalloproteinase-1 (MT1-MMP) and MMP2 adhere to collagen fibres. MMP1 and other collagenases cleave native collagens, along with other ECM macromolecules, into smaller fragments, which, in turn, are accessible to subsequent degradation by gelatinases (MMP2 and MMP9) or serine proteases. ECM degradation occurs while the advancing cell body gains

volume towards the ECM scaffold and is likely to provide the space required for cell expansion and migration, leaving behind tube-like matrix defects along the migration track [38]. This step is dependent on the cell type and the surrounding environment. Proteolytic strategies are indispensable for cells that cannot transmigrate narrow ECM gaps just by changing cell morphology and squeezing of their nuclei [40].

Actomyosin contraction: The contractile force, needed to move the cell body forward, is generated by the interactions of actin filaments with Myosin II, which controls the organization of actin filaments into stress fibers [21]. Powered by ATP hydrolysis, the actomyosin crossbridges inside these structures generate tension that contracts the cell body [41]. The tension generated by actomyosin contractile machinery is then transmitted to the ECM through focal adhesions (FAs) (Figure 1.3), which are located at both ends of the stress fiber and on the substrate or the ECM and hence physically connect the actin cytoskeleton to the ECM [42, 43]. The traction force at FA is in the range of tens of nano-Newtons [44]. FA is an assembly of ECM proteins, transmembrane receptors, and cytoplasmic structural and signaling proteins, including $\alpha v\beta 3$ and $\alpha 5\beta 1$ integrins, vinculin, paxillin, talin, zyxin, tensin, protein tyrosine kinases, and phosphatases [45]. Among these FA proteins, integrins are primary mediators that provide a physical linkage between the actin cytoskeleton and ECM and thus play a key role in cellular mechanotransduction [46, 47].

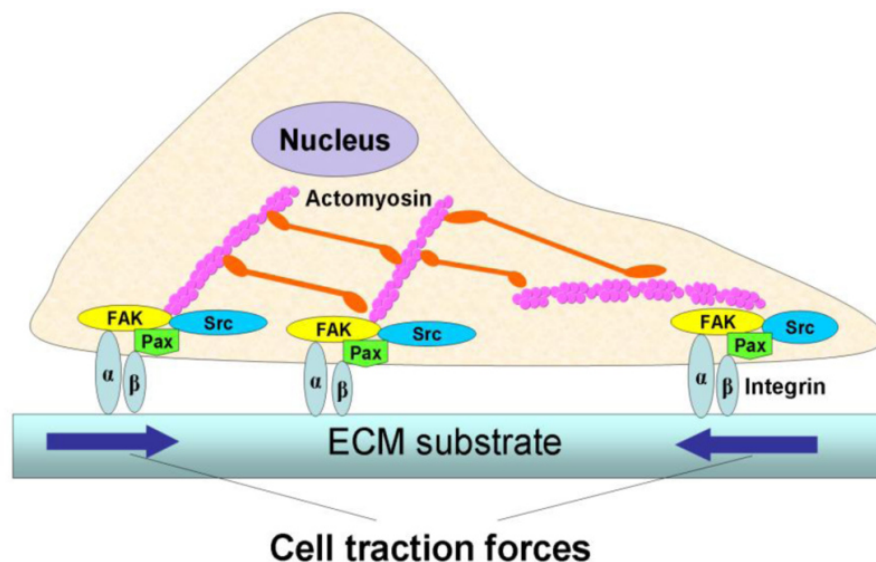


Figure 1.3: Force transmission within an adherent cell [42].

Detachment of the trailing edge: At the cell rear, adhesions need to be released, whereas at the front the formation of adhesion has to be controlled. Phosphatases play important roles in rear release, by limiting the assembly of cytoskeletal proteins. Focal contacts are further weakened through the proteolytic cleavage of adhesion receptors and the accumulation of collagen fragments that are generated while the cell moves forward. Moreover, in order to maintain a continuous retrograde flow of integrins on the cell surface, migrating cells must reload receptor at the leading edge. The recycling of these proteins takes place through endocytic vesicles [1].

Although fundamental cell migration mechanisms are shared between different migrating cells, the cell type and its environment are crucial for the migration response. Some cells, like fibroblasts, are known as slow-moving, while other cell types, like T-cells, are fast-moving [48]. In addition, different tumour cells can differ strongly in their intrinsic migratory capacity. Next to cell type, the nature of the surrounding matrix determines to great extent the migration response of cells. The composition of the ECM, availability of growth factors and cytokines, physiological circumstances like pH and pO₂ and, of course, intracellular constituents, all together regulate cell polarity and migration.

Besides this well-established mode of single cell migration, detailed knowledge obtained over the past 30 years suggests that at least one additional mechanism is involved in cell translocation within tissues. In fact, some cell types are able, under physiological conditions, to move in a collective mode in tightly or loosely associated groups, such as clusters, sheets or strands [49]. Cell movement in groups can be referred to as collective cell migration [2].

3.2. Cell proliferation

The cell cycle is the complex sequence of events by which the cells grow and divide. The time it takes for a cell to complete one cell cycle varies depending on the type of cell. Some cells, such as blood cells in bone marrow, skin cells, and cells lining the stomach and intestines, divide rapidly and constantly. Other cells divide when needed, to replace damaged or dead cells. These cell types include cells of the kidneys, liver and lungs. Still other cell types, including nerve cells, stop dividing once mature. In eukaryotic cells, this process occurs through a series of four distinct stages (Figure 1.4): mitosis phase (M), Gap 1 phase (G1), Synthesis phase (S), and Gap 2 phase (G2) [50]. The G 1, S, and G 2 phases of the cell cycle are collectively referred to as interphase.

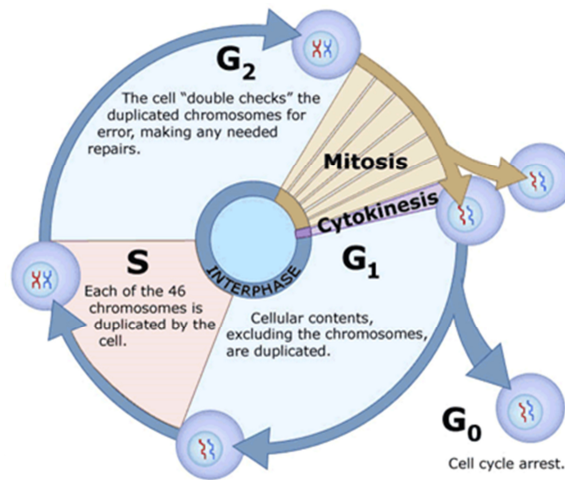


Figure 1.4: Cell cycle.

Interphase: The dividing cell spends most of its time in interphase, as it grows in preparation for cell division. In fact, during this stage the cell doubles its cytoplasm and synthesizes DNA. It is estimated that a dividing cell spends about 90-95 % of its time in this phase. The G₁ phase is the period prior to the synthesis of DNA. In this phase, the cell increases in mass and organelle number in preparation for cell division. The S phase is the period during which DNA is synthesized. In most cells, there is a narrow window of time during which DNA is synthesized. The chromosome content is doubled in this phase. During the G₂ phase, occurring after DNA synthesis but prior to the start of mitosis, the cell synthesizes additional proteins and continues to increase in size.

Mitosis: The mitosis phase of the cell division process involves the separation of nuclear chromosomes, followed by cytokinesis (division of the cytoplasm forming two distinct cells). At the end of the mitotic cell cycle, two distinct daughter cells are produced. Each cell contains identical genetic material. The mitosis includes four phases: prophase, metaphase, anaphase and telophase. During the prophase, the chromatin condenses into discrete chromosomes which migrate toward the cell center. The nuclear envelope breaks down and spindle fibers form at opposite poles of the cell. In the metaphase the nuclear membrane disappears completely, the spindle fully develops and the chromosomes align at the metaphase plate (a plane that is equally distant from the two poles). During the anaphase paired chromosomes separate and begin moving to opposite ends of the cell. Spindle fibers not connected to chromatids lengthen and elongate the cell. In the telophase the chromosomes are cordoned off into distinct new nuclei and the genetic content of the cell is divided equally

into two parts. Cytokinesis begins prior to the end of mitosis and completes shortly after telophase.

Once a cell has completed the cell cycle, it goes back into the G 1 phase and repeats the cycle again. Cells in the body can also be placed in a non-dividing state called the Gap 0 phase (G 0) at any point in their life. Cells may remain in this stage for very long periods of time until they are signaled to progress through the cell cycle as initiated by the presence of certain growth factors or other signals. In fact, normal animal cells have alternative modes of existence: either proliferative or quiescent. They survive well in either state. Several suboptimal nutritional conditions can bring about quiescence, including high cell density, nutrient or serum insufficiency, or high cAMP [51].

Progression through the eukaryotic cell cycle is known to be both regulated and accompanied by periodic fluctuation in the expression levels of numerous genes [52]. In particular, cyclin-dependent kinases (CDKs) play a crucial role in the control of the cell cycle and proliferation. Various CDKs activate the different stages of the cell cycle from G1 to mitosis. Each CDK/cyclin complex is responsible for transition or progression of a given phase within the cell cycle [53]. Loss of appropriate cell cycle regulation leads to genomic instability [54] and is believed to play a role in the etiology of both hereditary and spontaneous cancers [55]. In fact, uncontrolled proliferation is the hallmark of cancer and other proliferative disorders and abnormal cell cycle regulation is, therefore, common in these diseases.

3.3. Collective cell dynamics

Collective cell migration can be described as “collections of cells moving together and affecting one another while doing so” [56]. In fact, collective cell movement occurs when two or more cells retain their cell-cell junctions, coordinate their actin dynamics and intracellular signaling and thereby form a structural and functional unit that move across a two-dimensional layer of extracellular matrix (ECM) or through a three-dimensional scaffold [57, 58].

Like individual cell migration, the collective movement of cells plays a key role in several biological processes, including embryonic development, immune response, angiogenesis and tissue repair [59-61]. In addition, collective cell dynamics contribute to pathological situations such as metastasis formation, allowing malignant tumour cells to invade surrounding tissues [2, 3]. Specifically, invading cell groups may range from strands of only one or two cells in diameter, to broad masses that can include cells that do not contact the ECM [3].

However, despite the importance of collective cell migration, far less is known about exactly how cells migrate in a collective and coordinate way [62]. A better understanding of the underlying behaviors during collective cell movement will provide insight into morphogenesis and tissue reorganization during regeneration and disease. Furthermore, the ability to control collective migration will provide novel tools for tissue engineering [63].

The main question is why cells move collectively if they can move as individual units. Collective migration can actually keep a tissue or structure intact and continuous while remodeling it, allow mobile cells to carry immobile cell types along, allow migrating cells to influence each other, thereby ensuring appropriate cell distribution and shaping of a tissue, allow collective decisions that may be more robust for the system. In this scenario, collective migration can be considered the best example of how multicellular organisms are not just a collection of independent cells but interdependent cells that act together to make a whole [2].

Several examples of collective behavior involve epithelial tissues. Although epithelia are generally considered as a constrained environment where cells are fixed in position, it has been appreciated that morphogenesis in early embryos, for example, can involve cell movements within a tissue sheet [64]. Dramatic net tissue morphogenesis can occur when many cells in a tissue rearrange in a highly coordinated way, thus highlighting the ability of cells within an epithelium to move relative to one another while retaining tissue integrity [2].

Collective migration retains the principles of single cell migration. In fact, similarly to single-cell migration, collective cell movement results from actomyosin polymerization and contractility coupled to cell polarity [57]. On top of this, further additional constraints are relevant in collective movements, including direct cell-cell chemical signaling, physical interactions leading to mechanical integrity of clusters, the organization of follower cells guided by leader cells located on cluster edges, the coordinated polarization of leader cells, the coherent and cohesive movement, the secondary remodeling of the extracellular matrix along the migration track [2, 57]. The main features of collective cell migration will be described in more detail below.

Cell-cell coupling: In collective cell migration, the cells within the groups are held together by cell-cell junctions at the leading edge as well as in lateral regions and inside the moving cell group [49, 57, 65, 66], while migration of individual cells is often associated with the loss of cell-cell adhesion [67]. Cell-cell coupling is mediated by adherens-junction proteins, including cadherins and transmembrane proteins of the immunoglobulin superfamily, desmosomal proteins, integrins, tight junctions and gap junctions [68]. These cell-cell junctions determine chemical (signaling) as well as physical (mechanics) interactions, as they

mediate direct cell-cell signaling, cell-cell cohesion, mechanical integrity, and cell polarity [57].

The mechanical and chemical interactions are essential for cell movement but may also restrict and guide movement. When migration is performed by a group of cells that also affect one another mechanically and via signaling, new constraints and regulatory opportunities emerge. Thus, for collective migration the relevant cell biology is that of independently migrating cells plus the features added by the community effects [57].

Direct cell-cell signaling: One of the key aspects of collective migration is the direct chemical crosstalk among the cells; physical cell-cell contacts enable specific and efficient signaling interactions, as the cells in a group communicate with one another directly and compare signaling levels in a direct way [56].

Simultaneous coordinated polarization: The mechanisms that govern cell polarization and actin polymerization and lead to protrusion of a collective leading edge (i.e. a defined tip of cells that guides migrating cell groups and generates force) are most probably homologous to the polarity mechanisms of single cells. Several mechanisms polarize the cell cohort into “leader” or “pioneer” cells that guide “followers” at their rear. The polarized topology of a cohort is important for effective movement [56] and is a feature of all migrating groups [57]. The differences between leaders and followers are associated with clear differences in cell morphology and gene expression. Whereas cells at the leading edge are often less ordered and mesenchyme-like, cells at the rear tend to form more tightly packaged assemblies, such as rosettes or tubular networks [61]. Moreover, the presence of tight contacts in the aggregates mediates the simultaneous coordinated polarization of cells at the leading edge of the collective structure. In fact, front cells display a polarized morphology with their protrusions preferentially oriented outwards, into the free space; additionally, they detect extracellular guidance cues and generate greater cytoskeletal dynamics than follower cells in the cohort [61]. It is not completely clear how front cells become internally polarized; interaction with the substrate at the free edge might direct front cell polarization, as ECM anisotropy can produce intracellular polarization [69]. However, leader and follower cells should be considered as different cell states and not different cell types. In fact, live imaging of collective cell migration shows that leader and follower cells can interconvert and change roles [56].

Mechanical integrity and coordinated movement: Cell-cell coupling determines cell-cell cohesion, mediating the mechanical integrity of the cell aggregate during its movement [70]. Consequently, cells at different locations retain their position within the group; the movement

of the group, hence, occurs without disturbing its inner architecture [49]. The cells of the clusters are able to move in a collective and highly coordinate way via chemical signals and strong cadherin contacts [71]. If two cells adhere strongly to one another, the expectation is that they will be mechanically coupled and that their behavior will be highly coordinated. Thus, if both cells are motile, they should tend to move in the same direction with the same speed and so on. Conversely, adhesion to cells that are immotile can be a mechanical impediment to migration. The strength of a cell-cell adhesion bond depends on both the adhesion molecules themselves and on the associated cytoskeleton. It appears that most or all cells of the collective contribute directly to overall movement, as each cell gives an individual migratory contribution [2].

Secondary remodeling of 3D substrates: As single cell migration, collective cell migration through three-dimensional substrates depends upon cell-matrix interactions, but collective cell movement is characterized by the secondary remodelling of the extracellular matrix along the migration track. Thus, collective cell migration in 3D tissues is more space-consuming than single-cell migration [72]. To generate sufficient space to accommodate the volume of several cell diameters, collective cell migration through a 3D matrix involves local matrix degradation as well as the generation of paths of least mechanical resistance. Specifically, whereas single cancer cells generate small microtracks, collective structures form macrotracks of varying width (up to several hundreds of micrometers, or more) [39]. In migrating cell groups several proteases are preferentially localized to the leading edge of the cluster [57].

Cross-talk among cell groups: For the initiation or maintenance of collective migration, the migrating cell groups chemically interact with the neighboring ones through the release of soluble factors [57, 59]. These external guidance cues control group locomotion through the chemotaxis process, that is the directional movement of individual cells or cell aggregate according to chemicals in their environment. Each cell aggregate releases chemical molecules and, at the same time, senses the amount of chemoattractants released by the adjacent cell groups [2, 13]. As a consequence, there is an extensive communication among cell aggregates.

Long-range force transmission: Cell traction force is essential for cell migration, cell shape maintenance, mechanical signal generation and other cellular functions. In single cell migration, large traction forces are localized at the leading edge and at the trailing edge, acting in opposite directions [73]. When thinking about cells moving as a cohesive tissue, an important issue is the extent to which mechanical stress propagates within multicellular cohorts to control migration. It remains an open question whether the global motion is

coordinated by leader cells pulling on cells behind or by internal pressure due to cell division and proliferation that would expand cell sheets outwards. In fact different mechanical processes can promote the growth of cell sheets. In particular, proliferation of cells inside the sheet far from the leading edge can induce the build-up of an internal pressure that pushes neighboring cells outwards. In contrast, peripheral leader cells can generate mechanical tension in such a way as to drive the movement of passive followers [74]. Traction force microscopy was used to investigate how physical forces regulate the motion of epithelial cell sheets. By culturing epithelial cells on flexible gels, the traction forces exerted at the cell–substratum interface was analyzed by looking at the deformation pattern of embedded particles that act as markers (Figure 1.5) [75].

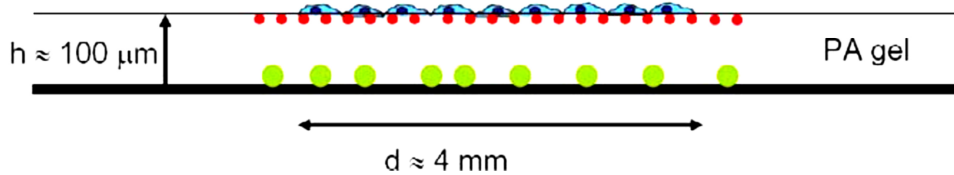


Figure 1.5: Experiment to measure traction forces during collective cell migration [75].

To determine the transmission of forces within an advancing cell sheet, the radial expansion of cell colonies was investigated as a function of time [75]. Traction force mapping shows long-range force transmission within sheets or clusters in a cooperative way; in fact, large traction forces are observed many cell rows behind the leading edge, suggesting a mechanical cooperation from cell to cell over large distances within the cell sheet. In summary, the collective motion in an advancing epithelial cell sheet results neither from leader cells dragging those behind, nor from cells that are individually self-propelled. These mechanisms are not sufficient to explain this complex mechanical process. Instead, each individual cell, both at the leading edge and inside the sheet, takes part in a global “tug-of-war” that maintains the collective into a global state of tensile stress [73-75]. Physical signals from the substrates tend to induce a migration of cells away from each other, whereas a stronger mechanical input from cell–cell interactions would drive them towards each other (Figure 1.6). Thus the importance of cell–cell junctions in the force transmission requires a cell sheet to transmit physical forces in a cooperative way [21, 73].

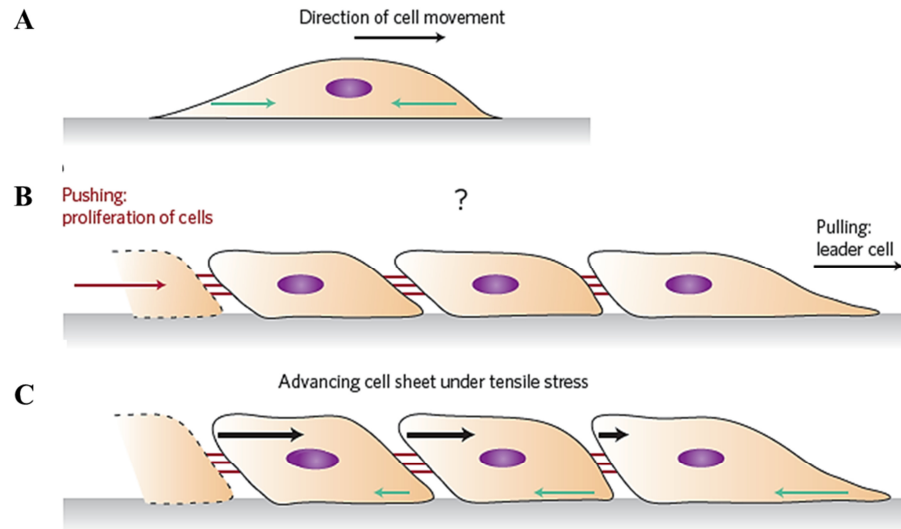


Figure 1.6: Force distributions during cell migration. (A) Schematic representation of the traction forces exerted by a single cell on the substrate; (B) Different mechanical processes promoting the growth of cell sheets; (C) Cell sheet are under mechanical tensile stress [73].

Depending on the context, collective movement can occur by two-dimensional sheet migration across a tissue surface or by multicellular strands or groups moving on a two-dimensional substrate or through a three-dimensional tissue scaffold [61].

3.4. Collective dynamics in cell sheets

Cell sheet migration is a form of collective cell behavior, especially characteristic of epithelial cells both *in vivo* and *in vitro*. In cell sheet migration, the cells maintain close contact and continuity while the sheet moves forward [2]. Cell sheet movement is characterized by the distinction between leader cells, which are located at the wound edge, and follower cells, located in the cell layer [61]. There is a clear front of the moving structure and a seemingly simple directionality of movement provided by where the free space is. Cell proliferation is involved in the dynamic evolution of a cell sheet as well.

One of the main features of epithelial monolayers is the contact inhibition of cell movement, that is a dramatic decrease of cell motility and growth with increasing cell density; this lead to the establishment of a stationary post-confluent state which is insensitive to nutrient renewal. It is widely believed that cell-cell contacts represent a necessary but not sufficient condition for growth inhibition. It has been suggested that mechanical compression may provide an inhibitory signal for mitosis. However, the nature of the signaling pathway leading to suppression of mitosis and the inhibition of cell movement remains still unclear [76].

Several analogies between confluent cell layer motion and classical glass-forming particulate systems were found. During collective migration within confluent cell layers, cell sheets flow like a fluid yet remain fixed and solid-like at short time scales, with the motion of each cell constrained by the crowding due to its neighbors [77]. This solid-like character over short times and collective flow over longer times is reminiscent of many crowded particulate systems, which undergo a transition from a supercooled fluid-like state to a glass-like state. By analogy, the collective motion of cells might be described by a similar transition: as cell density rises, neighboring cells restrict the motion of each cell, forcing cells to move in groups [78].

Experiments performed on Madin–Darby canine kidney (MDCK) cells, which are a model system to study collective cell dynamics, revealed that there are flows of cells within the epithelium. Specifically, complex displacement fields that exhibited remarkable long-range correlations can be found. Moreover, the velocity fields within the monolayer involve many cells in a coordinated way [79]. These flows are not necessarily directed toward the free surface; in fact, vortices of cells can be observed [79, 80]. Geometrical confinement of cells into well-defined circles also induces a coordinated, synchronized and persistent rotation of cells, which depends on cell density. In fact, the speed of such rotating large-scale movements slows down as the density increases. The rotating cells move as a solid body, with a uniform angular velocity. Interestingly, this upper limit leads to length scales that are similar to the natural correlation length observed for unconfined epithelial cell sheets [81].

3.5. Dynamic evolution of cell clusters

Free aggregates are characterized by tightly connected cells that migrate as cohesive structures. The dynamic evolution of cell clusters in space and time is mainly linked to three mechanisms: collective locomotion, cell proliferation within the clusters and aggregation of adjacent clusters.

As might be expected for such a free group, directional migration is controlled by localized external guidance cues. Recent results indicate that two different modes of guidance signaling operate in border cells. One mode is dependent on localized signaling within each cell, comparable to the situation in single cell chemotaxis. The other mode is described as collective guidance. Collective guidance relies on the fact that the moving cells are a group: each cell senses the amount of chemoattractant, and the cell with the highest level of signal migrates most effectively at each point in time. Cells at the edge of a group have a discreet

outer surface and internal contact surfaces; this provides an intrinsic cell polarity and thus potentially a vector along which each cell will attempt to pull the cluster. Whether such a collective guidance mechanism is sufficient to guide a migrating group has yet to be clarified [2].

One of the main feature of cell groups evolution is the expansion of the clusters driven by cell proliferation mechanism within the collective structures [82]. Daughter cells seem to occupy, on average, twice the area of their mother cell and the rate of colony growth should match exactly the rate of cell mitosis. Some articles support that cell colonies grow following a simple exponential law (Figure 1.7) [76, 83], as the cells within the collective structures grow exponentially through the following law:

$$n(t) = n_0 * 2^{(t/t_d)} \quad (1.1)$$

where t is a certain time interval, $n(t)$ the number of cells at time t , n_0 the number of cells at time 0 and t_d the duplication time of the cells [84].

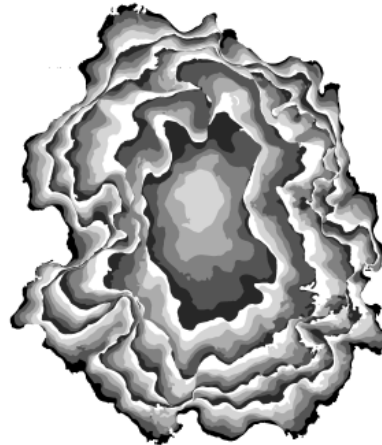


Figure 1.7: Schematic representation of epithelial colony growth, with superimposed snapshots of a single colony at different times, coded by different shades of gray [76].

Moreover, cell aggregation events may occur in collective behavior, as cell clusters can diffuse and spread until they meet to form new larger aggregates. Cell aggregation is the result of the attractive interaction between individual cells [85, 86] as well as cell groups that migrate in response to signals released and detected by themselves, through chemotactic mechanisms. Consequently, chemotaxis plays a key role in the aggregation process: the cells within a cluster secrete soluble chemokines that are detected by the cells of neighboring which carry specific receptors for these chemokines. Cell aggregates are able to sense the

clusters in their neighborhood and to communicate through chemokines release and detection. Following chemotactic signals, multicellular aggregates encounter and attach to each other. The cross-talk among cell aggregates plays an essential role, e.g. in tissue formation and function [87]. M. Eyiurekli et al. have considered that chemoattractants are secreted from the cell's surface symmetrically and diffuse within a fixed radius of influence. They have assumed that once the chemoattractant concentration falls below a certain value, cells in the environment can no longer detect its gradient. This assumption creates a circular field around each cell with a radius R_{\max} , corresponding to about two cell diameters. Any cell within a distance of R_{\max} to another cell is influenced by the other cell's chemoattractants. A cell that is further away than R_{\max} from an emitting does not detect its chemoattractant and the detecting cell's motion is not affected by the emitting cell. In summary, a cell senses the chemicals emitted from other cells when it enters their influence fields. The extent of the field is defined by a chemical concentration threshold. For example, the three cells on the left in Figure 1.8 are affected by each other's chemoattractant, because they are within each other's field of influence; therefore they move toward each other. The fourth cell is outside their influence fields, and therefore is unaffected by the other three and moves randomly [88].

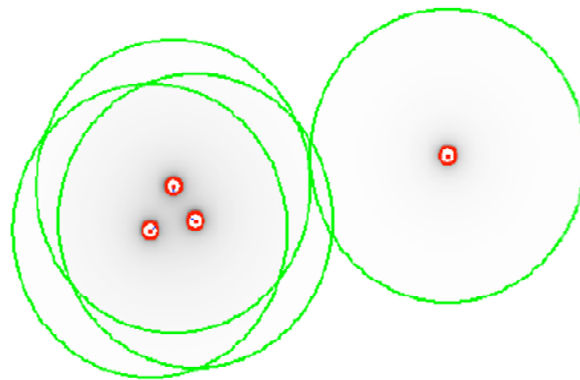


Figure 1.8: Four cells and their fields of influence.

Several papers support the idea that cell clustering and cluster aggregation can be seen as the coalescence of coagulating objects [89, 90]. In fact, the fusion of two contiguous cell aggregates may be described in terms of an effective interfacial tension [90] that promotes the formations of clusters with minimum external surface for a given number of cells; analogously cluster coalescence can be inhibited by an effective viscous friction of the surrounding matrix. Kosztin et al. observed that during the fusion of identical spherical soft

tissue aggregates the shape of the system is that of two contiguous spherical caps (Figure 1.9). This observation suggests that soft tissues behave like complex viscous liquids whose description requires an a priori unknown hydrodynamic constitutive model. However, the simplicity of the geometry allows to describe analytically the dynamics of the considered fusion process by employing conservation of mass and energy as proposed for the coalescence of highly viscous molten drops (Kosztin et al., 2012).

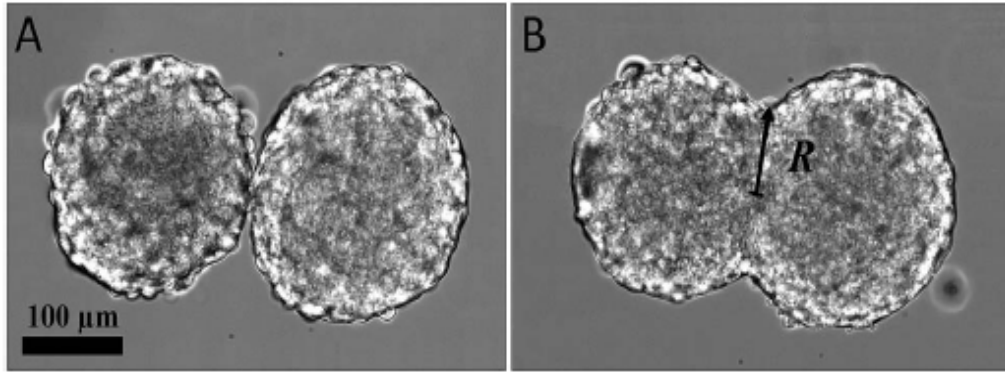


Figure 1.9: Fusion of two cell aggregates [89].

After aggregation, the fusing clusters are observed to become spherical, because they compact due to interfacial tension. In fact, the fusion of two contiguous cell aggregates may be described in terms of an effective interfacial tension that promotes the formation of clusters with minimum external surface, in analogy with the coalescence of droplets (Figure 1.10). The characteristic time for cluster retraction τ can be seen as the equivalent of the emulsion time for the case of a retracting droplet [89, 90], i.e. the time for an irregular liquid drop to take a spherical shape. Thus, it can be written

$$\tau = \frac{\eta d_{final}}{\gamma} \quad (1.2)$$

where d_{final} is the diameter of the final cluster, γ is the interfacial tension and η is the material viscosity. Despite several theories and mathematical models have been proposed, the mechanisms of cellular aggregation have yet to be clarified.

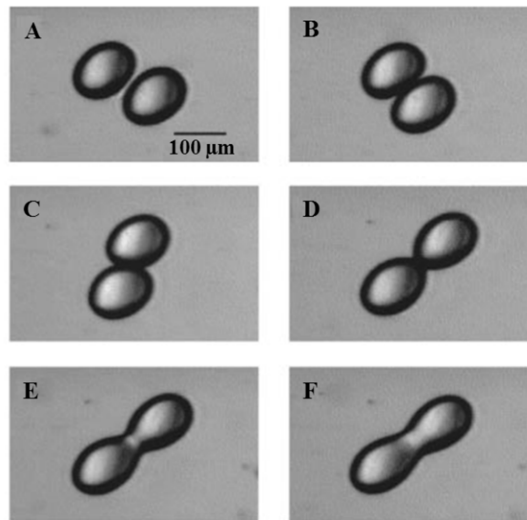


Figure 1.10: Sequence of images showing a collision of drops with coalescence [91].

3.6. Live cell imaging

Cell dynamics, led by proliferation and migration mechanisms [1], are crucial for many key biological processes, including morphogenesis, tissue repair, immune responses and cancer cell invasion [92]. Thus, a full comprehension of these mechanisms could lead to novel therapeutic approaches.

Cell motility as well as cell proliferation are the product of several complex, integrated, finely regulated and highly coordinated processes [16, 17]. Due to the tricky nature of these fascinating processes, reaching a better understanding of cell dynamic behavior represents a formidable intellectual challenge, which require a multidisciplinary approach (Horwitz and Webb, 2003).

Live cell imaging is becoming an increasingly popular tool for elucidation of biological mechanisms and is instrumental in unravelling the dynamics and functions of many cellular processes. The imaging of live cells poses many challenges, such as cell viability, complex microscope settings and the use of appropriate fluorescent components that vary in nature. The successful imaging of biological events in cells is largely dependent on the environmental conditions provided. Ideally, the conditions should be as close to physiological cellular environment as possible, in order to avoid the induction of cellular stress responses and artefactual cell behavior. Hence, the medium, pH and temperature must be maintained at a physiological level that does not alter biological processes of interest. The medium of choice is usually limited by the cell type of interest. In general, the medium should meet all the nutritional requirements for cell growth and this usually involves the addition of serum.

Live cell imaging can be efficiently performed by using time-lapse microscopy (TLM), which allows a powerful analytical tool that allows direct visualization of biological systems *in vitro* during their dynamic evolution [93]. TLM involves repeated capture of images in specific positions, i.e. of the same objects (e.g., cells in movement), at regular time intervals, within periods of time ranging from few minutes to several days. The duration of the intervals determines the temporal resolution, and the resulting video sequence shows cells or organisms in action, revealing the dynamic nature of cellular behavior and giving scientists a first look at some important biological processes. Briefly, the time-lapse station consists of a microscope equipped with motorized stage and focus for automated sample positioning, with the entire system sitting on a vibration-free table. The images are captured by a video camera. All the equipment are driven by a software that iteratively acquires images of selected regions at regular time intervals over several hours. In order to create the proper environmental conditions around the biological sample, video microscope are equipped with a cell incubator providing the appropriate temperature (around 37°C) and the atmosphere (5% CO₂ and humidity) necessary to keep cells alive and healthy throughout a TLM experiment [94].

TLM is coupled to a wide variety of *in vitro* assays to allow the quantitative characterization of the dynamical aspects of biological systems [95], such as random migration assays, wound healing assays and chemotaxis assays. Each method has its own advantages, limitations, and drawbacks [95, 96].

3.7. Random migration assays

Cell random motility assay is a well-established method to characterize cell migration [93]. It is based on the observation of individual cell motion in isotropic condition and provides intrinsic parameters of cell motility. In this assay, the cells are plated out at a low density on the surface of a culture dish, and cell position is typically tracked as a function of time. Cell trajectories are then reconstructed either manually or automatically by a cell matching algorithm [97] which allows a quantitative determination of cell motion parameters, including cell total travel length, net displacement and velocity [59]. Cell random motility can be also described by a persistent random walk model [98-100], which is associated with the persistence time between significant directional changes and the cell motility coefficient analogous to molecular diffusivity [101].

Cell random motility assays are probably the most widespread and have contributed to the fundamental understanding of cell migration processes at the molecular level [102]. The major advantage of the single cell migration assay is that it provides valuable insights into the

dynamical behavior of individual cells. The assay also allows the tracking of cell motions in two- or three-dimensional substrata, in which the cells are embedded within a matrix typically made of type I collagen.

The quantitative analysis of single cell migration, however, requires the tracking of large number of cells for long periods of time to obtain statistically robust results [96]. From this perspective, the single cell motility assay is sophisticated and the quantitative analysis is very time-consuming. The large amount of data acquired from this detailed analysis need to be further processed to extract simple parameters that can be considered representative for the entire population.

3.8. Chemotaxis assays

The ability of cells to migrate, adhere, and change shape, which is central for all eukaryotes, is primarily regulated by external signals, although there are instances when cells respond to internal cues as well. One of the most interesting and relevant cases of cell migration in response to external stimuli is chemotaxis, i.e., the directional movement of cells along a towards a concentration gradient of a soluble molecule.

This mechanism is implicated in a range of physiologically relevant processes, such as inflammatory response [103], homeostatic circulation, and development [104]. It also concerns a number of disorders and pathological processes including infectious and allergic diseases, wound healing [105], angiogenesis, atherosclerosis, and tumour dynamics [13, 106, 107]. In the latter case, it is well known that cancer cells can migrate both individually and in a collective manner [108]. Moreover, it has been recently shown that a diffusional instability mechanism [8] can induce the separation of single or clustered cells from the main tumour body, which can then migrate toward the source of nutrients, e.g. a blood vessel, thus invading wider areas and tissues.

A still open issue is how soluble gradients might be continuously maintained *in vivo*, where it is known that several physical events such as muscular contraction, convection of extravascular fluid, and lymphatic flow might perturb the graded diffusion of soluble substances.

Despite its ubiquity and importance, chemotaxis remains a difficult process to investigate in a quantitative way, partly because it occurs in complex 3D environments not easily reproducible *in vitro* and not readily compatible with live cell imaging. The development of physiologically relevant *in vitro* assays to study chemotaxis in a quantitative way is a topic of

growing interest. Early efforts to generate spatially linear and temporally stable chemical gradients led to the development of diffusion-based chambers.

Several experimental approaches have been proposed in the literature to investigate cell chemotaxis both qualitatively and quantitatively. In these assays, a gradient is established by diffusion inside a porous medium or through a small gap between two large reservoirs containing chemoattractant solutions of different concentrations. The most popular chemotaxis assay is based on the Boyden chamber [109]. It consists of two compartments, placed one into the other, which are separated by a porous membrane through which cells migrate. The pore size has to be chosen small enough in relation to the size of the investigated cells so that the cells actively migrate through the pores and cannot passively pass the membrane by just dropping through them. The cells are seeded on a porous membrane in the upper well, which is placed in a well containing a chemoattractant solution. It diffuses into the upper one creating a concentration gradient across the membrane. This stimulates the movement of the cells from the upper side to the bottom side of the membrane (Figure 1.11). The cells on the bottom side are then fixed, stained, and counted.

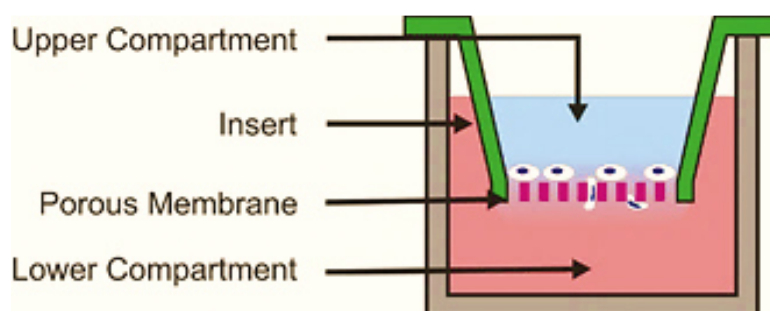


Figure 1.11: Boyden chamber.

This assay is widely used because it's unexpensive and easy to set up. In addition, the filter inserts with different pore sizes are commercially available and that the assay can be used to quickly screen chemotactic effect of many compounds. However, the Boyden assay shows many limitations due to the fact that it does not provide well defined concentration gradients. In fact, the chemokine becomes homogeneously diffused in the upper chamber and the cells will no longer migrate through the pores. Moreover, it is an end-point assays and cannot be used for live cell imaging. Consequently, the Boyden assay does not allow cell migration to be monitored as a function of time; therefore dynamic parameters of cell migration cannot be evaluated. Furthermore, chemotaxis and chemokinesis (undirected increase of cell speed)

cannot be discriminated in this assay because an equilibrium of the chemotactic factor to be investigated is quickly reached [110].

The under agarose assay [111] is also widely used to investigate cell chemotaxis, but as the Boyden assay, it suffers from several drawbacks, including that the cells are incubated in static conditions and dynamic parameter of cell migration cannot be evaluated. However, the *in vivo* environment is far more complex in comparison to conventional cell assay chambers. Microfluidic devices, usually fabricated in PDMS (PolyDiMethylSiloxane) by soft lithography [112-115], have also been recently proposed as a tool to observe cell behaviour and migration under chemotaxis or interstitial flow conditions [116]. Convective and diffusive transport can be decoupled by using microfluidic agarose membranes; the effect of shear stress can be also investigated by exposing the cells to static or pulsating flows [117, 118]. Bridge chambers provide a visualization platform for observing the behavior of cells between the two wells. The cells are plated onto cover slips, which are then inverted leaving a small gap between the bridge and the cover slip, too small for fluid flow to occur, but large enough to allow diffusion of the chemoattractant. Cells can then be observed using an inverted time-lapse microscope, which allows to capture the dynamic behavior of the cells. Commercially available chemotaxis bridge assays include the Zigmond and Dunn chambers (Figure 1.12). The Zigmond chamber [110] was designed for studying polymorphonuclear leukocytes capable of rapidly migrating at speeds of up to 30 $\mu\text{m}/\text{min}$ [119]. In this chamber, two compartments containing the chemoattractant and the cells, respectively, are connected side by side horizontally. This chamber allows the generation of shallow gradients and represent a great improvement on under agarose assays, due to its improved optical properties and near steady state linear gradient stable for 30–90 minutes. The Dunn chamber [120, 121] was introduced in 1991 for the investigation of chemotaxis in fibroblasts, which migrate much more slowly at 0.42-1.25 $\mu\text{m}/\text{min}$. Gradient characterization experiments for this chamber highlighted that it was able to generate a linear gradient within 1 h of setting up the chamber, with a gradient half-life of 10 to 30 h, due to the stable gap between the cover slip and bridge. A recent modification of this technique is the Insall chamber, shown in Figure 1.12 [122], whose advantages include easy handling, gradients with defined directions and two different gradient steepnesses in the same assay, compatibility with thin cover slips for optimal optical properties. As with the Dunn chamber, gradients are maintained for at least 24 hours, allowing slowly-moving cancer cells to be tracked. These assays are typically used to evaluate cell migration on 2D substrata. Direct observation chambers where the chemoattractant solution is in contact with a 3D gel containing cells have also been reported [123, 124], but quantitative

control of the concentration gradient was difficult to achieve. 2D assays are easy to handle and provide important tools for understanding the migratory activity in response to natural or pharmacological modulators, but there could be different mechanisms in 2D vs 3D cell migration [125-127], the latter being in principle more adequate to mimic the *in vivo* environment.

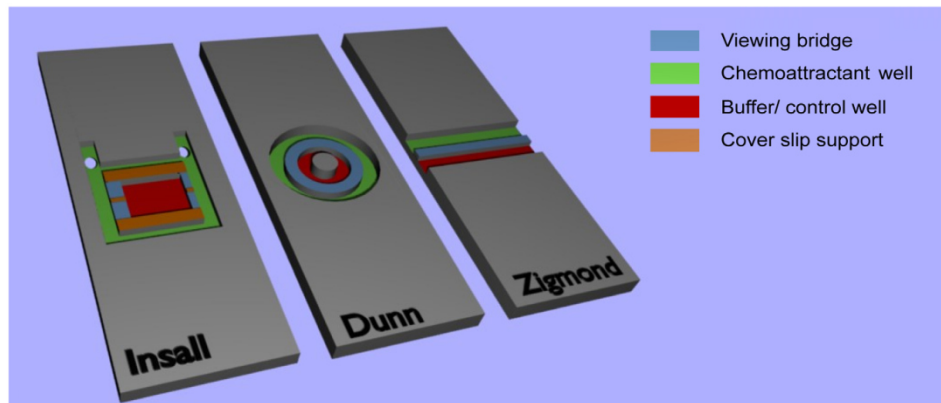


Figure 1.12: (A) Schematic representation of the Insall, Dunn and Zigmond chambers [122].

An ideal *in vitro* chemotaxis assay should be carried out in a tissue-like collagen or fibrin gel, allowing direct cell tracking [128] and imaging of the concentration gradient of the chemotactic factor (CF) within the (optically transparent) gel, and be relatively easy to set up with significant reproducibility [129]. Since cells are able to sense a spatial increase in chemokine concentration to direct their motion, chemotaxis studies require a way to deliver chemicals to cells in a controlled way. These criteria have been fulfilled in the *in vitro* assay of leukocyte chemotaxis reported by Moghe et al. [130], in which the cells are initially dispersed throughout the gel rather than concentrated on the filter surface as in the Boyden chamber, thus minimizing cell-cell interactions and cell alteration of the CF gradient. A simple modification of this leukocyte chemotaxis assay reported by Knapp et al. [131] allows a gradient of similar steepness to be realized for sufficiently long periods to investigate the chemotaxis of slow moving cells, such as fibroblasts. It involves the placement of a barrier between the two halves of a chamber (one-half initially containing CF at uniform concentration, the other initially containing none), leaving a small gap at one end of the barrier that serves to geometrically (or dimensionally) constrain the free diffusion; this small gap hinders the passage of the diffusing molecules, thereby slowing the decay rate of the spatial gradient, which emanates radially outward.

Recently, a novel chemotaxis assay in 3D collagen gels based on a direct-viewing chamber has been developed to overcome some of the limitations of the existing assays. The chamber, shown in Figure 1.13, consists in two steel blocks glued on top of a microscope slide by using a silicone adhesive. The blocks, separated by a porous membrane (0.22 μm pore size), are assembled together by two mounting screws. Part 1 in Figure 1.13 has two independent compartments; the first one (A) is used as control well while the second one (B) is the reservoir of the chemoattractant solution. In part 2 there is only one compartment (C) which is used for the cell seeded collagen gel. Once assembled, the membrane separating the chemoattractant (B) and the collagen gel (C) compartment is sandwiched between the two rectangular open frames in part 1 and 2, and the chemoattractant can diffuse through the membrane first and then into the cell-seeded collagen gel [132].

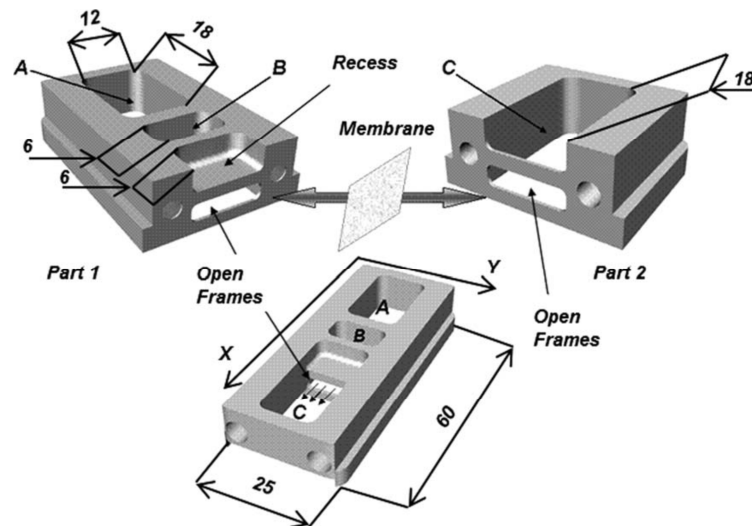


Figure 1.13: 3D rendering of a recently developed chemotaxis chamber [132].

This methodology provides an integration of features, which are not found altogether in other assays from the literature: an autoclavable chamber simple to operate and including a control well, live cell imaging with both low and high-resolution optics, a 3-D extracellular matrix, a well characterized concentration gradient lasting for extended time periods, quantitative data analysis based on cell tracking.

3.9. Wound healing assays

The wound healing (WH) assay is considered one of the most popular methods to evaluate cell dynamic behavior *in vitro* [96, 133], because of its low cost and simplicity to set up [134].

In the classical WH assay, also known as scratch assay, the cells are grown on a two-dimensional surface until they cover the entire available surface (100% confluence). An artificial scratch is then created on the confluent cell monolayer by mechanically removing the cells from a defined area with a pipette tip, a blade, a needle or similar [135]. Then the cells are washed with a desired medium to remove not attached damaged cells and cell debris. In response to the stimulus arising from the creation of the empty space in a previously intact tissue, the cells on the wound margins, which are no longer contact-inhibited, proliferate and move toward the center of the denuded region to fill the wound [136] until new cell-cell contacts are established again. It is not quite clear what triggers the wound closure process. The scratch process destroys the removed cells, which release their intracellular content into the medium; this process is also quite traumatic for the cells on the newly formed edges. Indeed these border cells may become partially permeable as a result of the brutal tearing off of the adhesive junctions they maintain with their neighbors. A sudden influx of the extracellular medium in these cells may potentially trigger their migration. It is also possible that a free edge is sufficient by itself to induce cell motility and proliferation to redensify the monolayer [79].

The process of wound healing is regulated by numerous growth factors, such as epidermal growth factor (EGF), transforming growth factor- β (TGF β), vascular endothelial growth factor (VEGF), platelet-derived growth factor (PDGF), and basic fibroblast growth factor (bFGF). In particular, bFGF is a member of a large FGF family of structurally related proteins that bind heparin or heparan sulfate, known to promote both proliferation and motility of a wide variety of cell types [137]. FGF binds to the different isoforms encoded by the four receptor tyrosine kinases designated FGFR1-4, and also binds to heparin or heparan sulfate proteoglycans. FGF-stimulation leads to the activation of the Ras/MAPK signaling pathway [138], which plays an important role in bFGF-induced cell proliferation [139].

Epithelial and fibroblast-like cell behavior in the WH assay

Two main mechanisms of wound healing, have been identified [2, 135, 140], depending on the type of cells involved. The first one is typical of fibroblast-like cells, which cover the

wound space as individual cells; the second mechanism is a typical feature of epithelial or endothelial cells, which close the wound in a collective mode [140].

Concerning the first wound healing mechanisms, fibroblasts migrate toward the wound area primarily as individual cells [140]. The availability of free space after the scratch is the initiating event for the induction of cell movement. bFGF seems to promote fibroblast migration through the PI3-kinase-Rac1-JNK pathway, which is a novel pathway of bFGF-induced cell migration. Overall, the cells can move with the same probability in any direction, due to the lack of cell-cell interactions. In addition, cell proliferation may also contribute to the wound closure [139], as it increases in response to the “sensation of free space” after wounding [134].

Concerning the second wound healing mechanism, epithelial-like cells maintain close contacts and continuity with each other while each sheet of cells moves forward as a coherent cluster, whose mechanical integrity is led by physical cell-cell interactions [79, 141]. The loss of spatial constraints in the epithelial layer stimulates cell migration [79, 142] and proliferation [143] within the cohort, thus enabling the wound closure through the spreading of one sheet of cells towards the other in a collective and coordinate manner [144, 145].

WH experiments performed on epithelial monolayers of Madin-Darby canine kidney (MDCK) cells showed that wounding in this model system is accompanied by two traveling waves of MAPK activation that propagate from the wound edge into the bulk of the monolayer. These dynamic signaling patterns were found to be essential for coordinated cell migration during the wound healing process, which involves the spreading of the monolayer, with essentially no cell proliferation. Furthermore, it has been proposed that MAPK participates in a positive feedback loop which is characterized by cell spreading, MAPK activation and cell motion, which drives the spreading of a wounded MDCK monolayer [146].

There is still some controversy regarding the triggering event for the induction of epithelial cell sheet movement. Cell damage was suggested to be a prerequisite for the initiation of cell movement [147]. To test whether cellular injury is required to trigger the healing response, Block et al. used agarose strips to create gaps in rabbit corneal epithelial monolayers minimizing the perturbation of the cells. Following strip removal, cellular sheets migrated at the same rates as sheets created in scraped monolayers. The findings support the idea that the triggering event for the induction of cell sheet movement seems to be the availability of empty space [148].

The injury seems to be not strictly necessary; in fact, injury-free WH assays performed on MDCK epithelial cells showed that the free surface is sufficient to induce cell migration. Complex and coordinated long-range motions within the epithelium were observed, supporting the hypothesis of a mechanical communication between the cells in response to the creation of free space [79]. However, Nikolic' et al. showed that the injury is essential for coordinated behavior of MDCK cells in the epithelial sheet. MDCK sheet migration was investigated under three different conditions: the classic scratch assay; empty space induction, where a confluent monolayer is grown adjacent to a slab of polydimethylsiloxane and the monolayer allowed to spread upon removal of the slab, without damage; injury via polydimethylsiloxane membrane peel-off, where an injured monolayer migrates onto plain tissue culture surface. It was observed that the damage in the confluent cell monolayer induces a the first wave of MAPK activation and that unconstraining of the sheet without injury induces only a second, slower wave of MAPK activation. It was also shown that the injury induces the generation of reactive oxygen species (ROS) at the wound interface, and that ROS are essential for the activation of the first wave of MAPK signaling pathway. Furthermore, in the absence of an external damage, cell motility within the sheet appears greatly attenuated in terms of speed, travelled distance and cell path persistency compared with the classical wound healing [149].

Mathematical modelling of the wound closure process

The wound closure dynamic process can be mathematically described using the Fisher-Kolmogoroff equation [150], which describes cell density evolution in space and time in terms of cell motility and proliferation [151]. Both these mechanisms are involved in the spatial spreading of the cells invading the wound area, strongly affecting the evolution of cell density [152]. According to the Fisher-Kolmogoroff equation, cell motility is modeled by Fickian diffusion, while cell proliferation is described by a logistic growth [153]:

$$\frac{\partial u}{\partial t} = D \frac{\partial^2 u}{\partial x^2} + ku \left(1 - \frac{u}{\hat{u}}\right) \quad (1.3)$$

where u is cell density at time t at a given distance x from the wound edge, D is the constant diffusivity (random motility coefficient), analogous to the diffusion term in Fick's law, k is the proliferation rate and \hat{u} is the carrying capacity of the surface, corresponding to the cell density at confluence, in which the cells cover the whole available surface. Consequently, according to the Fisher-Kolmogoroff equation the rate of change of cell density at position x

at time t depends on both the change in cell density due to the migration process and the change in cell density due to cell proliferation [154]. The diffusion term of the Fisher-Kolmogoroff equation is linear, with the diffusivity assumed to be constant. The logistic growth model is related to the cell doubling time t_d ($k = \frac{\ln 2}{t_d}$) and includes crowding effects by reducing the growth rate as the density approaches the confluence density, or threshold value, \hat{u} [155]. The Fisher-Kolmogoroff equation exhibits constant shape travelling wave solutions; in fact, the model predicts that after a short transient the movement of the invading cell front can be observed in terms of a traveling wave, which propagates with constant speed $s = \sqrt{4 \hat{u} k D}$ in the direction perpendicular to the wound [136, 152, 154-156]. If the cells do not move, which means that $D=0$, cell proliferation is the only mechanism driving cell density evolution. Under these conditions, the Fisher's equation can be simplified to the logistic equation (Eq. (1.4)):

$$\frac{\partial u}{\partial t} = ku \left(1 - \frac{u}{\hat{u}}\right) \quad (1.4)$$

In particular when $u \ll \hat{u}$, cell proliferation follows an exponential growth model.

When cell proliferation is suppressed, meaning that $k=0$, it can be written:

$$\frac{\partial u}{\partial t} = D \frac{\partial^2 u}{\partial x^2} \quad (1.5)$$

In this case (Eq. (1.5)), cell density evolution is only related to cell diffusion and the Fisher-Kolmogoroff equation is similar to the Fick's law. Several drugs working as cell division inhibitors, such as mitomycin-c, can be used to inhibit the proliferation process [139, 157].

Maini et al. experimentally measured the position of the invading cell front as a function of time and found that it moved at approximately a constant speed. They also determined the wave speed for wounds generated in cell monolayers grown on different substrates. Analytical results from the Fisher-Kolmogoroff equation then provided a relationship between the rate of cell proliferation and the diffusion coefficient. However, the details of the cell density behind the wound edge were not investigated [154].

Other approaches to identify parameters are based on the measurements of the cell density profile. For example, Sengers et al. fitted the solution of a reaction-diffusion equation to density profiles obtained from experiments, in order to match the experimental data [158, 159]. Similarly, Sherratt and Murray studied a WH assay and chose the parameters in two

different reaction–diffusion equations so that both models predicted the observed closure rates [160]. Takamizawa et al. calculated numerical solutions of the Fisher-Kolmogoroff equation using different values of the diffusivity and proliferation rate parameters and compared the numerical results with the experimental data of cell density within the wound. A trial and error method was used to estimate the two parameters that gave the best fit to the experimental data [161]. Savla et al. proposed a modification in the Fisher-Kolmogoroff equation to include a term that describes cell spreading and account for a time delay into the mitotic term. The contributions of spreading, migration, and mitosis were investigated both numerically and experimentally. The best fit parameter values between the numerical solutions and experimental data were obtained with a nonlinear least-squares algorithm [162]. Dale et al. used a cell diffusivity that was a function of an external chemical factor; they determined an analytic approximation for the speed of traveling wave solutions in terms of the parameters and verify the results numerically and compared the predicted speed with experimentally measured closure rates in corneal epithelial wound healing [163]. Simpson et al. used a combination of experimental and modelling techniques to isolate the role of cell motility and proliferation in a two-dimensional circular barrier assay. They obtained independent estimates of D and k and make independent modelling predictions about the position and shape of the leading edge as well as the evolution of the cell density profiles. Their results highlighted that continuum models, based on the Fisher–Kolmogorov equation, are a reliable platform upon which they can interpret and predict their experimental observations [164].

However, the previous models do not include the effects of contact inhibition of migration in the wound closure process. This effect is significant and should be included when modeling wound closure dynamics. As cell motility has been observed to decrease with increasing local density [155], an extension of the Fisher’s equation, incorporating non-linear diffusion, is available:

$$\frac{\partial u}{\partial t} = D_0 \frac{\partial}{\partial x} \left[D \frac{\partial u}{\partial x} \right] + ku \left(1 - \frac{u}{\bar{u}} \right) \quad (1.6)$$

Here, the constant parameter D_0 is the diffusivity coefficient for isolated cells, while D is a dimensionless diffusivity and is function of $\frac{u}{\bar{u}}$ with the properties $D(0)=1$ and $dD/du < 0$ [136], meaning that the diffusivity is a decreasing function of cell density. A function that fits these requirements is

$$D = \left(\frac{A}{A + \frac{u}{\bar{u}}} \right) \quad (1.7)$$

where A is a critical value of cell density and represents a measure of contact inhibition phenomenon. It depends on the cell line; for example $A=0.02$ cells/ μm^2 for neurons migrating from a dense cluster [165]. Eq. (1.7) captures the contact inhibition effect of cell movement, whereby cells slow down, stop or change direction when they encounter another cell in their path [136], therefore hindering and inhibiting cell movement. It is natural to consider the cell diffusivity decreasing with density, since the presence of other cells leads to more collisions [155].

Wound closure investigation

Two methodological approaches are typically used to capture the output of the WH assay, in order to gain quantitative information about cell spreading within the wound region. The most popular approach is related to the manual acquisition of images within the sample along the wound at the beginning and at fixed time intervals (for example every 6 h) until the wound is closed [139]. In this approach cell movement is typically quantified counting the number of cells which repopulate the wound region for each time step, or measuring the distance between the two wound edges or the wound area [166] in order to determine the percentage of wound closure at fixed time points [167]. However, this classical approach results to be approximate, as it doesn't allow to highlight the dynamic aspects of cell behavior. For example, Andújar et al. quantify the wound closure process by counting the migrated cells after 24 h from the beginning of the assay, in order to investigate the role of shikonin in the migration of intestinal epithelial cells [168]. Tsai et al. also determined the number of CCD-966SK cells migrating in the denuded zone after 12 and 36 h [169]. Zhang et al. measured the distance between the two edges of the scraped area at the beginning and after 24 h, in order to estimate the migratory distance of the cells within the wound region [170]. Yue et al. quantify cell migration toward the denuded area at 16 and 24 h and determined the percentage of wound closure [171]. In order to assess the role of Protein kinase C on the spreading and migration of intestinal epithelial cell during WH assays, Sumagin et al. also determined the rate of cell migration into scratch wounds by measuring the surface area devoid of epithelial cells immediately after wounding ($t=0$) and at subsequent time points (12, 24 and 48 h) [172]. An alternative, more reliable approach to quantify cell dynamics in a WH assay is based on live cell imaging performed by using time-lapse microscopy (TLM) which allows to iteratively acquire sample images with a defined time frequency [93], while controlling the

environmental parameters to ensure cell viability throughout the experiment, which can last up to a few weeks [94, 173]. This methodological approach allows to obtain the abovementioned measurements, i.e., the number of cells in the wound region or the percentage of wound closure, in a more accurate way. Moreover, the possibility to regularly observe over time exactly the same wound region, rather than roughly comparing randomly taken images, enables to estimate precise quantitative parameters, such as wound closure velocity, measuring the reduction of wound area over time, or the cell front propagation speed, quantifying the position of the wound front over time.

Overall, the wound healing process is typically investigated on the scale of the entire cell population, neglecting individual cell behavior. More precise information can be obtained coupling TLM approach with cell tracking, in order to quantify intrinsic cell motility from individual cell trajectories (Rosello et al., 2004). In fact, the possibility to regularly image over time exactly the same wound region allows to track the path of individual cells on the wound edges, in order to investigate the dynamics of wound healing also on the scale of the single cells. This approach enables to reconstruct cell trajectories and quantify cell motility parameters, such as the total length travelled by the cells, the net displacement and cell velocity [174, 175].

Advantages and disadvantages of the wound healing assay

One of the major advantages of the wound healing assay is that it mimics to some extent migration of cells *in vivo*. In comparison with other popular *in vitro* methods, such as the Boyden assay, the wound healing assay is particularly suitable to study the regulation of cell migration by cell interaction with extracellular matrix (ECM) and cell–cell interactions. In other popular methods such as Boyden chamber assays, preparation of cells in suspension before the assays disrupts cell–cell and cell–ECM interactions [135]. Moreover, the WH assay is also compatible with advanced microscopy techniques including live cell imaging, allowing analysis of intracellular signaling events (e.g., by visualization of green fluorescent protein (GFP)-tagged proteins for subcellular localization or fluorescent resonance energy transfer for protein–protein interactions) during cell migration. The wound healing assay is also probably the simplest method to study cell migration *in vitro* and only uses the common and inexpensive supplies found in most laboratories capable of cell culturing [140].

Although very powerful to investigate cell dynamics, the wound healing assay suffers from several disadvantages and limitations. For example it cannot be used to investigate the chemotactic behavior of the cells, and consequently, it does not replace other well-established

methods for chemotaxis such as the Boyden chamber assay, as no chemical gradient is established. In addition, it takes a relatively longer time to perform than some other methods, considering that a couple of days are needed for the formation of the cell monolayer before making the scratch and starting the experiment. Relatively large amount of cells and chemicals are required for the assay as it is usually performed in a tissue culture dish. Therefore, it is not the best method to choose if the availability of cells (e.g., specialized primary cells that are hard to get in sufficient amount) or chemicals (e.g., expensive reagents) is limited [140].

Furthermore, the outcomes of the WH assay are somewhat confounded by several factors, which may represent a limit in accomplishing reproducible and reliable quantitative results. First, the wound width can vary along its length and among different experiments [176]; it depends on the dimension of the tool used in making the wound as well as the scraping force and velocity [177]. The geometry of the initial wound is particularly relevant, since the complex force field that develops at the free edge of the monolayer depends on the size and shape of the cell-free region [178]. Second, the scratching process involves mechanical injuries to the cells located on the wound edges [149], which may potentially lose their original morphology and function; this may result in the transient contraction of the cell wave front [179]. Some damaged cells and cell debris can also keep attached to the wound margin, perturbing the motility of other cells moving around the obstacle to access the cell-free area [180], or they often reattach to the plate and move into the wounded area [133] or can cause leaking of the intracellular contents towards the wound region, leading to adulterated results. Additionally, the migrating surface, often coated with extracellular proteins prior to cell growth, can be damaged by the sharp objects typically used in the scraping process; alterations in surface topography may lead to preferential paths in cell movements (contact guidance) [181]. It is well established in the literature that substrate microtopography can influence cell adhesive and migratory properties, since substrate topography can alter the establishment and organization of cell membrane based focal adhesion complexes and can thereby invoke specific signaling pathways which may regulate cellular phenotype and function [182]. Furthermore, the relative cell confluence in the region where the scratch is made, is challenging to control and reproduce within the same culture dish and among different cell samples [183]. This makes it difficult to compare between experiments. The difficulty to obtain the same cell density in the samples primarily arises from anisotropies in the spatial spreading of the cells, mainly due to uneven cell attachment in the culture dish after plating. Moreover, it is arduous for the operator to plate exactly the same number of cells

in different culture dishes. Above all, several cell treatments, such as gene silencing, involve the use of invasive techniques, which may result in unwanted cell detachment from the bottom of the plates or cell death.

Overall, these factors might potentially influence the outcome of the WH assay, strongly limiting the reproducibility of the experiments. In order to implement the WH assay in a more controllable way, novel approaches have been developed.

Alternative approaches to the classical WH assay

Recent advancements in micromachining, optics, chemistry, and electronics in the past decades, have led to the development of novel techniques which can be used to overcome the limits of the classical wound healing assay. Specifically, wounding techniques based on non-mechanical methods such as chemical, electrical, and optical approaches have been recently developed (Figure 1.14).

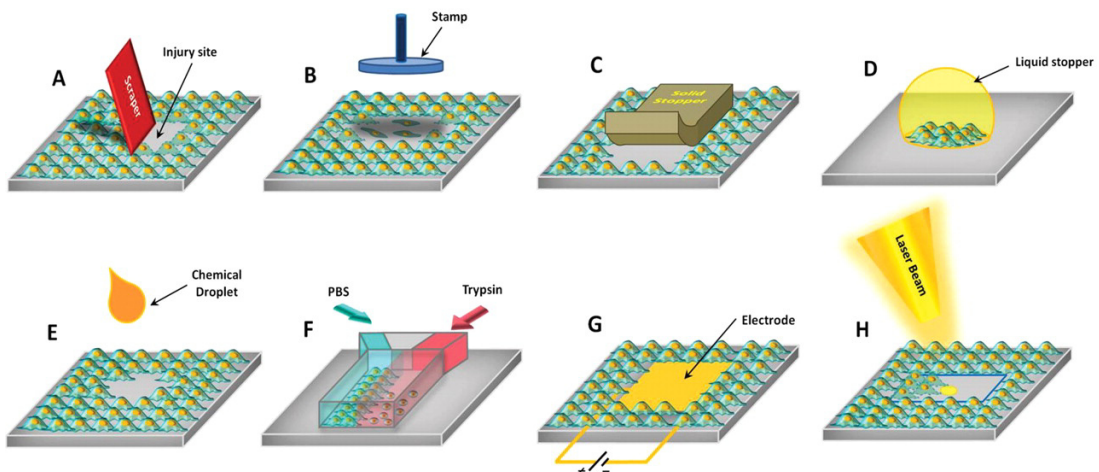


Figure 1.14: WH assays based on (A) scratching, (B) stamping, (C) solid barrier, (D) liquid barrier, (E) droplet chemical assay, (F) microfluidic chemical assay, (G) electrical assay, and (H) laser ablation [177].

The most common method for investigating cell dynamics by wound healing experiments is the mechanical approach because of its simplicity and cost-effectiveness. In a mechanical wounding assay, cells are disrupted physically. Mechanical wounding assays can be categorized into mechanical scratching and stamping assays. In a typical scratch assay, the cells are allowed to grow until they reach 100% confluence, and a mechanical wound is then created by physical scraping (Figure 1.14.A) with a pipette tip, needle, bladder, razor, rubber policeman, cotton bud, or Teflon spatula [184, 185]. The scratch assay can be achieved by using a robotic system, in order to standardize the process and increase the throughput [186]. To

improve the reproducibility and minimize the surface damage, a drill press assay has also been developed [187]. In this method, a stabilized, rotating, silicone-tipped drill press is used to create uniform circular lesions in an intact cell monolayer. Another reproducible scratching method is the hydrophilic polydimethylsiloxane (PDMS) slab assay [149, 188] in which a short hydrophilic PDMS slab is embedded onto the substrate pre-coated with the material of interest, allowing the cells to grow on top of the substrate as well as the PDMS. After a confluent cell monolayer is formed, the PDMS is removed, wounding reproducibly the cells near the boundary. This method allows to minimize cell debris and surface damage in the free region of the substrate. Mechanical wounding can also be performed using the stamping assay (Figure 1.14.B). In this method, a confluent cell monolayer is punched by a stamp, such as a PDMS mold, to create a reproducible and uniform pattern. Advantages of stamping assays include creation of wounds with arbitrary shapes and study of cell migration in the presence of cell debris. For example, a stamping assay has been reported to study phagocytosis of cell debris in the wound site during wound healing [189]. Another stamping assay for studying cell regeneration is the stamp-sliding assay [190], in which the cell monolayer is stamped by a Neoprene pattern under pressure control, followed by rotary or lateral movement of the stamp to create desired uniform cell patterns, such as circles and islands.

The cell monolayer can also be wounded using physical methods, in which a physical barrier is applied prior to cell seeding to block cell attachment; the removal of the physical barrier triggers the wound closure process. The repeatability and standardization of the physical barrier assay are more achievable compared with the scratch assay and ensure a good survival rate. The use of a physical barrier also minimizes cell damage and keeps the cell-free region intact for ECM deposition. The physical barrier assay can include the use of solid barriers, typically composed of biocompatible materials, (Figure 1.14.C) and liquid barriers. One of the early solid barriers for cell migration studies is the Teflon fence [191] in which a Teflon fence is placed in a culture dish, where the cells are plated at high density. After forming a confluent cell monolayer, the wound closure dynamics is studied after the release of the Teflon fence. Other solid stoppers are made of silicone or PDMS with desired shapes. These materials can adhere to smooth surfaces without glue and are able to create multiple wounding sites. In addition, they are biocompatible, ease of use, and show high adhesiveness. The barrier can have a closed or open shape [192]. The open-shape barriers, such as circular rings, consist of inner and outer compartments in which cells can be seated either inside or outside of the barrier [193, 194]. Another physical barrier assay for collective cell migration studies is called “detachable substrate” [195]. This method consists of two complementary parts composed of

PDMS and polystyrene and fabricated by replica molding. After seeding cells and forming a cell monolayer on one substrate, the intact complementary substrate is attached and allows cells to migrate onto the untouched surface for cell migration studies. Liquid stoppers are another barrier assay enrolling liquid or gel barriers in outward cell dynamics studies in which less substrate and cellular damages are required near the boundary (Figure 1.14.D). One of the most popular liquid stoppers is the agarose gel [196], in which the cells are embedded into a droplet of agarose gel. Another method to study cell sheet migration is the oil droplet migration assay, in which an aqueous drop of medium–cell suspension is pipetted into a light mineral oil, and the drop falls on the matrix surface due to the density difference. After a confluent monolayer is formed, cells are released from the liquid stopper by aspirating the oil out of the dish. To study cell migration on the various surface coatings without cellular damage, a multichannel migration device, which takes advantage of surface tension, can also serve as a liquid stopper in microchannels [183].

Alternatively, wounding can be achieved by using chemical method (Figure 1.14.E), in which a droplet of sodium hydroxide is pipetted onto the cell monolayer to selectively remove cells in contact with the droplet [197]. The size of the wound is controlled by the volume of the chemical applied. The chemical wounding method can also be implemented using microfluidics in order to selectively remove cells in a microchannel in an enzymatical way [144, 198]. The flow in a microchannel is generally laminar due to the low Reynolds number of fluid flows in the microscale (Figure 1.14.F) [198].

Wound healing assays can also be accomplished electrically. Electrical wounding methods (Figure 1.14.G) are based on the electrical cell–substrate impedance sensing (ECSI) technique [199], which allows to create wounds with different geometries. The electrical wound healing device is typically composed of a small gold film electrodes on which the cells are grown and a much larger counter electrode [200]. By applying a relatively large voltage between the electrodes, the cells of the monolayer are electropermeabilized permanently with subsequent death of the cells in a defined area. This enables to generate a wound in the cell monolayer on the surface of the electrode. The movement of the cells which repopulate the empty space can be characterized by measuring the electric variation of impedance of the cell monolayer on the cell–adhesion electrode [201].

Wounding of cell monolayers can also be performed using optical methods [202]. A laser can mediate photothermal, photochemical, and photomechanical effects on the cells determining

the removal of the cells from a defined area of the confluent cell monolayer (Figure 1.14.H) [203]. This method allows to create repeatable wounds or wounds with arbitrary shapes.

4. Aim of the work

Although the framework of cell dynamics has gained impetus in recent years, the current understanding of many mechanisms is still limited and cell dynamic behavior remains a challenging process to study under physiopathologically-relevant conditions *in vitro*.

This work is addressed to:

- investigate *in vitro* the dynamic evolution of cells, from single to collective cell dynamic behavior, by using an experimental approach based on direct visualization (time-lapse microscopy) of cell samples and image analysis techniques, in order to reach a better understanding of many physiological and pathological processes;
- compare several methodologies widely used in the literature to investigate cell dynamics *in vitro*;
- model the mechanisms governing single and collective cell dynamic evolution, i.e., migration and proliferation, by using mathematical equations based on the transport phenomena approach.

The main goal of this project is to improve the current understanding of the mechanisms governing cell dynamics by using an interdisciplinary approach, based on chemical engineering core disciplines combined with biological, biotechnological and biomedical sciences. A rigorous investigation, based on the application of transport phenomena concepts, is essential to measure cell movement and proliferation indices that describe cell dynamics in precise quantitative way. For this reason, the development of such analyses is nowadays within the core business of Chemical Engineering [18], which can contribute to the building of mathematical models, based on the transport phenomena approach, useful to describe and predict the mechanisms driving cell dynamics [19].

Chapter 2

Investigation of Cell Dynamics *in vitro* by Time Lapse Microscopy and Image Analysis

Abstract

Pharmacological research is continuously working on the development of new drugs. This research typically starts from the formulation of new molecules that are first investigated at the cell scale, finally is completed with clinical trials. Investigation on the cell scale requires simple, reproducible and reliable assays, able to simulate physiological conditions in the lab. A wide range of biological processes, such as angiogenesis, inflammation, tissue regeneration, tumour growth and invasion, are strongly linked to cell proliferation and migration mechanisms that govern the dynamic evolution of both individual cells and cell aggregates. In this work we present an experimental methodology for the quantitative investigation of cell dynamics *in vitro* by live imaging of biological soft matter. Cell motility is observed by means of a Time Lapse Microscopy workstation, consisting of a motorized video-microscope equipped with an incubating system, and quantified by image analysis techniques. We report some preliminary experimental results relative to the migration of a tumour cell line both in random condition and in presence of an external stimulus, such as a chemical concentration gradient. The ultimate goal of this research is the development of a standard assay to be used as a test for drug efficiency, suitable for routine application in the pharmaceutical research.

1. Introduction

The pharmacological industry is strongly addressed to discovering and testing of novel therapeutic drugs for the treatment of a wide range of diseases, including cancer, inflammations and cardio-vascular dysfunctions. In particular, the identification of novel chemotherapeutic molecules is a topic of growing interest, because of the limitations of the therapy approaches to the treatment of cancer, due to tumour invasion and metastasis formation.

The research process of novel drugs is complex, time-consuming, and expensive. A wide variety of *in vitro* assays are used to identify novel therapeutic molecules and assesses their

efficiency on the industrial scale. Among these, the Boyden chamber assay [204] is widely used to investigate cell motility and invasion capacity, due to its simplicity. However, it presents a number of limitations; it does not allow cell dynamics to be monitored as a function of time and does not provide well defined concentration gradients of the drug under evaluation.

The detection of novel drugs and the evaluation of their activity require the development of a standard assay aimed at the investigation of single cells and cell tissue dynamics in response to drug treatment, while mimicking physiological condition on the lab scale. An ideal assay should be economic, relatively simple to set up with significant reproducibility and reliability, and useful for high-throughput screening.

A large number of physiological and pathological processes, including embryonic development, immune response, inflammation and tumour metastasis, are intimately related to the dynamic evolution of individual cells and cell clusters [61]. Cell migration, proliferation and aggregation mechanisms, driven by mechanical and chemotactic cues [13], play also key roles in the growth of healthy as well as pathological tissues.

The above mentioned mechanisms of cell dynamic evolution can be described by using mathematical models based on transport phenomena concepts [205]. It is possible to describe cell motility in terms of a motility coefficient, analogue of the Fickian diffusion coefficient, while cell proliferation can be described by models of logistic growth [136]. The fusion of two contiguous cell aggregates may be described in terms of an effective interfacial tension that promotes the formation of clusters with minimum external surface. An interesting approach of this phenomenon can be hence based on the analogy with the case of drops of fluid surrounded by an immiscible matrix [206], that deform, break-up [207], retract to the spherical unperturbed shape, coalesce, or form complex structures [208].

A detailed analysis of the mechanisms leading cell dynamics requires a rigorous approach, based on the measurement of quantitative cell movement indices. Cell dynamics can be efficiently investigated experimentally *in vitro* by using live cell imaging by Time Lapse Microscopy (TLM), that allows the direct visualization of biological systems during their dynamic evolution [93]. This microscopy technique is based on automated sample repositioning by motorized x-y stage and focus control and iterative image acquisition of selected fields of view while controlling the environmental parameter to ensure cell viability throughout the experiment, which can last up to a few weeks. The application of image analysis techniques allows the reconstruction of cell trajectories and the calculation of the

relevant cell migration parameters [175], or the quantification of the growth dynamic of tissues [173].

TLM is coupled to a large variety of *in vitro* assays, ranging from single cell random motility assays to chemotaxis assays, that allow a quantitative characterization of cell dynamics [133]. In single cell random motility assays, the cells are plated at low density, in order to reconstruct cell trajectories in 2-D or 3-D substrata. The trajectories are further analyzed according to mathematical model, such as the persistent random walk model [100], in order to measure motility parameters, i.e. cell velocity, the persistence time between significant changes in the direction of motion, and the cell motility coefficient, that is an analogous of the random walk diffusivity.

Chemotaxis assays allow to quantitatively analyze the directional cell response to chemical gradients. The investigation of chemotaxis *in vitro* presents several challenging experimental difficulties, mainly due to the problem of creating a stable gradient on a time scale long enough to elicit a significant cell migration response [132]. Chemotactic movement of the cells can be described in terms of a directionality index, defined as the ratio between the net movement in the direction of the gradient and the total curvilinear length of cell trajectories [129].

In this work, we propose an experimental methodology for the quantitative investigation of cell dynamics *in vitro* by live imaging of biological soft matter. Cell motility was observed by means of time lapse imaging and quantified by image analysis techniques. We report some preliminary experimental results relative to a case study aimed at the investigation of tumour invasion. In particular, we performed 2D single cell migration assays in order to quantitatively investigate the dynamic behavior of two populations of tumour cells, i.e. HT1080 NG2- and HT1080 NG2+ fibroblasts. The latter are characterized by high expression of the NG2 transmembrane proteoglycan. It is thought to be involved in tumour progression (Cattaruzza et al., 2013) because it accentuates growth responses, mediates the tumour cell-host microenvironment interaction and promotes neoangiogenesis [209].

In order to investigate the chemotactic response of the cells to several molecules, we applied a novel chemotaxis assay in 3-D collagen gels based on a direct-viewing chamber [129, 132] that is reusable, and can be coupled to a Time Lapse Microscopy and image analysis workstation. In the chamber a chemoattractant concentration gradient in the collagen gel sample seeded with cells is generated by diffusion through a porous membrane. We analyzed the migration of HT1080 tumour fibroblasts under a concentration gradient of FGF2 growth factor, that is known to be implicated in the progression of human cancer [210].

2. Materials and methods

2.1. Cell culture

HT1080 is a cell line of fibrosarcoma from connective tissue. This cell line presents good cell motility and a significant morphological polarization. HT1080 fibroblasts and two subpopulations of this cell line (HT1080 NG2+ and NG2-) were cultured in Dulbecco's Modified Eagle Medium (DMEM) supplemented with 10 % (v/v) Fetal Bovine Serum (FBS), sodium pyruvate 1 % and antibiotics (50 units/mL penicillin and 50 µg/mL streptomycin) and maintained in a humidified incubator at 37 °C under an atmosphere of 5 % CO₂ in air.

2.2. Chemotaxis chamber

Chemotaxis assays were performed by using a chamber [129] consisting of a single aluminium block glued on top of a microscope slide by using a silicone adhesive. A porous membrane (0.22 µm pores), sandwiched between two rectangular metal frames, separates two compartments, one for the cell seeded collagen gel (sample well), and the other as a reservoir of the chemoattractant solution (chemoattractant reservoir). During the experiment the chemoattractant, loaded in the reservoir, diffuses through the membrane, and thereby generates a concentration gradient in the cell seeded collagen gel. In Figure 2.1, a 3D rendering shows the chamber in an assembled view, where the membrane supporting frames are housed in the chamber.

During the experiment the chemoattractant, loaded in the reservoir, diffuses through the membrane, thereby generates a concentration gradient in the cell seeded collagen gel. The chemoattractant concentration profile in the collagen gel can be described according to the model of Fickian diffusion in a semi-infinite slab [132]:

$$C(x,t) = \frac{C_0}{2} \left[1 - \operatorname{erf} \left(\frac{y}{\sqrt{4Dt}} \right) \right] \quad (1)$$

where $C(x,t)$ is the chemoattractant concentration as function of the space x and time t , C_0 is the initial concentration in the chemoattractant reservoir, D is the diffusion coefficient of the molecule in the gel.

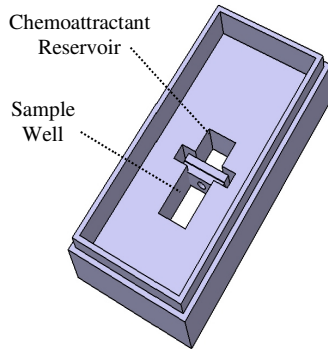


Figure 2.1: View rendering of the chemotaxis chamber.

2.3. Time Lapse Microscopy workstation

Time Lapse Microscopy experiments were performed using an automated workstation based on an inverted optical microscope with a long working distance 10x objective in phase contrast. A scheme of the workstation is reported in Figure 2.2. The microscope, placed on an anti-vibrating table, is equipped with motorized stage and focus, that allow to automatically position the field of view within the sample under observation. In order to mimic environmental conditions, the microscope is enclosed in a homemade incubator that keeps the sample temperature at 37 ± 0.1 °C in a saturate moisture atmosphere with 5 % CO₂. Images are acquired using a high-resolution high-sensitivity monochromatic CCD video camera. The whole workstation is driven by homemade control software in Labview. Images were stored on hard drive for off line analysis.

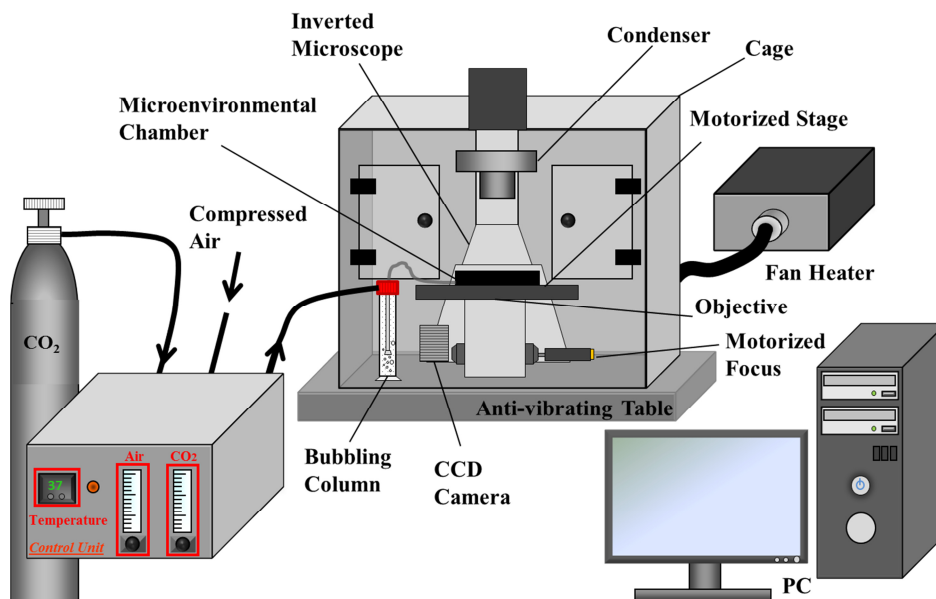


Figure 2.2: Scheme of the Time Lapse Microscopy workstation.

2.4. Experimental methods

In 2D random motility experiments, HT1080 NG2+ and NG2- fibroblasts were plated on an uncoated twelve-well culture dish at a density of 9×10^4 cells per well and allowed to attach overnight, incubating under standard conditions at 37 °C in a 5 % CO₂/Air atmosphere before starting the experiments.

Collagen gel was prepared with the following composition (volume basis): DMEM medium, 0.1 M NaOH (5 %), 10x MEM medium (5 %), FBS (0.5 %), antibiotics (50 units/mL penicillin and 50 µg/mL streptomycin) (1 %) and collagen solution (2 mg/mL). All components were kept on ice during the preparation, except for the cell suspension that was added at the end. The solution was placed in the sample well of the chamber. The chamber was then incubated at 37 °C and 5 % CO₂ for 20 min to induce collagen polymerization.

2.5. Image analysis

Image analysis of random motility assays and chemotaxis experiments was performed using a semi-automated Cell Tracking software. For each time step, all the cells were individually followed to determine cell contour and the coordinates of the center of mass. The trajectory of each cell was reconstructed for the whole experiment starting from the center of mass coordinates. Furthermore, average motility parameters of the cell population were calculated as a function of time using a Matlab script.

3. Results and discussion

We performed 2D single cell migration assays, in order to quantitatively investigate the dynamic behavior of two populations of cancer cells, i.e. HT1080 NG2- and HT1080 NG2+ fibroblasts.

A detailed analysis of the motility of the two fibroblast populations on a planar surface is reported in the following. In Figure 2.3.A and 2.3.B we report the trajectories described by HT1080 NG2- and HT1080 NG2+ fibroblasts respectively; cell paths are plotted starting from the same initial position. In both fibroblast populations, the trajectories showed a random orientation being uniformly distributed on the XY plane (i.e., no preferential direction in cell motion can be distinguished). However, more extended trajectories were detected in NG2+ compared to NG2- fibroblasts.

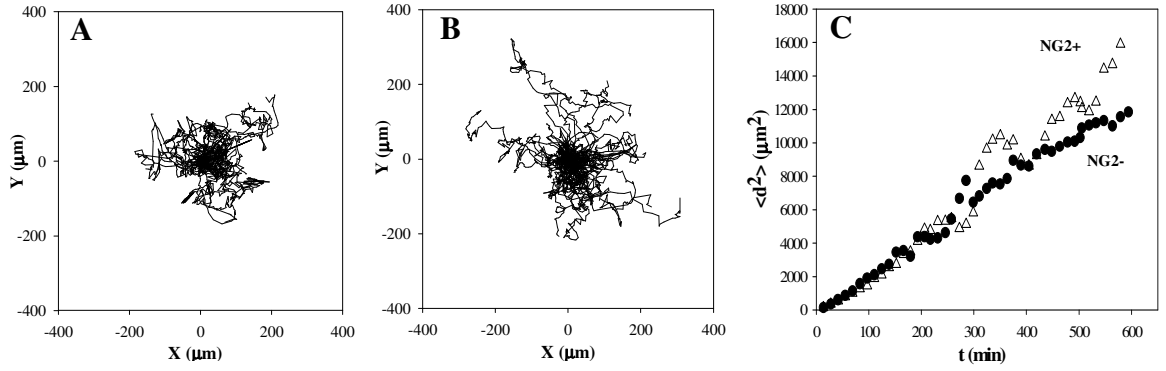


Figure 2.3: Fibroblast trajectory analysis and mean square displacements. A direct analysis of cell trajectories is used to characterize the motion of NG2- (A) and NG2+ fibroblasts (B). To quantitatively assess cell movement, the mean square displacements are calculated (C).

Cell motility was quantified by measuring quantitative motility indices, according to the persistent random walk theory [100], where it is assumed that cell motion is characterized by a diffusion coefficient (also referred to as the random motility coefficient) μ ($\mu\text{m}^2/\text{min}$) and a persistence time P (min), that is, the characteristic time in which cell movement persists in the same direction. The value of μ is related both to the average speed of the cells and to the persistence time. According to the theory, the mean square displacements are given by the equation Eq. (2.3):

$$\langle d^2(t) \rangle = 4\mu \left[t - P \left(1 - e^{-t/P} \right) \right] \quad (2.3)$$

where $\langle d^2(t) \rangle$ (μm^2) is the mean squared displacement of the tracked cell sample at time t . The trend predicted by Eq. (2.3) is linear for $t \gg P$, with a slope proportional to the diffusion coefficient (i.e., $\langle d^2(t) \rangle \approx 4\mu t$). The squared displacement was measured for every interval by calculating the Euclidean distance between the two positions occupied by the cell at the beginning and at the end of the interval. The mean squared displacements $\langle d^2(t) \rangle$ (μm^2) were then calculated as an average over the number of measurements done for each cell over the entire trajectory, and then over the entire cell population. In Figure 2.3.C we report the mean squared displacements as a function of time, for HT1080 NG2- and NG2+ fibroblasts. Eq. (2.3) was fit to the experimental data of mean squared displacements as a function of time, with μ and P as the only adjustable parameters. The velocity of the cells V was also calculated

as the ratio between the curvilinear trajectory described and the elapsed time, averaged over the entire cell population.

The statistical significance of the results was verified by repeating the analysis on another identical cell population, for each sample.

In Table 2.1 we report the estimate of the motility parameters (μ , P and V) for the two fibroblast populations; the standard deviation is reported as uncertainty.

Cell sample	μ ($\mu\text{m}^2/\text{min}$)	P (min)	V ($\mu\text{m}/\text{min}$)
HT1080 NG2-	5.50 \pm 0.15	32.19 \pm 0.10	0.59 \pm 0.01
HT1080 NG2+	7.11 \pm 0.31	39.58 \pm 1.85	0.61 \pm 0.03

Table 2.1: Motility parameters for HT1080 NG2+ and HT1080 NG2- fibroblasts.

HT1080 NG2+ fibroblasts show higher motility compared to NG2- fibroblasts, as evident by the higher value of all the parameters examined, especially the random diffusion coefficient μ and the persistence time P.

Our preliminary results support the hypothesis that the NG2 proteoglycan is involved in the regulation of cell motility. Further experimental investigation is in progress to confirm this result.

We also analyzed the chemotactic response of HT1080 cancer fibroblasts under a concentration gradient of FGF2. This growth factor is known to be implicated in the progression of human cancer.

The directionality of cell movement during chemotaxis assays was quantified by defining a directionality index I, that is the ratio between the net movement in the direction of the gradient and the total curvilinear length of the cell trajectory. It ranges from +1 (trajectory fully oriented towards the source of chemoattractant) to -1 (negative chemotaxis). I = 0 corresponds to a random motion where no preferential direction is observed.

In Figure 2.4.A we report the quantitative measure of the y component of the chemotaxis index (I_y), i.e., the ratio between the net displacement in the direction (y) of the gradient and the total curvilinear trajectory of the cells, as a function of time. I_y fluctuates around 0, meaning that the fibroblasts seem to move in a random fashion. The average cell velocity on the other hand shows a progressive increases in the first 7 hours, as shown in Figure 2.4.B.

This result suggests a chemokinetic, rather than chemotactic, effect of FGF2 growth factor on HT1080 fibroblasts.

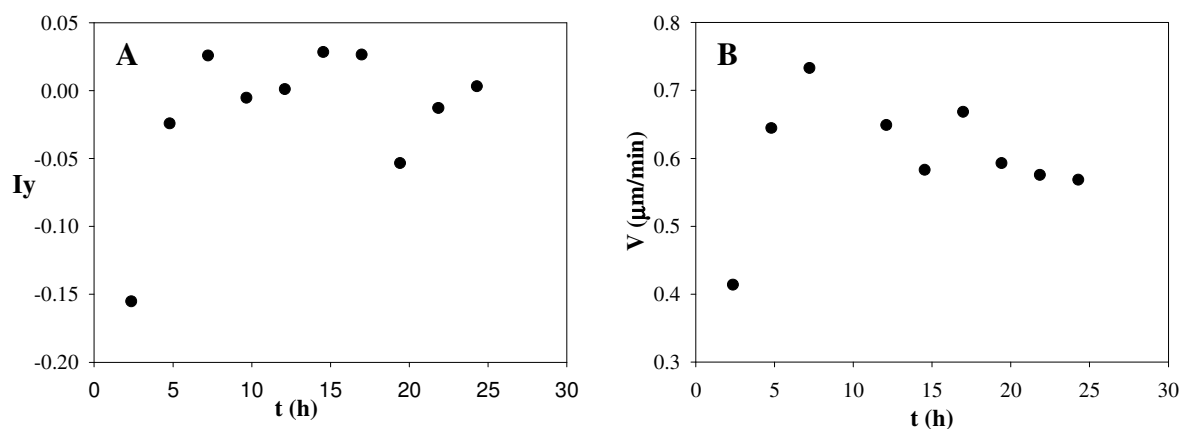


Figure 2.4: Analysis of motility for HT1080 fibroblasts under FGF2 chemotactic gradient: the y component of the chemotactic index (A) and average cell velocity modulus (B) as a function of time.

4. Conclusions

The development of physiologically relevant *in vitro* assays to identify novel therapeutic molecules and test drug efficiency is a topic of growing interest in the pharmaceutical industry, mostly due to the wide application in the treatment of cancer.

Due to the complexity of the cell response, a detailed quantitative assay requires an interdisciplinary approach based on chemical engineering core disciplines combined with biological and biomedical sciences [205]. A rigorous investigation, based on the application of transport phenomena concepts, is essential to measure cell movement indices that describe the dynamic response of cells to drug treatments.

In this work we present an experimental methodology to investigate the dynamics of biological soft matter in a quantitative way, while mimicking physiological condition on the lab scale. In particular, we used Time Lapse Microscopy in order to analyze the motility of a tumour cell line both in random condition and in presence of an external stimulus, such as a chemical concentration gradient. We applied a novel methodology for the experimental investigation of drug efficiency *in vitro* by time-lapse live cell imaging of cell movement under a controlled gradient of a soluble molecule. In this assay, a concentration gradient in a collagen gel sample seeded with cells was generated by diffusion through a porous membrane. Preliminary results are reported to validate the technique.

The aim of this work is the development of a standard assay to be used as a test for drug efficiency. The technique proposed provides highly reproducible results [129, 132] and is promising for routine application in the pharmaceutical industry.

Chapter 3

Comparison between fibroblast wound healing and cell random migration assays *in vitro*

Abstract

Cell proliferation and migration play a key role in many biological mechanisms involved in the dynamic evolution of individual cells or tissues, including cancer growth and invasion, embryogenesis, angiogenesis, inflammatory response, and tissue repair. In this work, we compare two established experimental approaches for the investigation of cell motility *in vitro*: the cell random migration (CRM) and the wound healing (WH) assay. In the former, extensive tracking of live cells in time-lapse microscopy images and elaborate data processing are used to calculate two intrinsic motility parameters of the cell population under investigation, i.e., the diffusion coefficient and the persistence time. In the WH assay, a wound is made in a confluent cell monolayer and the temporal reduction of wound area is taken as an empirical measure of cell migration ability, provided that cell proliferation is accounted for. To compare WH and CRM we applied the two assays to investigate the motility of skin fibroblasts isolated from wild type and transgenic mice for PED/PEA-15 (TgPED), a protein known to be overexpressed in patients with type 2 diabetes. Overall, we found a substantial agreement between independent measurements of cell migration based on the two techniques, both of which showed a slower migration ability of TgPED cells. In particular, our results highlight that the cell motility parameters derived from CRM analysis can be also estimated from a WH assay, thus suggesting it as an easier and faster approach for the quantitative characterization of cell migration. To our knowledge this is the first, quantitative comparison of these two widely used techniques.

1. Introduction

The dynamic evolution of cells, governed by proliferation and migration mechanisms [1], plays a key role in a wide range of physiological as well as pathological processes, including morphogenesis, immune responses, angiogenesis, tissue repair and tumour progression [92,

211]. Nevertheless the complex mechanisms governing cell dynamic behavior are still far from full comprehension [16, 17]. A detailed analysis of these processes requires a rigorous approach to quantitatively measure well-defined cell movement and proliferation indices. The wound healing (WH), or scratch assay, and the cell random motility (CRM) assay are among the most commonly used methods to investigate cell dynamic behavior [96, 133].

Specifically, WH assay is a well-known, low-cost, and relatively easy assay which is widely used for the characterization and quantification of cell migration *in vitro* [134]. In this assay, an artificial scratch is created mechanically on confluent cell monolayers by scraping off an area of cells [135]; In alternative, more recent versions are based on removable inserts that limit the area initially covered by cells [212]. In response to the injury, the cells on the edges of the newly created gap proliferate and move toward the center of the denuded area until the wound is closed [136]. The time required for wound closure is taken as a measure of the migration ability of the cell population under investigation, although the results can be influenced by cell proliferation as well [79].

The WH kinetics can be also assessed by monitoring wound area as a function of time [200], which is best carried out by using a time-lapse microscopy (TLM) workstation [213]. By TLM, sample images at given positions can be iteratively acquired with a defined frequency over periods of time ranging from few minutes to several days [93]. Such possibility of regularly observing over time exactly the same area of the sample, i.e., the same wound region (rather than comparing randomly taken images), enables stable and consistent measurement of the reduction of wound area over time. To maintain cell viability during TLM experiments, video microscopes can be equipped with an incubator to control environmental conditions [94, 173, 214].

In all these experiments, the WH process is usually investigated in a “macroscopic” sense, i.e., on the scale of the entire wound. At the cell level, two main modes of wound healing have been identified [2, 133, 135, 140]. The first mode is typical of cell lines of epithelial or endothelial origin, which are able to create cellular sheets or monolayers at confluence. Once a wound is made by scratching the monolayer, the cells on either side tend to maintain close contacts and continuity with each other while moving forward in a collective mode as a coherent cluster, whose mechanical integrity is ensured by cell-cell interactions [79, 141, 215]. The triggering event for the induction of cell sheet movement is the availability of empty space [148] rather than the injury itself, which is not strictly necessary [79], although in absence of an external damage the migration appears predominant in the cells at the leading edges [144] and attenuated in the rear or sub marginal cells in terms of speed and cell path

persistence [142]. In other words, the loss of spatial constraints itself in the monolayer stimulates cell migration [79, 142, 144] and proliferation [143, 145], thus enabling the wound closure, but in the presence of an external damage, sub-marginal cells following the ones at the leading edge have a stronger contribution to the movement of the cell sheets and therefore to the wound closure.

The second wound healing mechanism, more relevant to this article, is a typical feature of fibroblast-like cells, which migrate toward the wound area primarily as individual cells [140], rather than as cohorts [146]. Also in this case, the availability of free space upon the scratch is the initiating event for the induction of cell movement. Overall, the cells can move with the same probability in any direction, due to the lack of strong cell-cell interactions. In addition, cell proliferation may also contribute to wound closure [139], as it increases in response to the “sensation of free space” after wounding [134].

The different mechanisms underlying the two above described WH modes are not clearly distinguished in the output of the test, which is just wound closure as a function of time. So, the WH assay, though simple and straightforward, provides limited information at the single cell level [187]. In addition, the question arises whether WH can provide an intrinsic measure of cell motility due to a possible dependence of the results on the manual operation of the assay (e.g., in terms of size and extent of the wound) [177]. On the contrary, the cell random motility (CRM) assay, which is another well-established method to characterize cell migration [93], is based on the observation of individual cell motion and provides intrinsic parameters of cell motility. In the CRM assay, cells are plated out at a low density on the surface of a culture well, and cell position is tracked as a function of time. The cell trajectories are then reconstructed either manually or automatically by a cell matching algorithm which allows a quantitative determination of cell motion parameters, including cell total travel length, net displacement and velocity [59]. Cell random motility can be also described by a persistent random walk model [98-100], which is based on two fitting parameters: the persistence time between significant directional changes and the cell motility coefficient (analogous to molecular diffusivity).

Major advantages of the CRM assay are that it provides insight into the dynamical behavior of individual cells, and allows the tracking of cell motion in two but also in three-dimensional substrata, where the cells are embedded in an extracellular matrix (e.g., a collagen gel). In addition, the assay can be used to study directional migration in anisotropic substrata where cell movement is biased towards a concentration gradient of a soluble or substrate-bound factor (e.g. chemotaxis and haptotaxis) [132]. All these features (single cell level of the

investigation, 3D migration and directional migration) are not supported by the WH assay and necessitate a more laborious assay. In fact, quantitative analysis of single cell migration requires the tracking of large number of cells for extended periods of time in order to obtain statistically robust results [96]. Moreover, the large amount of tracking data needs to be further processed to extract model parameters representative of the entire cell population. From this perspective, the CRM assay is more laborious and time-consuming compared to the WH assay. The CRM assay should be considered as a gold standard to investigate cell migration, because it allows a comprehensive and multi-scale analysis of cell motility at the level of both the entire population and the individual cells.

Although the abovementioned experimental techniques are valuable in assessing cell motility parameters, a quantitative comparison between the WH and CRM assays is however lacking in the literature. In this work, we aim to compare the motility behavior of two different fibroblast-like cell populations obtained by WH and CRM tests simultaneously carried out in the same experiment. The results provided by the two assays are quantitatively analyzed to assess whether they yield comparable information on cell motility. The comparison between the two assays is based on the persistent random walk model combined with a solution of the diffusion equation for cell density including cell proliferation [154].

As a case study to illustrate the comparison between the two assays, we used two cultured primary fibroblast populations, with known differences in migratory ability [175], isolated from wild-type (Wt) control mice and genetically modified TgPED mice, overexpressing the protein PED/PEA-15, which is highly expressed in several tissues and cell types, including fibroblasts, from type 2 diabetic patients [216, 217]. Transgenic mice overexpressing PED/PEA-15 (TgPED) have also been shown to display glucose tolerance abnormalities [218], accompanied by wound healing defects typical of diabetes mellitus [175].

It was previously reported [175] that fibroblasts isolated from TgPED mice showed a significant reduction in the migratory ability compared to Wt fibroblasts. It was also observed that cytoplasmic spreading was significantly reduced in TgPED fibroblasts; this was paralleled by a decreased cellular content of focal adhesion plaques and actin stress fibers.

We performed WH experiments on both, Wt and TgPED fibroblasts. We did not limit our investigation at the cell population level, i.e. measuring the wound closure kinetics, but we also applied the tracking method, typically used for CRM assay, to quantify the movement of the cells during the wound closure process, and we further investigated the directionality of cell motions. We finally estimated migration parameters by CRM assay as well on the two

cell populations. These independent quantifications of cell motility parameters based on either cell population dynamic analysis or individual cell behavior are here compared and discussed.

2. Materials and Methods

2.1. Cell cultures

Skin fibroblasts were obtained by punch biopsy from TgPED and Wt mice that were generated and characterized as described previously [218]. Mice were housed in the animal facilities in a temperature-controlled (22°C) room with a 12 h light/dark cycle and were killed by cervical dislocation.

Cultures were established and grown at 37°C in Dulbecco's Modified Eagle Medium (Lonza, Switzerland) supplemented with 10% fetal calf serum (Lonza, Switzerland) in a 5% CO₂-95% air humidified atmosphere, as described elsewhere [175]. Cultures between passages 8 and 15 were used in this study. For all experiments, cells were maintained in culture for an equal number of generations.

The duplication time of both TgPED and Wt fibroblasts was measured to be about 16 h, no significant differences was observed between the two populations, as also proved by thymidine incorporation experiments [175].

2.2. Time-lapse microscopy

Time-lapse microscopy experiments were performed using an automated workstation with an inverted microscope (Zeiss Axiovert 200; Carl Zeiss, Jena, Germany) and a long working distance 10× objective in phase contrast (CP Achromat Ph1). The microscope was equipped with a motorized stage and a motorized focus (Prior, Cambridge, UK) for automated sample positioning and was enclosed in a homemade incubator consisting of a plexiglass cage kept at 37°C ± 0.1°C by warm air flux from a heater tuned by a PID controller. To surround samples with a controlled atmosphere and prevent water evaporation and pH changes in cell culture medium, air premixed with 5% CO₂ was blown through a bubbling column for humidity saturation and fed to a microenvironmental chamber placed on the stage. Live-cell imaging was performed using a high-resolution, high-sensitivity monochromatic CCD video camera (Orca AG; Hamamatsu, Japan). The whole workstation was driven by homemade control software in LabView. The image acquisition frequency was set to 10 min, and the overall experimental duration was 24 h. Images were stored on a hard drive for subsequent offline analysis.

2.3. Experimental methods

In this study, two different types of experiments, CRM and WH, were carried out to investigate cell behavior.

In CRM experiments, Wt and TgPED fibroblasts plated on uncoated 6-well culture dishes at a density of 2×10^5 cells/well were allowed to attach overnight and incubated under standard conditions at 37°C in a 5% CO₂/air atmosphere prior to experiments. Figure 3.1.A shows a typical image of random migration experiments.

To perform WH assays, Wt and TgPED fibroblasts plated on uncoated 6-well culture dishes at a density of 5×10^5 cells/well were incubated until 100% confluence. Cell monolayers were wounded manually by scratching with a p200 pipette tip, and in each well, cells in an area with a width ranging between 380 and 580 μm were removed. Fibroblasts were then washed twice with phosphate-buffered saline (PBS) to remove cellular debris. Prior to experiments, culture medium was replaced with fresh medium. Figure 3.1.B shows a typical image of WH experiments.

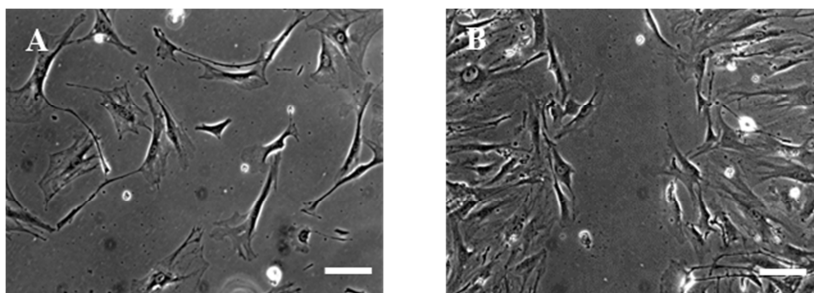


Figure 3.1: Typical images acquired during CRM experiments (A) and WH experiments (B). Scale bar = 100 μm .

2.4. Image analysis

At each time point, individual cells were identified by means of a semi-automated image analysis macro based on standard software libraries (Image Pro Plus). The cell contour, orientation, and coordinates of the centroid (center of mass) were determined and stored. The centroid coordinates were used to reconstruct the trajectory of each cell throughout the experiment.

In WH assays, the cell-free area representing the wound was measured by segmenting images for each time point by an homemade automated image analysis software.

2.5. Data analysis

To estimate cell motility parameters, cell position arrays were processed by a Matlab script.

Average values of cell population parameters, such as velocity and orientation angles of the cell major axis, were calculated as a function of time. For each cell trajectory, several non-overlapping intervals [100, 219] of size t were identified, and squared displacement was measured for every interval by calculating the Euclidean distance between two positions occupied by the cell at the beginning and the end of the interval. The mean squared displacement relative to an interval of size t , $\langle d^2(t) \rangle$ (μm^2), was then calculated as the average of all the measurements taken for each cell over its entire trajectory, and then further averaged over the entire cell population. The calculation was iterated for different values of t , the smallest size of the investigated time intervals corresponding to the delay time between consecutive TLM image acquisitions, the largest size corresponding to the entire experiment length. It is worth mentioning that low values of t correspond to higher numbers of independent measurements, whereas approaching the maximum available value of t , i.e. the entire experiment length, it is possible to average only few measurements. For this reason low values of t are associated with higher statistical significance. The analysis of cell motility was based on the persistent random walk theory [99, 220], where it is assumed that cell motion is characterized by a diffusion coefficient (also referred to as the random motility coefficient) D ($\mu\text{m}^2/\text{min}$) and a persistence time P (min), the characteristic time during which cell movement persists in the same direction. The value of D is a quantitative measurement of cell migration and is related to both the average speed of cells and the persistence time. According to the theory [100], the mean squared displacements are given by the following equation (Eq. (3.1)):

$$\langle d^2(t) \rangle = 4D[t - P(1 - e^{-t/P})] \quad (3.1)$$

The trend predicted by Eq. (3.1) is linear at $t \gg P$ (i.e., $\langle d^2(t) \rangle \approx 4Dt$), with a slope proportional to the diffusion coefficient. Eq. (3.1) was fit to the experimental data of mean squared displacements as a function of time, with D and P as the only adjustable parameters.

Cell velocity V ($\mu\text{m}/\text{min}$) was also calculated as the ratio between the curvilinear trajectory described and the elapsed time, and it was averaged over the entire cell population. As another parameter of cell movement, the fraction of motile cells was defined as the proportion of cells showing a total trajectory length over the entire experiment length (25 h) greater than about $180 \mu\text{m}$, calculated as 3 times the average cell diameter (about $60 \mu\text{m}$).

2.6. Statistical analysis

To find possible differences in cell velocity between the two fibroblast genotypes analyzed, statistical significance was assessed by the t-test analysis.

The parameters D and P were calculated out of the trajectories measured for 68 TgPED and 78 Wt for CRM assays, and 46 TgPED and 48 Wt fibroblasts for WH assays. This sample size can be considered as statistically relevant [221]; however, in order to estimate the statistical error, the overall number of cells tracked for each sample was divided in two subpopulations, and the calculation repeated twice.

3. Results and Discussion

The effects of PED/PEA-15 on fibroblast motility have been recently described [175]. Here, we confirmed the differences in terms of cell migration between Wt and TgPED fibroblasts by using WH and CRM assays, and used this result to compare the two experimental techniques.

In the WH experiments, the kinetics of wound closure was determined for both the Wt and TgPED fibroblast populations. In Figure 3.2, the wound area (A), as measured by image analysis at each time point and normalized to the initial value (A_0), is shown as a function of time. Each data point in Figure 3.2 represents the average of three measurements taken from three different positions of the same well, standard deviation is reported as error bar. For each data set, a linear fit is also plotted, whose slope can be considered a quantitative measurement of the wound closure velocity. These velocities were 0.021 h^{-1} and 0.015 h^{-1} for Wt and TgPED fibroblasts, respectively, meaning that TgPED was 1.4 times slower than Wt. The images shown in the lower panel of Figure 3.2 correspond to the data points A, B, and C, respectively, and represent one of the three fields of view analyzed for the Wt sample. The top row corresponds to the raw images, while the bottom row shows the result of image processing with the cell-free area highlighted in black.

According to the Fisher's model [150], the wound healing process depends on both cell proliferation and motility [136]. In our case study, the contribution of the proliferation mechanism to the wound healing process can be considered identical for Wt and TgPED fibroblasts. In fact, no difference between the two cell populations was detected in terms of proliferation rate in thymidine incorporation experiments, as reported in previous work [175]. The motility of the two fibroblast populations was analyzed in details, in order to compare the different samples. Figure 3.3 shows cell trajectories, as determined by image analysis of CRM experiments, in random, non-confluent conditions. The paths of 68 TgPED and 78 Wt fibroblasts are plotted starting from the same initial position in Figure 3.3.A and 3.3.B, respectively. The trajectories are uniformly distributed on the XY plane and show random

orientations, as a consequence of the absence of any preferential direction in cell motion. At a visual inspection of the two charts, the trajectories in the Wt sample appear somewhat more spread out; this observation was later analyzed in detail through the measurement of motility indices, quantitative results are reported in Figure 3.7 and Table 3.1, and are discussed below.

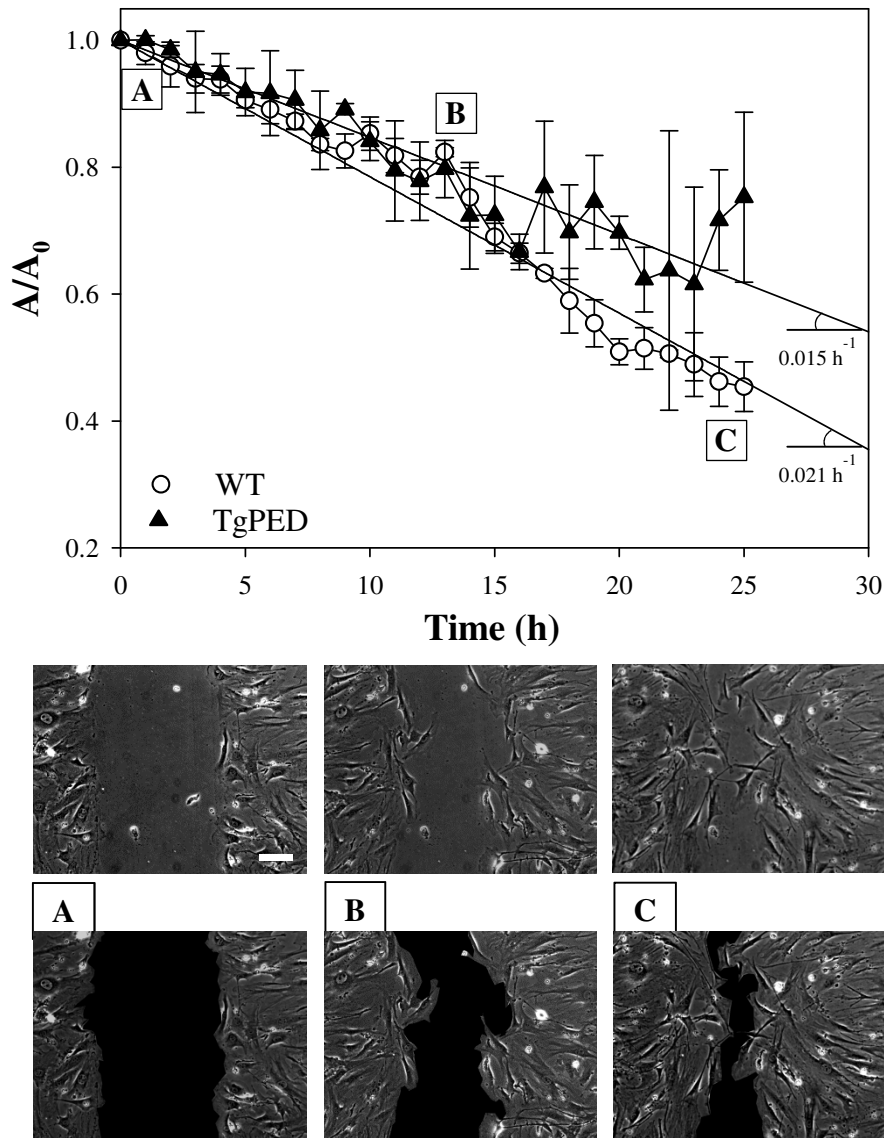


Figure 3.2: Dynamic evolution of wound closure. The wound area A was normalized with respect to the initial value A_0 and plotted as a function of time for the two fibroblast populations (Wt and TgPED). Images of the Wt sample are shown (top and bottom, raw and processed images, respectively), with the wound area shown in black. Scale bar = 100 μm . Error bars represent the standard deviation.

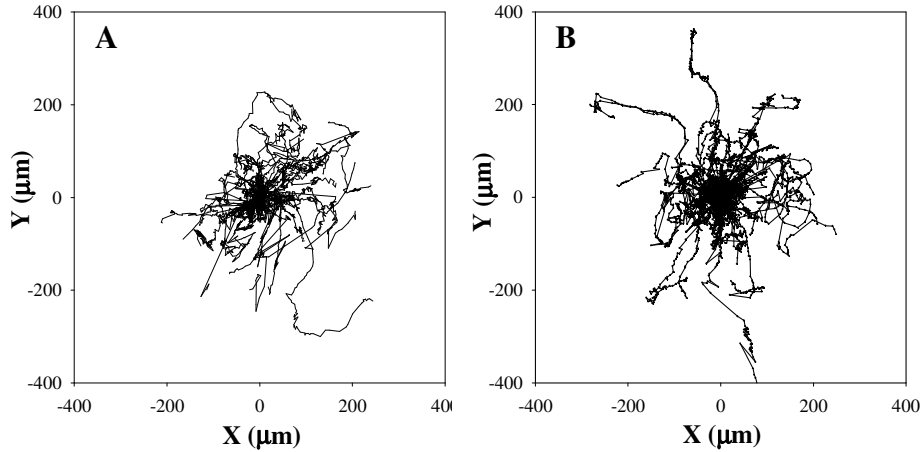


Figure 3.3: Trajectories of 68 TgPED (A) and 78 Wt (B) fibroblasts under random conditions.

We compared cell motion in the WH experiments to cell motility under unstimulated random conditions as in the CRM assays. The comparison was done by applying the tracking method, typically used for the CRM assay, to quantify the movement of the cells invading the cell-free area in the wound closure process. In order to analyze the data in more detail, the trajectories described by 46 TgPED and 48 Wt fibroblasts are reported in Figure 3.4 using a color code: the cells on the right edge of each wound are labeled in red, cells on the left edge are labeled in black, the trajectory in blue is relative to one of the cells on the left edge (see below). Figure 3.4.A and 3.4.B show the trajectories described during the wound closure by TgPED and Wt fibroblasts, respectively, referred to the same initial positions, in analogy to what we reported in Figure 3.3 for CRM assays. The trajectories in Figure 3.4.A and 3.4.B are uniformly distributed in the XY plane, hence the migration of Wt and TgPED fibroblasts toward the wound area can be considered as random. This enables a direct comparison between the results obtained using the CRM and the WH assay. As expected, most of the cell paths were preferentially directed toward the center of the cell-free area to close the wound. Indeed, the trajectories reported in black, corresponding to cells on the left edge of the wound, were oriented toward the right (i.e., positive X abscissa values), whereas the trajectories in red, corresponding to cells on the right edge, showed a preferential orientation toward the left (i.e., negative X abscissa values). Figure 3.4.C and 4.D show the X component of the trajectories as a function of time for the TgPED and Wt samples, respectively. It is evident that the black trajectories developed mostly over the positive semi-plane, whereas the cells from the right edge (in red) moved toward the negative direction. For comparison, the

dynamic evolution of the Y component of TgPED and Wt cell trajectories is shown in Figure 3.4.E and 3.4.F, respectively. For both samples, the red and black data series merge with each other, showing that the trajectories developed randomly toward either the positive or the negative Y direction. It is worth noting that some of the cells in the Wt sample show a folding trajectory. In particular, some cells from the left edge initially moved toward the left direction and then at later times reverted to the right direction, i.e., the positive X abscissa (for example, see the trajectory in blue in Figure 3.4.B, 3.4.D and 3.4.F, that refers to a cell laying on the left edge of the wound). This behavior may be related to the presence of local damages to the cell monolayer. For instance, cell debris removed during the scratch was not properly washed off, or the cells that were partially damaged by the scratch and did not move altered the motility of other cells, that were forced to move around the obstacle to access the cell-free area. In general cell trajectories can be also influenced by damages on the dish surface, due to the scratching [222], which may lead to preferential paths in cell movements (contact guidance).

The directionality of cell movement during wound closure was quantified by defining the directionality index I , which is analogous to the chemotactic index [130]. For every single cell, the ratio between the net displacement (S) along the X or Y direction and the overall curvilinear trajectory (C_T) over the same time interval was calculated. The directionality index I in a given time interval was then calculated as a weighted average over the entire cell population, with the trajectory length being the weight [129]. Figure 3.5 shows two images of a WH experiment corresponding to 0 and 25 h, with the trajectories described by some of the cells superimposed in white. The net displacements (S) along both the X and Y axes were also shown. We measured the average values of the directionality indices I_x and I_y for both TgPED and Wt cell genotypes, calculated over the subpopulations of cells moving from the left and right edges of the wound (indicated as L and R, respectively). As expected, due to the orientation of the X axis, I_x was systematically positive for the cells from the left edge that moved preferentially from the left to the right (i.e., following the positive orientation of the X axis) and was always negative for the cells from the right edge. For direct comparisons among different populations, the absolute values of I_x and I_y is shown in Figure 3.6. $|I_y|$ seems to fluctuate around 0, proving that cell movement along the Y direction was random, whereas $|I_x|$ was significantly higher for both edges. The Wt cells exhibit a less pronounced difference between $|I_x|$ and $|I_y|$ for the subpopulation along the left edge, compared to the TgPED sample, due to the presence of some cells that showed folding trajectories, as reported in Figure 3.4 and discussed above.

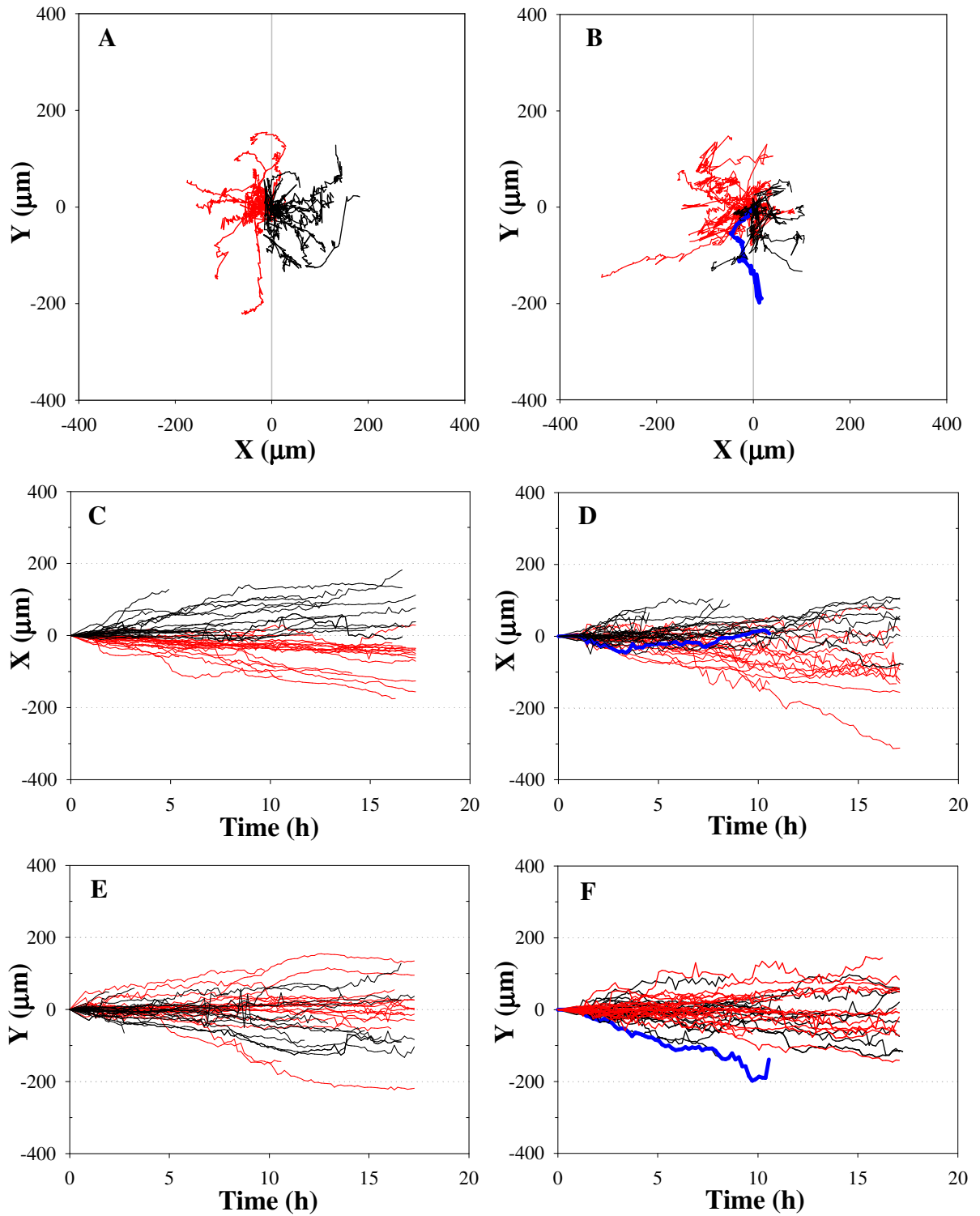


Figure 3.4: (A, B) Trajectories of 46 TgPED (A) and 48 Wt (B) fibroblasts during WH experiments. (C, D) Real-time evolution of the X coordinate for TgPED (C) and Wt (D). (E, F) Real-time evolution of the Y coordinate for TgPED (E) and Wt (F). The cells on the left and right edges of the wound are shown in black and red, respectively. The trajectory in blue is relative to a cell on the left edge that shows a folding trajectory to move around an obstacle and reach the cell-free area.

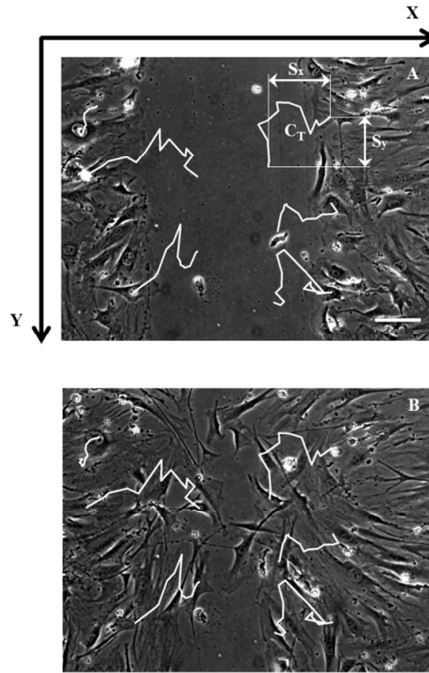


Figure 3.5: Trajectories described for some of the cells were superimposed on the initial (A) and final (B, 25 h) images of a WH experiment. The curvilinear trajectory (C_T) and the net displacements (S_x and S_y) over the two directions are also indicated. Scale bar = 100 μm .

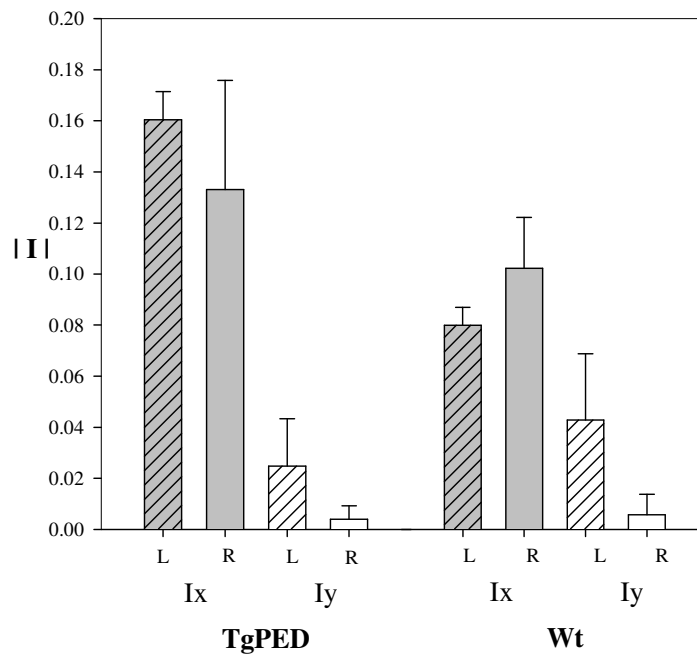


Figure 3.6: Directionality indices along the X and Y directions for the TgPED and Wt samples in the WH experiments. Bars indicate the absolute value of the average indices calculated over the cells moving from the left (L) and right (R) edges. Error bars represent the standard deviation.

The image analysis used for cell tracking also provides the orientation angle of the major axis of each cell [132] at any time point, which is related to the direction of cell movement at that specific instant. The distribution of the cell orientation angles at several time points was also calculated. Despite the clear presence of a preferential movement along the X direction, no defined preferential orientation was observed over the cell population (data not shown for the sake of brevity). A possible cause of this random orientation is the presence of two competing effects, one being that the cells prefer to move along the X direction to close the wound and the other being that the scratch induced initial stress over the cell monolayer along the Y direction, thereby orienting some of the cells orthogonally to the wound closure direction. The scratch may also accidentally induce micro abrasions on the dish surface that can contribute to drive the cells along the Y direction (i.e. the direction of the scratch). The effect of the scratch was also observed in terms of folding trajectories suggesting that, on average, the cell polarization was random. In other words, at any given time, different cells were oriented along different directions, even if the overall movement of the cell population remained directed toward the X direction, as measured by the directionality index.

Cell motility was quantified by means of specific parameters, as described in the Material and Methods section. Figure 3.7 reports the values of the mean squared displacement as a function of time for the Wt and TgPED samples under random motility conditions (Figure 3.7.A) and during wound closure (Figure 3.7.B). For any given value of time, the $\langle d^2(t) \rangle$ value was higher in the Wt fibroblasts under both conditions, indicating higher motility. The difference in mean squared displacement between the two cell populations was reduced in the WH experiments, suggesting that the wound may act to somehow depress cell motility in Wt cells, while no significant differences were measured for TgPED. For instance, for a value t of 700 min, $\langle d^2(t) \rangle$ for the Wt cells was 2-fold higher than that for the TgPED cells under random conditions, whereas the difference was only 1.4-fold for the WH assay. Cell-cell interactions or stress-induced mechanisms might account for such apparent discrepancy. By fitting the experimental measurements of the mean squared displacement according to Eq. (3.1), the random motility coefficient D and the persistence time P were estimated for both CRM and WH experiments. The resulting fitting curves are shown in Figure 3.7.

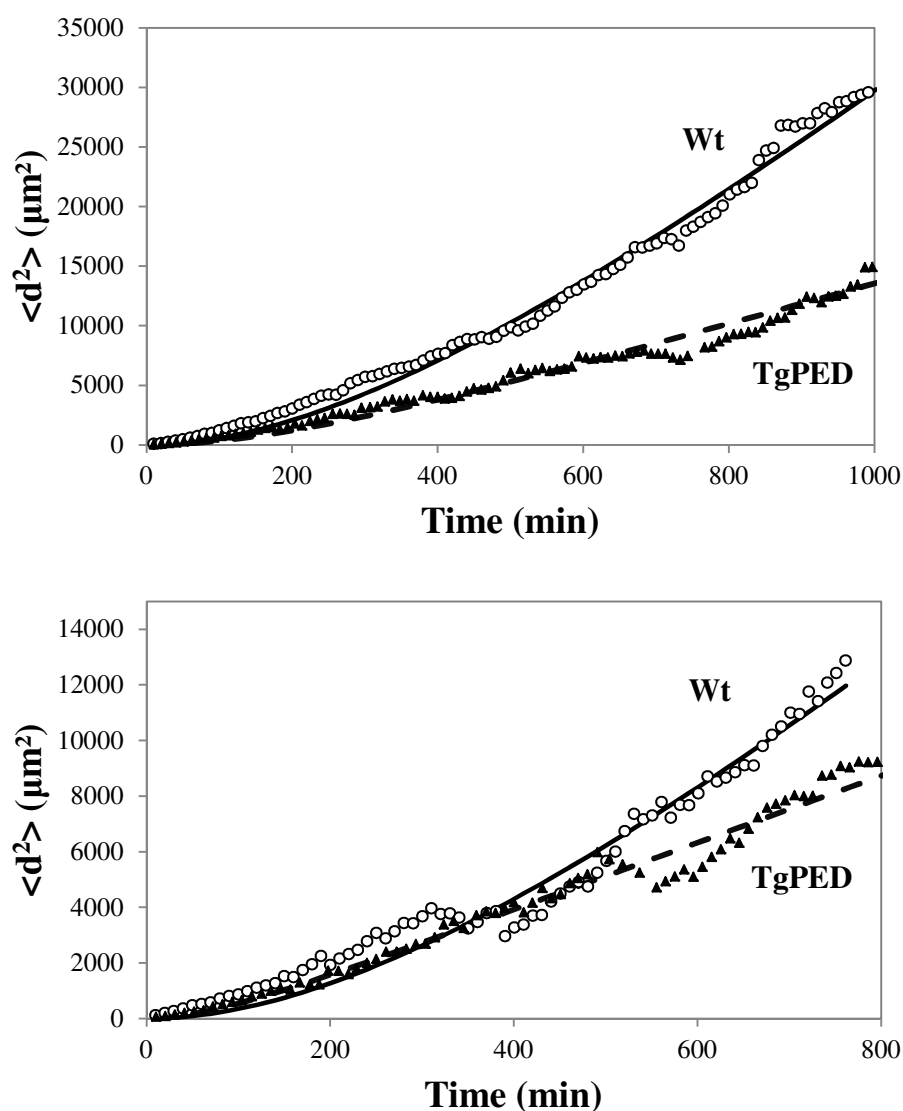


Figure 3.7: Mean squared displacement for the TgPED and Wt samples measured during CRM (A) and WH (B) experiments.

Table 3.1 summarizes the estimated motility parameters for the two cell populations under random and WH conditions. Compared to Wt, the TgPED fibroblasts showed limited motility, as evident by the lower values of all the parameters examined, including the random motility coefficient (D), the persistence time (P), the mean velocity (V), and the fraction of motile cells. This observation is in agreement with the detected difference in the wound closure rate reported in Figure 3.2 and also confirms that PED/PEA-15 indeed inhibits cell motility. The results provided by WH and CRM assays are in agreement. Consistent with the results shown in Figure 3.7, the increment in the motility parameters for the Wt cells was higher, compared

to the TgPED cells, under random conditions, in contrast to WH. In particular, the random motility coefficient D for Wt was 3.6 higher than that for TgPED in the CRM assay, whereas the increment was limited to 2.2 in the WH assay.

Experiment	Genotype	Fraction of mobile cells	D [$\mu\text{m}^2/\text{min}$]	P [min]	V [$\mu\text{m}/\text{min}$]
Random motility	Wt	71 % \pm 0.09	11.4 \pm 3.5	370.0 \pm 70	0.6 \pm 0.05
	TgPED	54 % \pm 0.02	3.2 \pm 1.0	68.2 \pm 15.0	0.47 \pm 0.01
Wound healing	Wt	85 % \pm 0.05	6.7 \pm 2.1	343.8 \pm 100	0.83 \pm 0.1
	TgPED	54 % \pm 0.03	3.1 \pm 1.1	74.8 \pm 16.0	0.54 \pm 0.15

Table 3.1: Motility parameters determined for the two cell populations under random motility conditions and during wound healing experiments. For each sample the calculation was repeated on two cell subpopulations, randomly selected; we reported the average of the two measures of each motility parameter, and the standard deviation as uncertainty.

Concerning the persistence time, the increments were 5.4 and 4.6 for CRM and WH, respectively. The differences in the fraction of motile cells and the mean velocity (V) were less significant. Statistical significance of the differences in the V for the two genotypes was also assessed ($p < 0.0001$) for both random and WH conditions. Figure 3.8 shows the mean velocity module calculated over the entire experimental length for each cell analyzed in the CRM and WH experiments.

The comparison of motility parameters of the two cell populations under WH and random conditions, showed that random motility coefficient for Wt cells is reduced under WH, while the fraction of motile cells and velocity are both increased. In particular the differences in the mean velocity can be considered as statistically relevant ($p < 0.0001$, see Figure 3.8). However, for TgPED cells no significant differences were observed comparing the WH and CRM assays, in terms of fraction of motile cells, D and P , while only limited differences are measured for the mean cell velocity V , that are less relevant than the previous case ($p = 0.0047$).

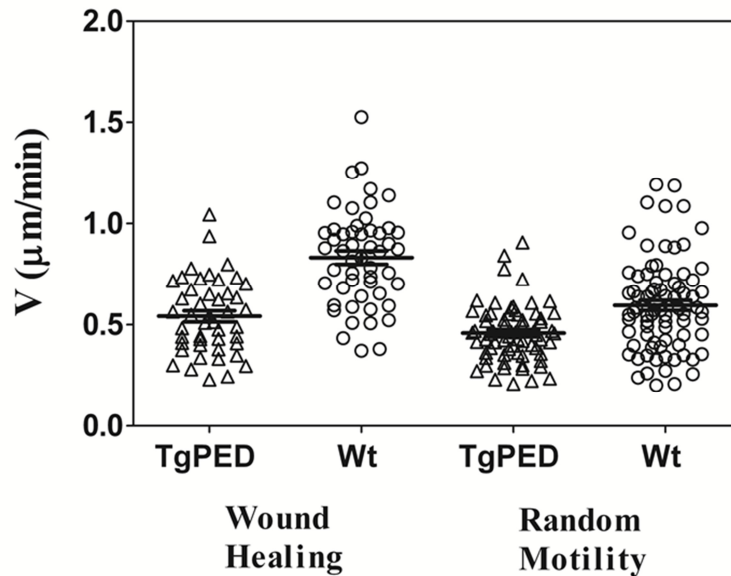


Figure 3.8: Average velocity module ($\mu\text{m}/\text{min}$) calculated over the entire experimental length for each cell analyzed. Four data sets are relative to the two genotypes (TgPED and Wt) as analyzed during random motility and WH experiments. The continuous line and error bars represent the average value and the standard deviation, respectively. The differences in the average velocity for the two genotypes can be considered as significant ($p < 0.0001$) for both random and WH conditions. The differences in the average velocity for Wt cells under random and WH conditions is also significant ($p < 0.0001$), while only limited differences are measured for TgPED comparing WH and CRM assays ($p = 0.0047$).

We can speculate that this difference in the behavior of the two cell populations can be attributed to the decrease in focal adhesion plaques of the TgPED fibroblasts compared to Wt. Due to the reduced adhesion to the support, it is likely that TgPED cells are less affected by the mechanical stress the scratch induces along the Y direction; furthermore any contact guidance due to the possible presence of micro abrasions on the culture dish is also less relevant. For this reason the two experimental conditions (WH and CRM) can be considered equivalent for TgPED cells, whose motility, limited compared to Wt, due to the limited adhesion, is not further depleted by the secondary damages induced during the scratch. Wt cells, on the contrary, show higher adhesion on the substratum and suffer more from the stress induced during the scratch. In our scenario we speculate that for Wt cells the wound closure process stimulates cell velocity, that is in fact incremented in the WH compared to CRM assay, but this increment does not correspond to an increment in the random motility coefficient, due to the contrasting effect on the cell orientation along the two directions, as discussed above. It is worth mentioning that the substratum micro-topography can influence

cell adhesion and migration [182]; in all our experiments cells have been plated on multiwell uncoated culture dishes.

Cell migration and invasion models, based on the Fisher's equation [150], can be used to describe the WH process. This approach predicts that the invading cell front moves as a traveling wave at constant speed $s = \sqrt{\frac{4D \ln(2)}{\tau}}$ [152, 155], where D is the random motility coefficient and τ is the cell doubling time (in our case study τ is about 16 h for both cell populations). The measured values of the cell front speed during the WH assay were 5.1 and 4.3 $\mu\text{m}/\text{h}$ for Wt and TgPED, respectively; these values are of the same order of magnitude of the typical cell velocity, as calculated according to the persistent random walk model (Table 3.1). The random motility coefficients D , estimated according to the Fischer's approach ($D = \frac{s^2 \tau}{4 \ln(2)}$), were 2.6 and 1.8 $\mu\text{m}^2/\text{min}$ for Wt and TgPED respectively, i.e., Wt motility was about 1.4-fold higher than that of TgPED. These estimates are comparable to the data of Table 3.1 for CRM and WH assays.

It's worth mentioning that a rough approximation of the order of magnitude of the random motility coefficient D can be also obtained by dividing the squared distance covered by the cell front by the elapsed time; the values so estimated were about 10 and 8 $\mu\text{m}^2/\text{min}$ for Wt and TgPED fibroblasts, respectively. This last approach assumes that the cell front movement is driven by simple diffusion [132], neglecting the contribution of the proliferation; for this reason, this calculation can lead to an overestimation of the random motility coefficient. However, also in this case the order of magnitude of the estimated random motility coefficient is in agreement with the reference measurement obtained by cell tracking, reported in Table 3.1.

Overall, we can state that the differences in the WH rate between the two considered samples is mainly due to differences in the cell motility, and that the contribution of the proliferation is limited and identical for the two cell types.

4. Conclusions

In this study, we performed a direct comparison of two different experimental methods for the investigation of cell motility using *in vitro* live-cell imaging by time-lapse microscopy. Single Cell Random Migration assays and Wound Healing assays were performed to analyze cell behavior under random conditions and in presence of an external stimulus, such as a mechanical damage on a cell monolayer. Both these experimental approaches are widely used

in the literature for the quantification of cell motion through the determination of several cell motility parameters. The first assay requires more elaborate data processing, and allows the determination of specific quantitative parameters, such as the random motility coefficient and the persistence time, and can be considered as a golden standard. The WH assay requires an easier analysis, and is more widely used in the literature; typically a wound closure velocity is measured, but sometimes the investigation is only limited to obtain a qualitative visualization of the cell motility. The aim of this study is to perform a detailed analysis of cell motility in the two experimental conditions and to make a direct comparison of the abovementioned methodologies, still lacking in the literature.

In order to compare WH and CRM, we applied the two assays to a case study in which the motility of two skin fibroblast populations, isolated from Wt control mice and TgPED mice, overexpressing the protein PED/PEA-15, was investigated. In addition to its involvement in cell motility, PED/PEA-15 is known to be overexpressed in patients with type 2 diabetes, which represents a relevant issue since wound repair abnormalities are common features of type 2 diabetes. In a previous report [175], it was shown that PED/PEA-15 controls fibroblast motility and wound closure by ERK 1/2-dependent mechanisms. In fact, a reduced migratory ability was observed in TgPED fibroblasts compared to Wt control fibroblasts. In this work, we used the known difference in terms of migration ability between Wt and TgPED cells to compare the two experimental techniques, i.e., WH and CRM assays.

In the WH assays, we analyzed the wound closure dynamics by quantifying the wound closure velocity based on real-time measurement of the reduction of the denuded area. We found that the TgPED fibroblasts healed the wound more slowly than the Wt cells. Cell spreading and proliferation are the dominant biological mechanisms governing the wound healing process [150, 154]. We focused on the analysis of cell motility, as the contribution of the proliferation mechanism to the wound closure process can be considered identical for Wt and TgPED fibroblasts.

We reported a detailed phenomenological and quantitative description of Wt and TgPED cell motility under different experimental conditions, i.e., in random conditions and during WH assays. The results show that WH assays are characterized by directionality in cell movement, induced by the presence of a gap; this directionality is relevant for the wound closure process. We referred to the persistent random walk model, in which cell division was not taken into account, and calculated typical parameters, including the persistence time, the random motility coefficient, the percentage of motile cells, and the cell velocity for both WH and CRM experiments. All the estimated motility parameters were lower in the TgPED fibroblasts

compared to Wt in both assays, supporting the hypothesis that the PED/PEA-15 protein plays a significant role in the regulation of cell motility, as shown in a previous work. However, the differences were less pronounced in the WH assays, resulting in a reduced decrement of the random motility coefficient and the persistence time. This result may be interpreted by postulating a direct involvement of cell-cell interaction-driven mechanisms or a modification of cell motility induced by the wounding itself, which may represent a significant cellular stressing event. Nevertheless, TgPED cell motility remained significantly reduced, compared to the Wt control fibroblasts, also during WH assays.

We made a cross comparison between the WH and CRM measurements, proving that the result of one assay can be estimated, at least as order of magnitude, given the result of the other. In particular the random motility coefficient, or the cell velocity, usually measured by CRM assays, can be estimated from the measurement of the wound closure velocity, obtained by WH assay. On the other hand, the time required for the wound closure can be estimated, given the random motility coefficient as determined from a CRM assay. This proves that the two assays are intimately linked with each other for the fibroblast populations here considered.

Overall, we found a substantial agreement between independent quantifications of cell migration based on the cell population dynamic analysis, WH assays, and the reconstruction of individual cell trajectories in both WH and CRM assays. In conclusion, the experimental techniques used in this study allow the acquisition of analogous information in terms of cell motility. In other words, we proved that the same conclusions can be drawn from the complex and time consuming single cell motility analysis, and from the simpler Wound Healing assay. To our knowledge this is the first, quantitative comparison of these two widely used techniques, based on the analysis of two different cell genotypes. Nevertheless, the CRM and WH assays are not equivalent from a biological point of view, because of the presence of damage in the cell monolayer in the WH assay. Cell migration in the WH assay may be qualitatively predicted from a detailed analysis of random motility, and vice versa, despite different quantitative terms. These findings could be applied to express the results of the WH assay, which is quite used in the literature due to its simple operation, in terms of intrinsic cell motility parameters. We believe our result can be relevant for future experimental and modelling works.

Chapter 4

The wound healing assay revisited: a transport phenomena approach

1. Introduction

The dynamic behavior of the cells, driven by proliferation and migration mechanisms [1], is essential for a wide spectrum of physiological as well as pathological processes, including morphogenesis, immune responses, angiogenesis, tissue repair, tumor growth and invasion [92, 211]. The complex mechanisms that lead cell dynamic behavior are still poorly understood [16, 17]. In order to achieve a better comprehension of such mechanisms, a detailed analysis of these processes requires a rigorous approach to quantitatively measure well-defined cell movement and proliferation indices. For this reason, the development of such analyses is nowadays within the core business of Chemical Engineering [18], which can contribute to the building of mathematical models, based on a transport phenomena approach, useful to describe and predict the mechanisms driving cell dynamics [19].

Biological processes can be investigated *in vitro* by using several conventional assays, which allow to quantitatively characterize the dynamical aspects of cell behavior. These assays range from simple and inexpensive ones, like the Boyden assay [204], to technically laborious, time-consuming and expensive experimental solutions, such as the cell random motility assay [214]. The latter one should be considered as a gold standard to investigate cell migration, because it enables a comprehensive and multi-scale analysis of cell migration at the level of both the entire population and the individual cells.

Nevertheless, one of the most popular methods to evaluate cell dynamic behavior *in vitro* is the wound healing (WH) assay [133, 223], because of its low cost and simplicity to set up [134]. In the classical WH assay, also referred as scratch test, the cells are grown on a two-dimensional surface up to a condition defined as confluence, corresponding to the carrying capacity of the surface, where all the available space is completely covered by the cells, which have the tendency to form continuous monolayers. An artificial scratch is then created on the confluent cell monolayer by mechanically scraping off an area of cells with a pipette tip, a blade, a needle or similar [135]. Then the cells are washed with a desired medium to remove cell debris and suspended cells. Novel approaches have been developed to implement the WH assay in a more controllable way [177]. For example, more recent versions are based on removable inserts that limit the area initially covered by the cells [212]. Alternatively,

wounding can be achieved by laser [202, 203] or electric [200] removal of the cells from a defined area. A number of circular WH assays have also been established; many of them involve the creation of a circular exclusion zone using a stopper positioned prior to cell adhesion and spreading [192, 224]. Furthermore, novel microfluidics-based WH assays use laminar flows in microfluidic channels to selectively detach the cells from a portion of confluent cell monolayers in an enzymatical way [144, 198].

In response to the stimulus arising from the creation of the empty space in a previously intact tissue, the cells on the wound margins, which are no longer contact-inhibited, proliferate and move toward the center of the denuded region to cover the wound area [136].

Depending on the cell types involved, two main mechanisms of wound healing have been identified [2, 133, 135, 140]. Specifically, the first mode is typical of epithelial-like cells, which repopulate the wound area in a collective mode, ensured by strong cell-cell interactions, moving as two coherent sheets [79, 141]. The second wound healing mechanism, more relevant to this article, is typical of fibroblastic cells, which fill the wound region moving primarily as dispersing individual units [140], rather than as cohorts [146]. Due to the lack of strict cell-cell interactions, overall the cells can move omnidirectionally, i.e. with the same probability in any direction.

The driving force for the spreading of the two cell sheets one toward the other in the wound healing process is the availability of free space, corresponding to the loss of spatial constraints [148]; the injury in the monolayer is not strictly necessary [79], even if in the presence of an external damage the movement is extended to the cells behind the wound margin. In addition, the sensation of available space by the cells also induces cell proliferation [134], which may contribute to the wound closure process [139].

The wound closure process can be mathematically described using the Fisher-Kolmogoroff equation, which includes terms for modeling cell motility and proliferation. Both these mechanisms are involved in the spatial spreading of the invading cells in the wound area, strongly affecting the evolution of cell density in time. According to the Fisher-Kolmogoroff equation, cell motility is modeled by Fickian diffusion, while cell proliferation is described by a logistic growth:

$$\frac{\partial u}{\partial t} = D \frac{\partial^2 u}{\partial x^2} + ku \left(1 - \frac{u}{\hat{u}}\right) \quad (4.1)$$

where u is cell density at time t at a given distance x from the wound edge, D is the constant diffusivity (random motility coefficient), k is the proliferation rate and \hat{u} is cell density at

confluence [154]. The model predicts that after a short transient, the movement of the invading cell front can be observed in terms of a traveling wave, which propagates with constant speed $s = \sqrt{4 \hat{u} k D}$ in the direction perpendicular to the wound [136, 152, 154].

An extension of the Fisher-Kolmogoroff equation, incorporating non-linear diffusion, also exhibits travelling wave solutions:

$$\frac{\partial u}{\partial t} = D_0 \frac{\partial}{\partial x} \left[D \frac{\partial u}{\partial x} \right] + ku \left(1 - \frac{u}{\hat{u}} \right) \quad (4.2)$$

Here, the constant parameter D_0 is the diffusivity for isolated cells, while D is a dimensionless diffusivity, function of $\frac{u}{\hat{u}}$ with the property $D \rightarrow 1$ as $\hat{u} \rightarrow 0$. In this form of the Fisher-Kolmogoroff equation, cell diffusivity is not constant, in analogy with the basic diffusive model in which the diffusion coefficient depends on the concentration of the molecule [225]. In Eq. (4.2), cell diffusivity is considered as a decreasing function of cell density:

$$D = \left(\frac{A}{A + \frac{u}{\hat{u}}} \right) \quad (4.3)$$

where A is a critical value of cell density corresponding to a measure of contact inhibition and depends on the cell line. Hence, this functional form captures the phenomenon of contact inhibition of cell movement, whereby the collisions of the cells can cause cell reorientation and lead to a change in the direction of cell path, therefore hindering and inhibiting cell movement [155, 165].

The measurement of cell density is a challenging task from an experimental point of view; for this reason, the analysis of the wound closure process is simplified quantifying the phenomenon in terms of change in the wound size over time. In order to gain this quantitative information over long periods of time, it is necessary to observe dynamically the cells while covering the wound space. As the wound healing process can last up to a few days, the cells must be taken in culture to ensure their viability during the experiment.

Two methodological approaches are typically used to capture the output of the WH assay, in order to gain information about cell dynamics. The most popular approach is related to the manual acquisition of images within the sample along the wound at the beginning and at fixed time intervals (for example every 6 h) until the gap is closed [139]. In this approach cell movement is typically quantified counting the number of cells that repopulate the wound region for each time step [168, 169], or measuring the percentage of wound closure at fixed

time points [167, 171, 172]. However, this classical approach results to be approximate, as it doesn't allow to investigate the dynamic aspects of cell behavior.

An alternative and more reliable approach is based on direct visualization by time-lapse microscopy (TLM) which enables to dynamically monitor the free surface area, iteratively acquiring sample images with a defined time frequency [93], while controlling the environmental parameter to ensure cell viability [94, 173]. This methodological approach, allows to obtain the abovementioned measurements, i.e., the number of cells in the wound region or the percentage of wound closure, in a more accurate way. Furthermore, the possibility to regularly observe over time exactly the same wound region, rather than roughly comparing randomly taken images, enables to estimate precise quantitative parameters, such as wound closure velocity, measuring the reduction of wound area over time, or the cell front propagation speed, quantifying the position of the wound front over time [79, 134].

Although the WH assay provides a valuable experimental approach for studying cell dynamics *in vitro*, it suffers from several drawbacks [180]. In fact, the outcomes of the WH assay are somewhat confounded by several factors, which may represent a limit in accomplishing reproducible and reliable quantitative results. For example, the wound width can vary along its length and among different experiments [176]; it depends on the dimension of the tool used in making the wound as well as the scraping force and velocity [177]. Moreover, the scratching process involves mechanical injuries to the cells located on the wound edges, which may potentially lose their original morphology and function [179]; this may result in the transient contraction of the cell wave front. Some cells and cell debris can also keep attached to the wound margin, perturbing the motility of other cells moving around the obstacle to access the cell-free area [180]. Additionally, the migrating surface, often coated with extracellular proteins prior to cell growth, can be damaged by the sharp objects typically used in the scraping process; alterations in surface topography may lead to preferential paths in cell movements (contact guidance) [181].

Furthermore, the relative cell confluence in the region where the scratch is made, is challenging to control and reproduce within the same culture dish and among different cell samples [183]. This makes it difficult to compare independent experiments. The difficulty to obtain the same cell density in the samples primarily arises from anisotropies in the spatial spreading of the cells, mainly due to uneven cell attachment in the culture dish after plating. Moreover, it is arduous for the operator to plate exactly the same number of cells in different culture dishes. Above all, several cell treatments, including cell staining and gene silencing, involve the use of invasive techniques, which may result in unpredictable efficiency of cell

adhesion, undesired cell detachment from the bottom of the plates or cell death. Overall, these factors might potentially influence the outcome of the WH assay, strongly limiting the reproducibility of the experiments.

In this work, we revisited the methodological approach typically used to quantify the wound closure dynamic in a WH assay, by using a novel approach based on transport phenomena concepts. In particular, we focused on the difficulty to achieve reproducible and reliable quantitative results in the WH assay, strongly linked to several bias. In order to investigate the potential effect of cell density on the wound healing process, we performed WH experiments on a population of fibroblasts by using *in vitro* TLM image acquisition. Overall, our work is addressed to overcome, at least in part, the limitations related to the conventional quantitative analysis of the WH assay. In particular, in this work we propose a phenomenological scaling of the experimental data, in order to overcome the effect of cell density on wound closure velocity in WH assays.

2. Materials and Methods

2.1. Cell cultures

HT1080 human fibrosarcoma cells were grown at 37°C in Dulbecco's Modified Eagle Medium (Lonza, Switzerland) supplemented with 10% fetal bovine serum (Lonza, Switzerland) and antibiotics (50 units/mL penicillin and 50 µg/mL streptomycin) (Lonza, Switzerland) in a humidified atmosphere containing 5% CO₂ in air. Cultures between passages 18 and 22 were used for WH experiments.

2.2. Time Lapse Microscopy

Time-lapse Microscopy (TLM) experiments were carried out using an automated workstation based on an inverted microscope (Zeiss Axiovert 200; Carl Zeiss, Jena, Germany) and a long working distance 10× objective in phase contrast (CP Achromat Ph1), described elsewhere [129]. The microscope was enclosed in a homemade incubator that allows to keep the sample at constant temperature (37 ± 0.1 °C) and under 5% CO₂, 100% humidified atmosphere. Live-cell imaging was performed by a high-resolution, high-sensitivity monochromatic CCD video camera (Orca AG; Hamamatsu, Japan). The whole workstation was driven by a homemade control software in Labview. The images were iteratively acquired at several locations within the sample using a motorized x–y stage and focus control. The delay between

two successive images of the same field of view was set to 10 min; the overall experiment duration was about 60 h.

2.3. WH assays

To perform WH assays, HT1080 fibrosarcoma cells were plated on uncoated 24-well culture dishes at different initial densities: 6×10^5 , 3×10^5 , 1.5×10^5 , 0.75×10^5 , 0.3×10^5 cells/well, corresponding to 34×10^{-4} , 17×10^{-4} , 8.5×10^{-4} , 4.3×10^{-4} and 1.7×10^{-4} and $\frac{\text{cells}}{\mu\text{m}^2}$ respectively. The cells were incubated at 37°C for about 24 h, until 100 % confluence was reached. Cell monolayers were scratched manually with a p200 pipette tip to scrape away an area of cells, in order to mimic a wound. Cell debris were then removed washing the fibroblasts twice with phosphate-buffered saline (PBS). Before starting the experiments, the wounded cell monolayer was rinsed with fresh culture medium.

The experiments were performed in the absence and in the presence of 5 $\mu\text{g/ml}$ of mitomycin-C (Sigma-Aldrich, Australia), an inhibitor of cell proliferation [226].

2.4. Image analysis

The size of the cell-free area (A), representing the wound, was measured by segmenting images for each time step using an homemade automated image analysis algorithm.

The wound width (b) was calculated for each time point as the ratio between the area of an equivalent rectangle with size A and the height of the image (h). Then, the position of the invading cell front $x = \frac{b_0 - b}{2}$, where b_0 is the wound width at time 0, was calculated. A schematic representation of the measured parameters is reported in Figure 4.1, which shows two images of a WH experiment, corresponding to 0 h and $t > 0$ h. The dotted lines indicate the wound edge on the right and left side of the scratch, whereas the double arrowed line shows the wound width.

Cell density was measured using the image analysis software Image ProPlus, which allowed to manually count the cells in a selected region, whose size was determined drawing manually its contour.

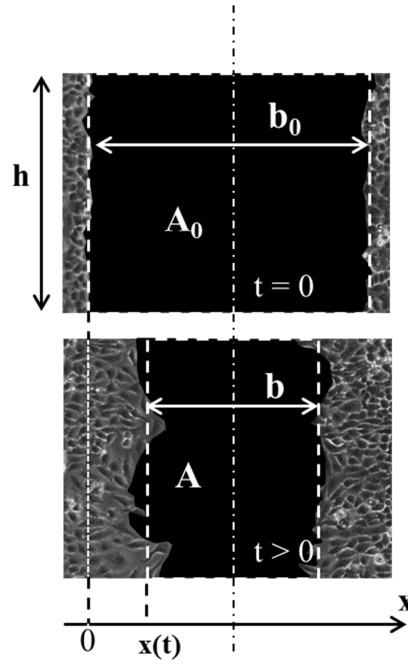


Figure 4.1: Images acquired during a WH experiment at the initial time ($t=0$) and $t>0$. The area of the wound at time 0 (A_0) and at $t>0$ (A) is shown in black. The height of the image (h) and the wound width (b_0 and b for $t=0$ and $t>0$, respectively) are also indicated. $x(t)$ is the position of the invading cell front, which changes along the x axis as a function of time.

3. Results and Discussion

In order to investigate the potential effect of cell density on the wound healing process, we performed WH experiments on HT1080 human fibrosarcoma cells by using *in vitro* TLM image acquisition.

The cells were plated for three times at different initial densities D_p : 34×10^{-4} , 17×10^{-4} , 8.5×10^{-4} , 4.3×10^{-4} and 1.7×10^{-4} and $\frac{\text{cells}}{\mu\text{m}^2}$ (Figure 4.1). The cell density D_m on the wound edges at the initial time step was measured by image analysis. As shown in Figure 4.2, the same value of D_p corresponds to different real values of cell density D_m , suggesting that the cell density in the region where the scratch is made, is challenging to control and reproduce.

In Figure 4.3, the cell density D_m is reported as a function of the theoretical cell density D_p . The data suggest that the higher the value of the theoretical cell density is, the higher the probability to make error in plating the cells. For example, for $D_p = 34 \times 10^{-4} \frac{\text{cells}}{\mu\text{m}^2}$ we obtained three different values of D_m : 27×10^{-4} , 29×10^{-4} , $44 \times 10^{-4} \frac{\text{cells}}{\mu\text{m}^2}$, $33 \pm 9 \frac{\text{cells}}{\mu\text{m}^2}$ being the mean value with the standard deviation, as shown in Figure 4.2.

The cell densities at various distances behind the cell front during the wound closure process was measured at several time points for three samples. Cell density evolution over time and location (along the direction of wound closure x) is shown in Figure 4.4. Specifically, in Figure 4.4.A, 4.4.B and 4.4.C we report the evolution in space of the cell density for increasing time steps, for samples corresponding to different initial cell densities D_m : $27 \times 10^{-4} \frac{\text{cells}}{\mu\text{m}^2}$, $12 \times 10^{-4} \frac{\text{cells}}{\mu\text{m}^2}$ and $3 \times 10^{-4} \frac{\text{cells}}{\mu\text{m}^2}$, respectively. In the first and second time step, a gradient of cell density can be observed; in fact, cell density decreases moving from the edges to the wound area. The curve describing cell density evolution in space exhibits the form of a travelling wave, according to the Fisher-Kolmogoroff equation. Figure 4.4.A and 4.4.B show that cell density on the edges of the wound do not change significantly over time, whereas in Figure 4.4.C cell density on wound edges increases over time.

The kinetics of wound closure was determined for all samples with different initial cell density. The process was quantified by measuring the reduction of the cell-free area (A/A_0) or the position of the invading cell front (x) over time. In Figure 4.5.A, the wound area (A), as measured by image analysis at each time point and normalized to the initial value (A_0), is shown as a function of time for each sample under investigation. In the inset, the mean value of the wound area (A) normalized to the initial value (A_0) is shown as a function of time. Each data point in the inset represents the average of all the measurements taken for each sample and the standard deviation is reported as error bar. In Figure 4.5.B the position of the invading cell front (x), measured as described in 2.4 paragraph, is reported as a function of time for each cell sample. Each data point in the inset represents the average of all the measurements x taken for each sample; the standard deviation is reported as error bar. It's worth mentioning that in Figure 4.5.B the curves reach different final values of x , corresponding to $\frac{b_0}{2}$, because no normalization was done in this case. The graphs in Figure 4.5 suggest that the cell samples require different time to complete the wound healing process. This can be related to the differences in the local cell density at time 0.

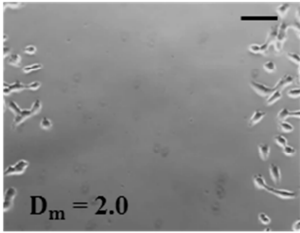
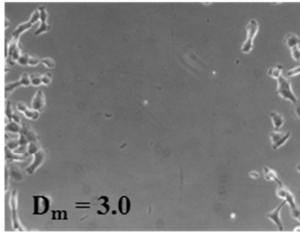
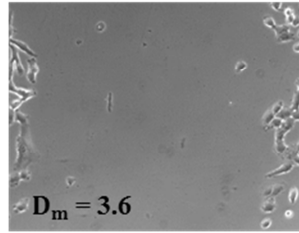
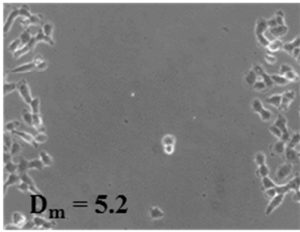
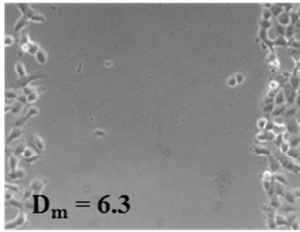
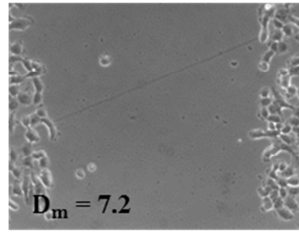
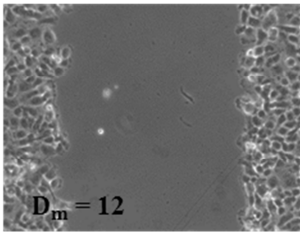
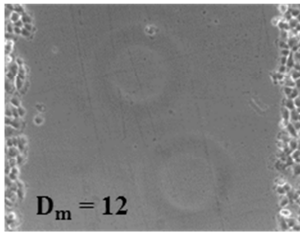
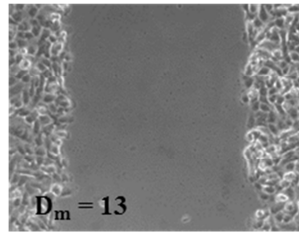
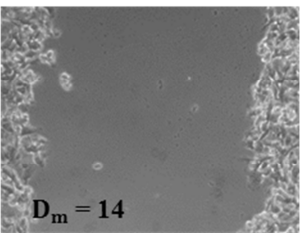
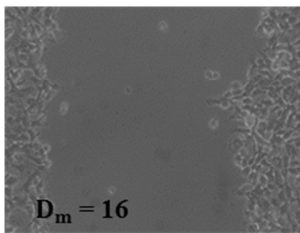
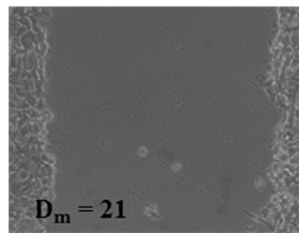
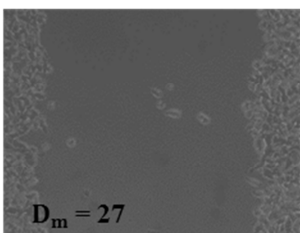
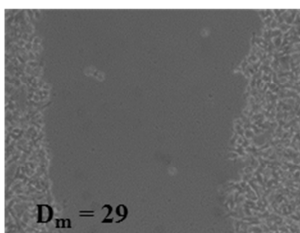
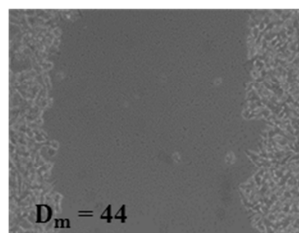
D_p	$\overline{D_m}$	Densities expressed as $\frac{\text{cells}}{\mu\text{m}^2} * 10^4$		
1.7	2.9 ± 0.8	 $D_m = 2.0$	 $D_m = 3.0$	 $D_m = 3.6$
4.3	6.2 ± 1.0	 $D_m = 5.2$	 $D_m = 6.3$	 $D_m = 7.2$
8.5	12 ± 0.8	 $D_m = 12$	 $D_m = 12$	 $D_m = 13$
17	17 ± 3	 $D_m = 14$	 $D_m = 16$	 $D_m = 21$
34	33 ± 9	 $D_m = 27$	 $D_m = 29$	 $D_m = 44$

Figure 4.2: Images of cell samples acquired at $t = 0$, corresponding to different initial cell densities. D_p is the theoretical value of the cell density, D_m is the real value of cell density according to the measure obtained by image analysis, and $\overline{D_m}$ is the average value of cell density for samples corresponding to the same D_p . Scale bar = $100 \mu\text{m}$.

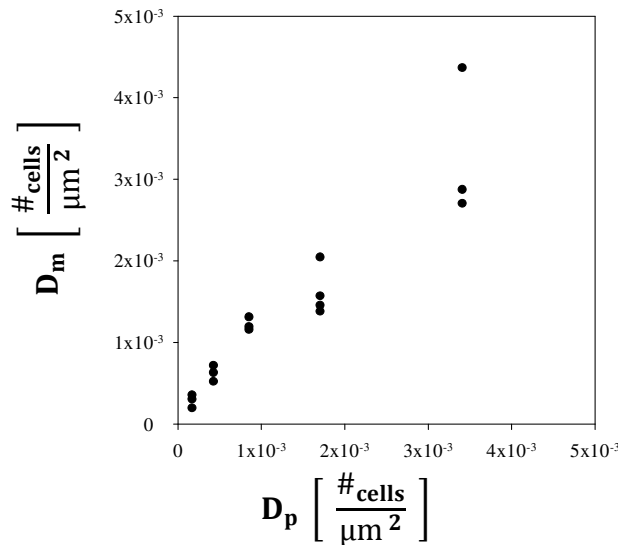


Figure 4.3: Cell density (D_m) measured by image analysis, reported as a function of the theoretical cell density (D_p).

Moreover, the curves describing the evolution of A and x in time show a linear trend, suggesting that the wound closure process occurs at constant speed. This result is in agreement with the Fisher-Kolmogoroff equation, which predicts that the progression of the invading cell front can be observed in terms of a traveling wave, which propagates with constant speed. We fit a linear equation to each data set reported in the graphs describing the evolution in time of A/A_0 (Figure 4.5.A) and x (Figure 4.5.B); the slope can be considered a quantitative measurement of the wound closure velocity (α) and the velocity of cell front progression (v), respectively.

In Figure 4.6, the wound closure velocity (α) and the velocity of cell front progression (v) are shown as a function of the cell density D_m measured at time 0. We found a linear relationship between the α or v and the cell density.

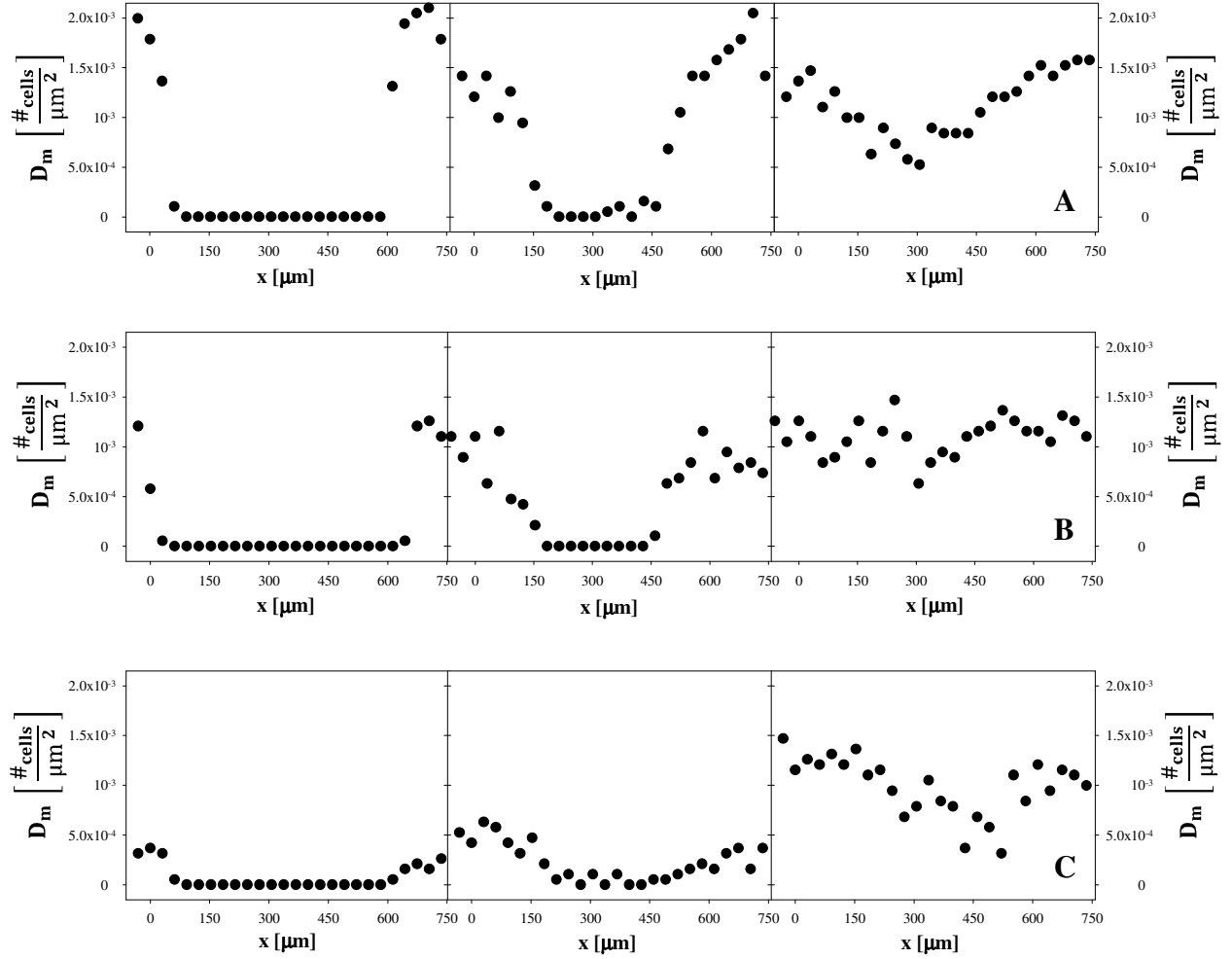


Figure 4.4: Cell density profile in space (along the x direction) and time, for samples corresponding to different initial cell densities: $27 \times 10^{-4} \frac{\text{cells}}{\mu\text{m}^2}$ (A), $12 \times 10^{-4} \frac{\text{cells}}{\mu\text{m}^2}$ (B) and $3 \times 10^{-4} \frac{\text{cells}}{\mu\text{m}^2}$ (C).

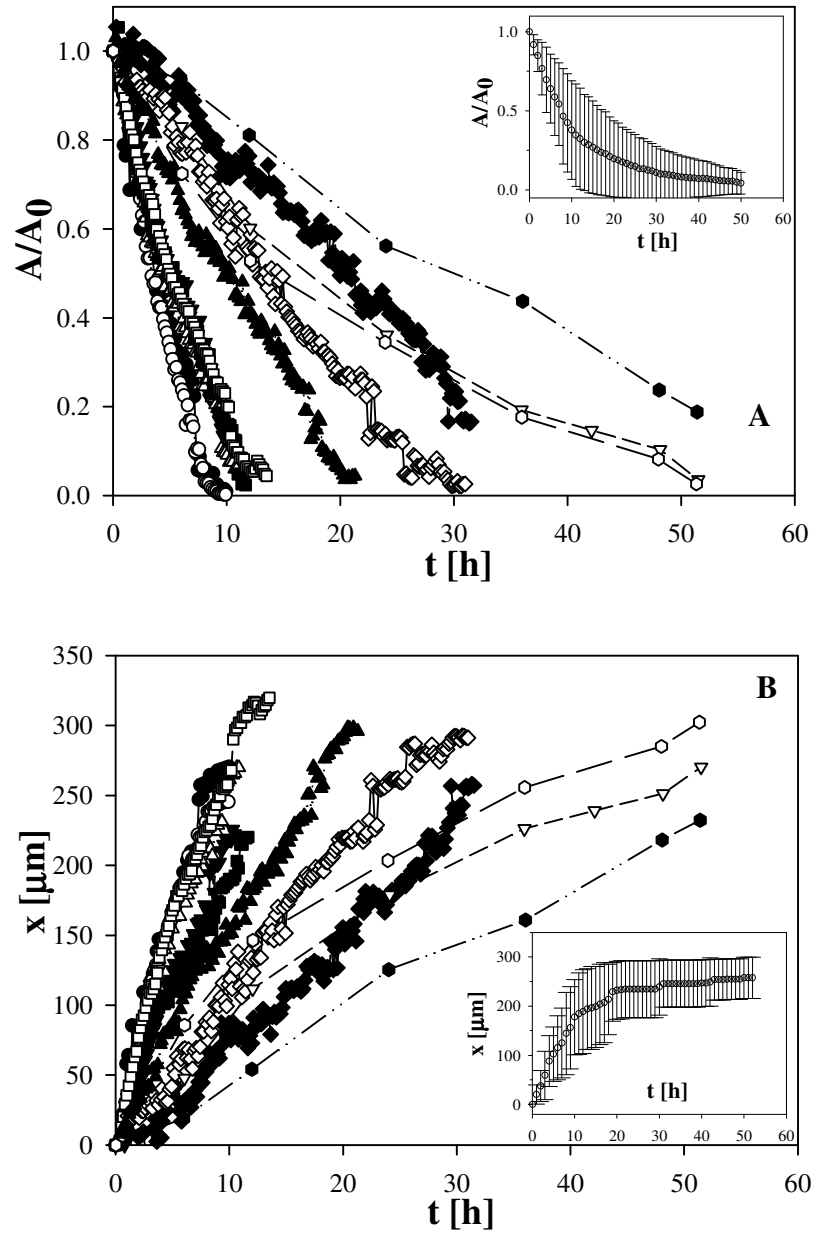


Figure 4.5: Dynamic evolution of wound closure. Evolution with time of the wound area A , normalized with respect to the initial value A_0 (A), and of the position of the invading cell front (B) for cell samples with different densities at time 0.

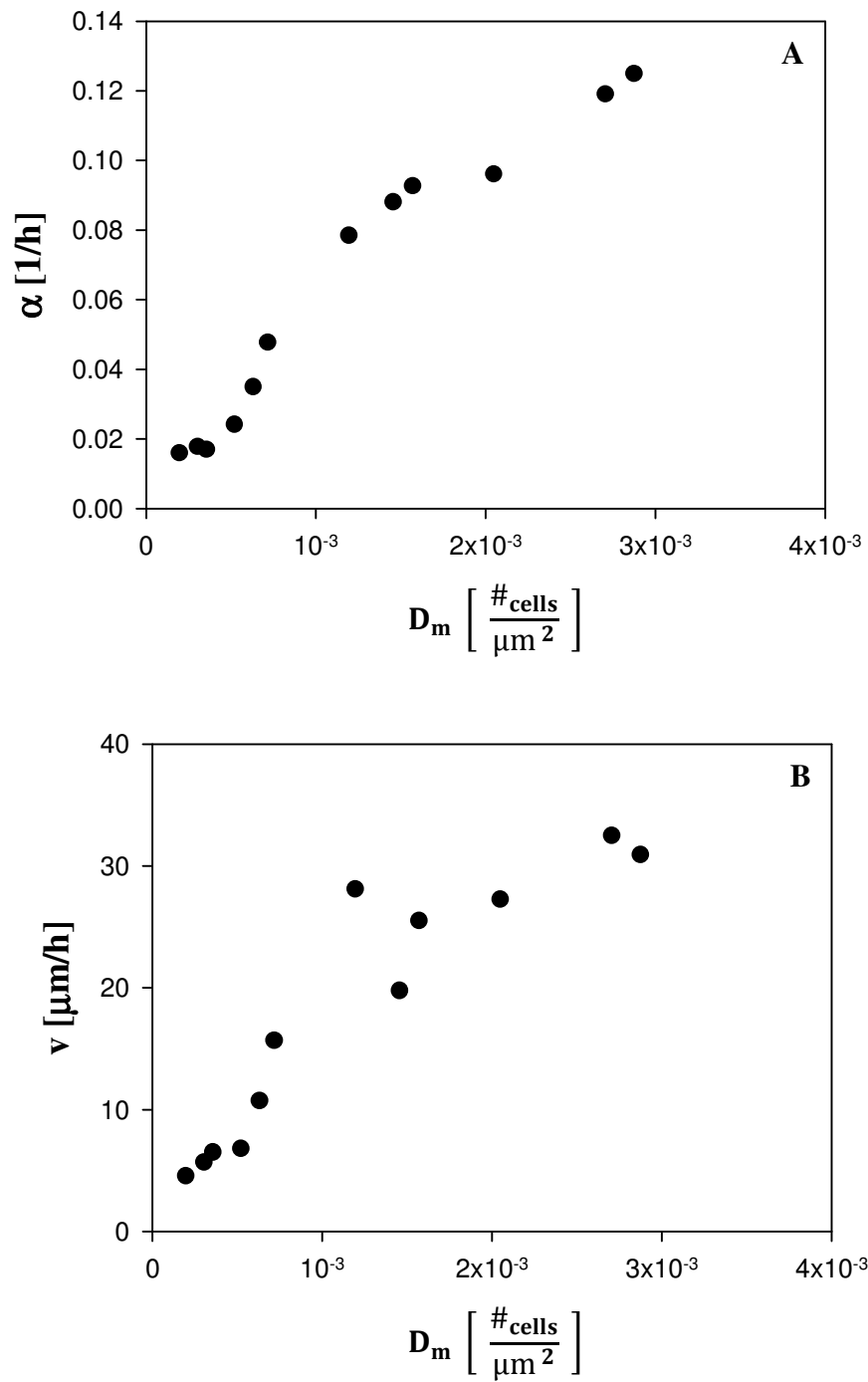


Figure 4.6: The wound closure velocity (α) and the velocity of cell front progression (v) are plotted as a function of the cell density at time 0.

We proposed a phenomenological scaling of the experimental data in order to overcome the effect of cell density on wound closure velocity. Our scaling on the time axis is based on the linear relationship between A/A_0 (or x) and the time, and between the wound closure velocity α (or the velocity of cell front progression v) and the cell density D_m . The scale factor (F) is the ratio between the cell density at time 0 of each sample (D_{m_i}) and the cell density at time 0 of a representative sample (D_{m_R}):

$$F = \frac{D_{m_i}}{D_{m_R}} \quad (4.4)$$

The scaled time t_c can be calculated with the following equation:

$$t_c = t F \quad (4.5)$$

We report the evolution in time of the cell-free area reduction (A/A_0) (Figure 4.7.A) and the position of the invading cell front (x) (Figure 4.7.B) after data scaling. In the inset, the average values of A/A_0 and x are shown as a function of time; the standard deviation is reported as error bar. Comparing Figure 4.5 and Figure 4.7, we found that after the scaling the curves are really close to each other, as suggested by the shorter error bars in the insets in Figure 4.7.

The same approach was used in a WH experiment performed in the presence of mitomycin-C, used to inhibit cell proliferation mechanism. Figure 4.8 shows the evolution in time of the cell-free area reduction (A/A_0) before (Figure 4.8.A) and after (Figure 4.8.B) data scaling. In the inset, the average values of A/A_0 are shown as a function of time and the standard deviation is reported as error bar. In Figure 4.9, the wound closure velocity (α) and the velocity of cell front progression (v) are shown as a function of the cell density at time 0. We found a linear relationship between the α or v and the cell density. Also in this case, after the scaling the curves are closer to each other, as suggested by the shorter error bars in the insets in Figure 4.8.B.

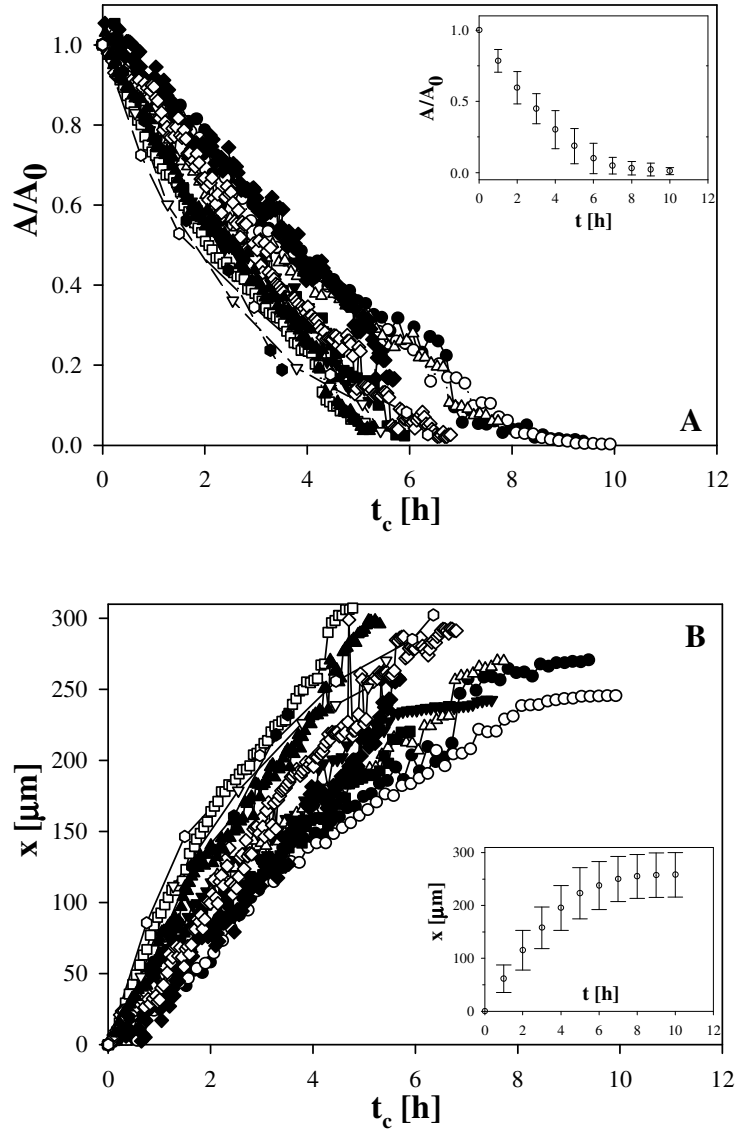


Figure 4.7: Dynamic evolution of wound closure after data scaling. Evolution with time of the wound area A , normalized with respect to the initial value A_0 (A), and of the position of the invading cell front (B) for cell samples with different densities at time 0.

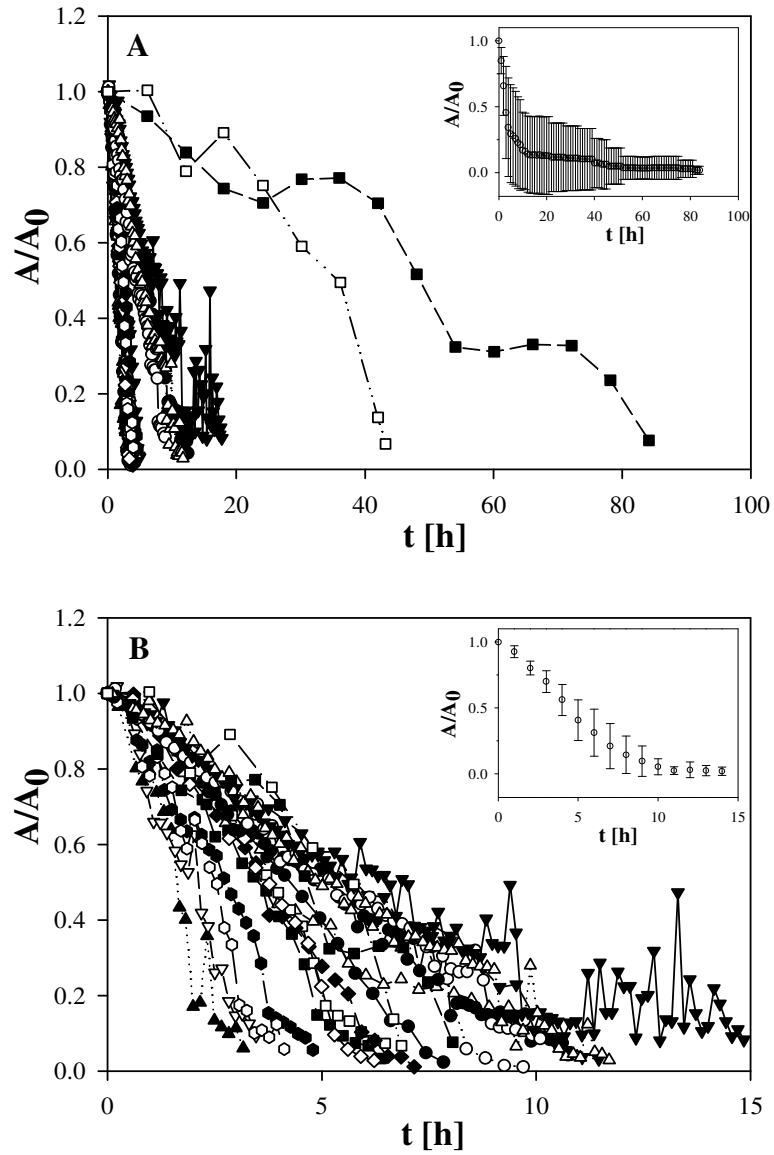


Figure 4.8: Dynamic evolution of wound closure before (A) and after (B) data scaling for samples (with different initial cell densities) in the WH experiment performed in presence of mitomycin-C.

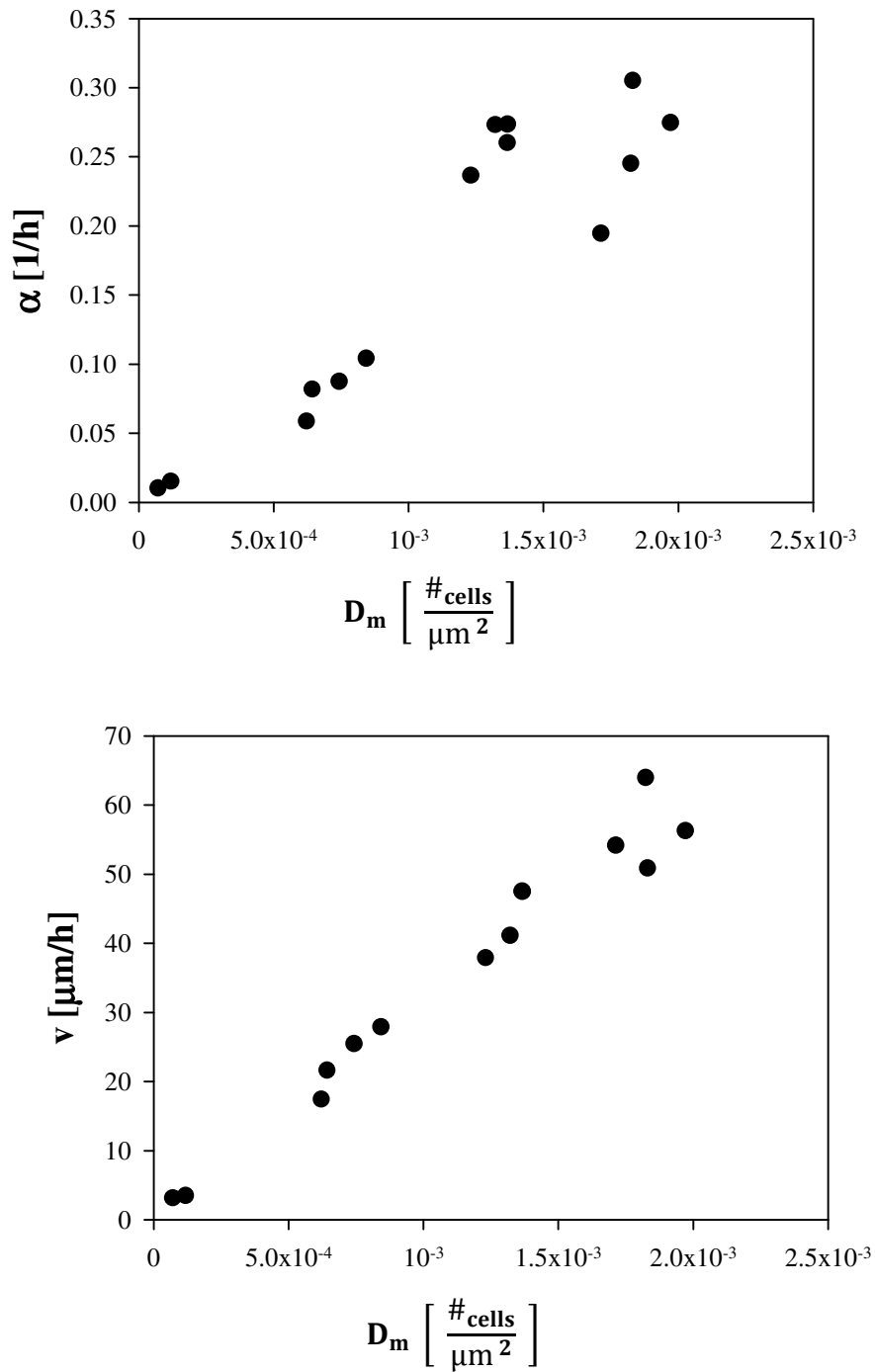


Figure 4.9: The wound closure velocity (α) and the velocity of cell front progression (v) are plotted as a function of the cell density at time 0, for the WH experiment performed in presence of mitomycin-C.

4. Conclusion

We revisited the methodological approach typically used to quantify the wound closure dynamic in a WH assay, by using a novel approach based on transport phenomena concepts. In order to investigate the potential effect of cell density on the wound healing process, we performed WH experiments on a population of HT1080 fibrosarcoma cells by using *in vitro* time-lapse microscopy technique.

We assessed that the relative cell confluence in the region where the scratch is made, is challenging to control and reproduce within the same culture dish and among different cell samples. This factor may influence the outcome of the WH assay, strongly limiting the reproducibility of the experiments and making the comparison between different cell samples very difficult.

In order to overcome the effect of cell density on wound closure velocity, we proposed a phenomenological scaling of the experimental data. This approach can be useful to avoid to trash the experiments when the samples under investigation exhibit different cell densities. The difficulty to obtain the same cell density in the samples can be due to anisotropies in the spatial spreading of the cells, led by uneven cell attachment in the culture dish after plating. In addition, it is arduous for the operator to plate exactly the same number of cells in different culture dishes. Several cell treatments, involving the use of invasive techniques such as gene silencing, may also determine unwanted cell detachment from the bottom of the plates or cell death.

Our future work will be addressed to rationalize the analysis and description of the wound healing process, taking into account the parameters involved in the wound closure kinetic. We will model the healing process of a wound using mathematical equations, which describe the main mechanisms involved, i.e., cell movement and proliferation. Mathematical descriptions of the wound healing assay are typically based on the Fisher-Kolmogoroff equation, which describes the cell density evolution in time as a function of cell motility, described by a diffusive flux, and cell proliferation, modeled by a logistic growth [155]. We will test the sensitivity of the parameters involved in the model by using a simulative approach and compare the numerical solutions obtained by the simulations with the experimental data.

Chapter 5

Dynamics of monolayer formation in T84 epithelial cells

1. Introduction

The movement of cell groups, sheets or strands, also known as Collective Cell Migration [56], plays a key role in several physiological as well as pathological processes including morphogenesis, tissue repair, immune response, and cancer progression [59-61]. In tumour invasion, collective cell movement allows malignant tumour cells to escape the primary tumour and invade surrounding tissues [2, 3].

Similarly to single-cell migration, collective cell movement results from actomyosin polymerization and contractility coupled to cell polarity [57]. However, collective movement occurs under additional constraints, determined by cell-cell junctions [57, 58]. The main features of collective cell dynamics are direct cell-cell chemical signaling, physical interactions leading to mechanical integrity of clusters, the organization of follower cells guided by leader cells located on cluster edges, the coordinated polarization of leader cells, the secondary remodeling of the extracellular matrix along the migration track (Rorth, 2009). Traction force mapping shows long-range force transmission within sheets or clusters in a cooperative way; each cell, at the leading edge as well as inside, takes part in a global “tug-of-war” that maintains the collective into a global state of tensile stress (X. Trepat, 2009; B. Ladoux, 2009). Physical signals from the substrates tend to induce a migration of cells away from each other, whereas a stronger mechanical input from cell-cell interactions would drive them towards each other. Thus the importance of cell-cell junctions in the force transmission requires a cell sheet to transmit physical forces in a cooperative way [21, 73].

Collective cell dynamics are also characterized by the expansion of cell clusters driven by the proliferation process within the collective structures. Daughter cells seem to occupy, on average, twice the area of their mother cell and the rate of colony growth should match exactly the rate of cell mitosis. Some articles support that cell groups grow follow a simple exponential growth law [76, 83].

Moreover, cell aggregation events may occur in collective behavior, as cell clusters may diffuse and grow until they meet to form new larger aggregates. Cell aggregation is the result of the attractive interaction between individual cells [85] as well as cell groups that migrate in response to chemical signals released and detected by themselves, through chemotactic

mechanisms. As the coalescence of coagulating objects, the fusion of two contiguous cell aggregates may be driven by interfacial tension and inhibited by viscosity [89, 90]. An interesting approach of this phenomenon is based on the analogy with case of drops of fluid surrounded by an immiscible matrix, that deform [208], retract to the spherical unperturbed shape, or coalesce [91, 227].

Collective cell dynamics can be observed in epithelial tissues. Although epithelia are generally considered as a constrained environment where cells are fixed in position, it has been appreciated that morphogenesis in early embryos, for example, can involve cell movements within a tissue sheet [64]. Dramatic net tissue morphogenesis can occur when many cells in a tissue rearrange in a highly coordinated way, thus highlighting the ability of cells within an epithelium to move relative to one another while retaining tissue integrity [2].

Despite the importance of collective cell migration, far less is known about exactly how cells migrate in a collective and coordinate way [62]. A better understanding of the underlying behaviors during collective cell movement will provide insight into morphogenesis and tissue reorganization during regeneration and disease. Furthermore, the ability to control collective migration will provide novel tools for engineering [63].

In order to reach a better understanding of collective cell behaviors, we used T84 intestinal epithelial cells as a model system. The epithelial lining of the intestinal lumen provides an essential barrier to diffusion of noxious agents [228]. Effective repair of injuries in such barrier is a process of strong physiopathological relevance. In addition, T84 epithelial cells show the characteristics of collective cell dynamics.

In order to dynamically investigate *in vitro* the collective behavior of T84 epithelial cells on a 2D substrate, we performed time lapse microscopy experiments. We analyzed the growth of isolated clusters of T84 cells, the spreading of cell aggregates to form a monolayer and the dynamic behavior of the single cells within the aggregates.

2. Materials and Methods

2.1. Cell cultures

Human colon adenocarcinoma T84 cells were cultured in Dulbecco's Modified Eagle Medium (DMEM) F12 supplemented with 10 % (v/v) Fetal Bovine Serum (FBS) and antibiotics (50 units/mL penicillin and 50 µg/mL streptomycin) and maintained in a humidified incubator at 37 °C under an atmosphere of 5 % CO₂ in air.

2.2. Experimental methods

T84 cells were plated on multi-well culture dishes at varying initial cell density. The multi-well plate was placed on the stage of an inverted microscope equipped with motorized sample positioning and focusing. The microscope was enclosed in a plastic cage to control environmental conditions (temperature: 37°C, CO₂ concentration: 5%, humidity level: close to saturation). Live cell imaging was performed in phase contrast by a high resolution monochromatic CCD video camera. Microscope operations were controlled by a time-lapse software allowing to select multiple fields of view and the time interval between consecutive image acquisitions during the experiment. To follow T84 collective behavior, images were iteratively acquired using a 5x objective at several locations within the culture dish, with an image acquisition frequency of 2 h; the overall experimental duration was 14 days. The cells were rinsed with fresh culture medium every two days, while the culture dish was under the microscope.

In order to capture the dynamic behavior of individual cells within the aggregates, images were iteratively acquired using a 20x objective. The time delay between the acquisition of consecutive images was 10 min, for a total of 70 h. Images were stored on a hard drive for subsequent offline analysis.

2.3. Image analysis

The number of cells within the clusters was determined using the image analysis software Image ProPlus, which allowed to manually count the cells in a selected region. The same software was used to measure the size of individual cells or colonies, by manually drawing their contour.

The trajectories of individual cells within the clusters were reconstructed using a cell tracking software (ImageJ). For each time step, individual cells were individually followed to determine the X and Y coordinates of the center of mass. The trajectory of each cell was reconstructed for the whole experiment starting from the center of mass coordinates. In order to quantify the movement of the cells in the clusters, the radial (V_{ρ}) and angular (V_{θ}) velocity of the cells were calculated for 12 h. V_{ρ} and V_{θ} were calculated in intervals of 2 h, as the ratio between the displacement along the radial and the angular direction, respectively, and the time interval.

3. Results and discussion

In vitro time-lapse microscopy experiments were performed to investigate the dynamics of monolayer formation in T84 epithelial cells, which show the features of collective cell migration.

Preliminary observations show that at early times T84 cells are arranged in 2D clusters or islands of different area depending on the initial cell density. As time goes on, the clusters tend to grow by cell proliferation and to fuse together leading to the formation of larger clusters or eventually of a single cell monolayer spanning the entire available surface. We analyzed the growth of isolated clusters of T84 cells, the spreading of cell aggregates to form a monolayer and the dynamic behavior of the single cells within the aggregates.

In Figure 5.1 the number of T84 cells (n) within several clusters is shown as a function of time. Some articles support that the cells within collective structures grow exponentially through the following law:

$$n(t) = n_0 * 2^{(t/t_d)} \quad (5.1)$$

where t is the time, $n(t)$ the number of cells at time t , n_0 the number of cells at time 0 and t_d the duplication time of the cells [84]. Eq. (5.1) was fit to the experimental data of the number of cells as a function of time, with t_d as the only adjustable parameter. The exponential fitting curve is also plotted in the graph in Figure 5.1. The duplication time of the cells within the clusters was 71 h.

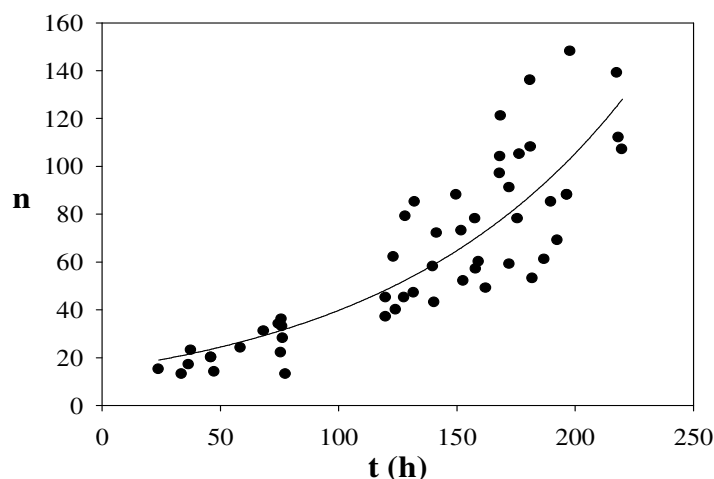


Figure 5.1: Dynamic evolution of the number of cells within the clusters. The number of cells (n) is reported as a function of time. An exponential fit is also plotted.

We also investigated the dynamic evolution of the cell size within the clusters. In Figure 5.2 the cell area (A_{cell}) is reported as a function of time. We fit the following exponential equation to the experimental data, in analogy with Eq. (5.1):

$$A_{\text{cell}}(t) = A_{\text{cell},0} * 2^{(t/\lambda)} \quad (5.2)$$

Here, t is the time, $A_{\text{cell}}(t)$ is the size of the cell at time t , $A_{\text{cell},0}$ is the size of the cell at time 0 and λ is the doubling time of the cell size. λ is the only adjustable parameter in the equation. The doubling time of the cell size was 120 h. The lower panel in Figure 5.2 shows two images of a representative cluster corresponding to 0 (A) and 10 h (B), with the contour of the same cell, taken as an example, superimposed in red.

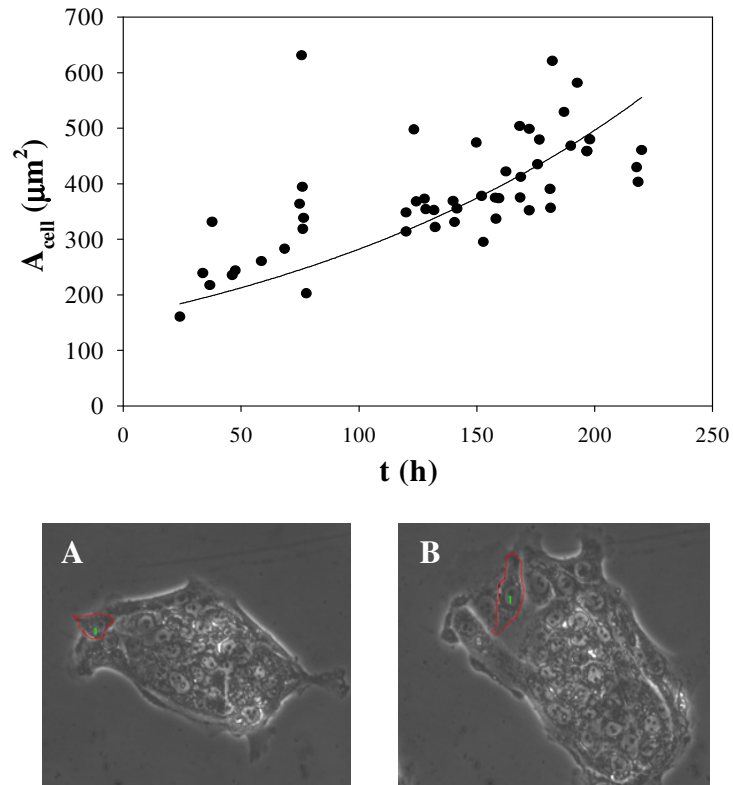


Figure 5.2: Dynamic evolution of the cell size. The area of the cells (A_{cell}) is reported as a function of time. An exponential fit is also shown. Two images of a representative cluster, corresponding to $t = 0$ (A) and $t = 10$ h (B) are shown. The contour of the same cell is superimposed in red in both the images.

Then, we investigated the relationship between the size of the whole clusters and the number of cells contained. In Figure 5.3 the number of cells (n) within the aggregates is reported as a function of the cluster size (A_{cluster}). We found that the number of cells linearly increases with the colony size. However, this linear relationship is not valid for higher values of cluster size.

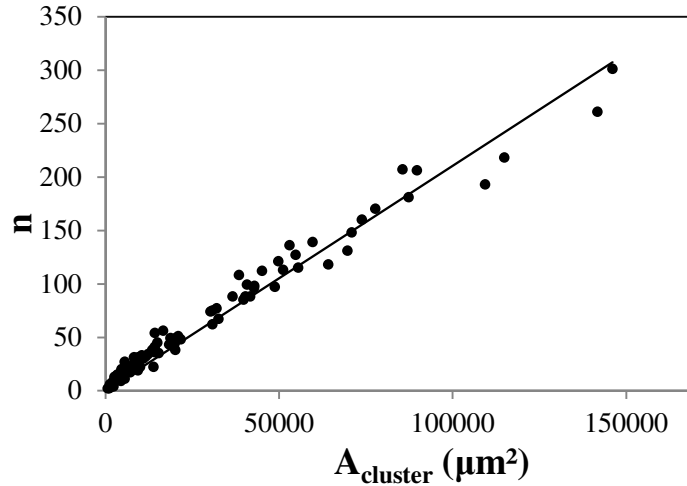


Figure 5.3: The number of cells (n) within the cluster is reported as a function of the cluster area (A_{cluster}). A linear fit is also reported.

In order to study the growth of the aggregates, we measured the area of the clusters as a function of time (Figure 5.4). Similarly to the number of cells and the cell area, cell cluster growth follows a simple exponential law, in agreement with cell population balances. Assessed the linear relationship between the number of cells and the aggregate size, we fit the following equation to our experimental data, in analogy with Eq. (5.1):

$$A_{\text{cluster}}(t) = A_{\text{cluster},0} * 2^{(t/\beta)} \quad (5.3)$$

Here, t is the time, $A_{\text{cluster}}(t)$ is the size of the aggregate at time t , $A_{\text{cluster},0}$ is the size of the aggregate at time 0 and β is the doubling time of the aggregate size, with β as the only adjustable parameter. The lower panel in Figure 5.4 shows two images corresponding to 0 (A) and 24 h (B), with the contour of the same representative cell aggregate superimposed in red. The doubling time of the colony size was 46 h.

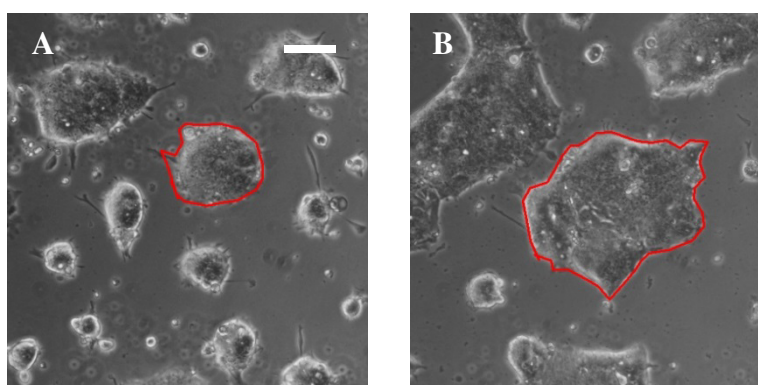
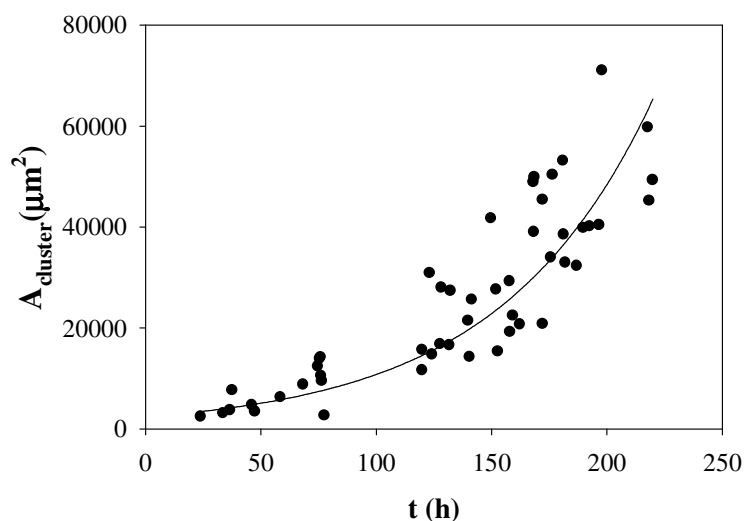


Figure 5.4: Cell cluster evolution in time. The area of the aggregates (A_{cluster}) is reported as a function of time (t). An exponential fit is also plotted. Two images of the clusters, corresponding to 0 (A) and 24 h (B) are shown. The contour of the same cell aggregate is superimposed in red in both images. Scale bar = 200 μm .

We observed that cell clusters grow and fuse together leading to the formation of larger aggregates and then of a continuous cell monolayer spanning the entire well surface. We investigated the dynamics of monolayer formation on a culture dish for T84 cells. The cells were plated at different cell densities on a multi-well culture dish and their spreading was dynamically observed by using time-lapse microscopy. We calculated A_s as the ratio between the area occupied by the cells in the image for each time step and the size of the image. This was a measure of cell confluence in time. In Figure 5.5, A_s is reported as a function of time for different cell samples corresponding to different initial cell densities. Overall, the curves follow an exponential trend up to 100% confluence. This suggests that cell confluence evolution in time shows the same behaviour of cell clusters growth. The lower panel in Figure 5.5 shows three images of cell spreading corresponding to 0 (A), 80 (B) and 160 h (C); the

area occupied by the cells is superimposed in red. The doubling time of the colony size was 46 h.

In Figure 5.6 all curves are reported as a unique data series; we fit the following equation to our experimental data, in analogy with Eq. (5.3):

$$As(t) = As_0 * 2^{\frac{t}{\tau}} \quad (5.4)$$

where t is the time, $As(t)$ is the confluence at time t , As_0 is the confluence at time 0, and τ is the doubling time of cell confluence, with τ as the only adjustable parameter. The characteristic growth time of the cell line (τ) was 50.8 h.

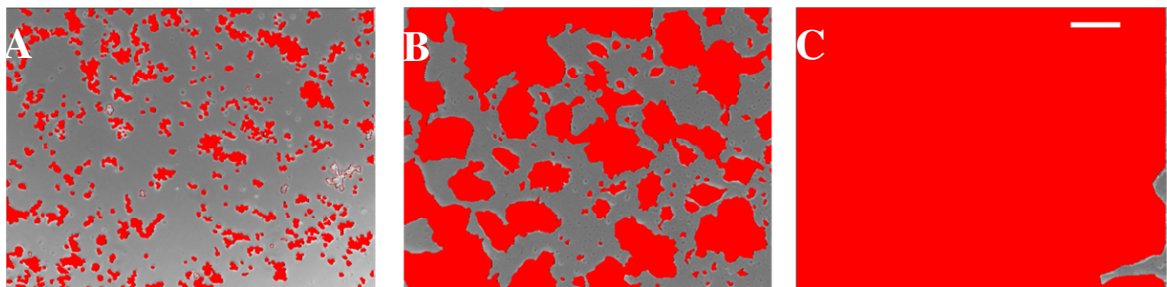
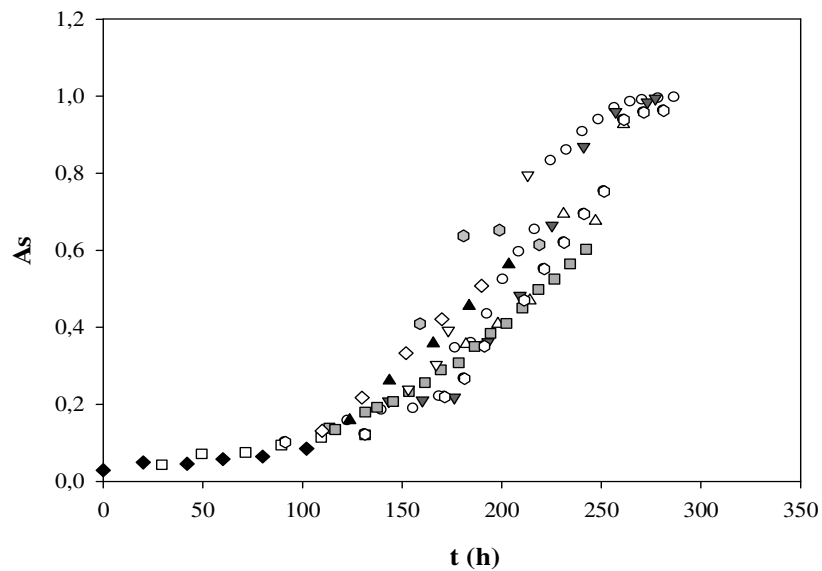


Figure 5.5: Dynamics of monolayer formation for different initial cell densities. Cell confluence (As) is reported as a function of time for each sample under investigation. Images of monolayer spreading at 0 (A), 80 (B) and 160 h (C) are shown, with the area occupied by the cells reported in red. Scale bar = 200 μm .

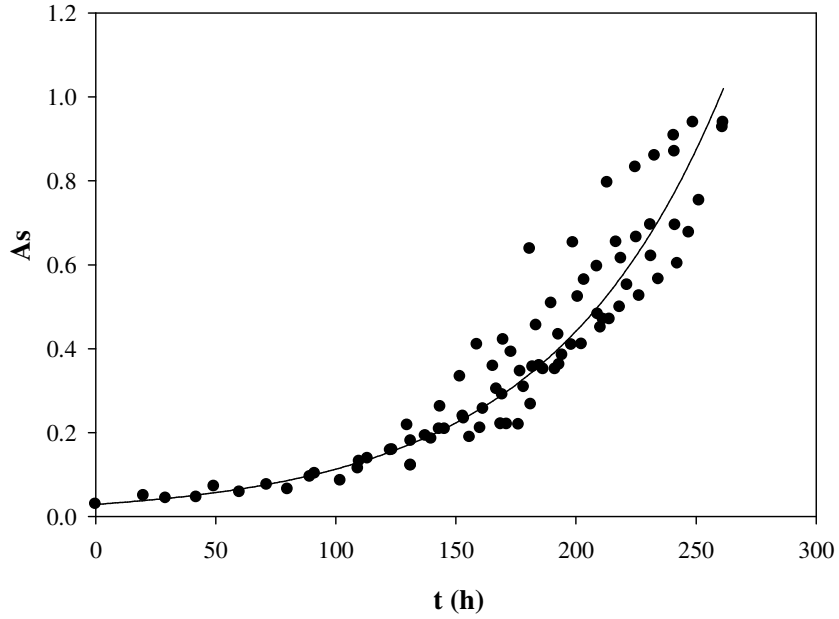


Figure 5.6: Dynamics of monolayer formation. Cell confluence (A_s) is reported as a function of time. All curves in Figure 5.5 are reported as a unique data series. An exponential fit is also shown.

Our data show that T84 cells monolayer formation is determined by cell proliferation mechanism, led by the exponential growth of the number of cells, as well as of the cell area. The characteristic growth time (τ) of the cell line under investigation can be estimated using the duplication time of the cells (t_d) and the doubling time of the cell size (λ), according to the following mathematical approach:

$$A_s(t) = n(t) * A_{cell}(t) \quad (5.5)$$

Considering Eq. (5.1) and Eq. (5.2), we obtained

$$A_{S_0} * 2^{(t/\tau)} = n_0 * 2^{(t/t_d)} * A_{cell,0} * 2^{(t/\lambda)} \quad (5.6)$$

Moreover

$$A_{S_0} = n_0 * A_{cell,0} \quad (5.7)$$

As a consequence, we obtained the following equation:

$$\tau = \frac{t_d * \lambda}{t_d + \lambda} \quad (5.8)$$

The characteristic growth time of the cell line (τ), estimated according to Eq. (5.8) was about 40 h. This estimate is comparable to the characteristic growth time estimated by the experimental data using Eq. (5.4).

Overall, our results suggest that the growth of the cell line under investigation is not dependent on the aggregation events between adjacent clusters; in fact, the growth of individual colonies as well as the spreading of the monolayer follows the same exponential law. Cell clusters aggregation seems to be due only to cluster growth, that lead close clusters accidentally to merge, and not to clusters active interactions, since clusters' motility is limited. However, it's worth mentioning that the extension of lamellipodia and filopodia-like structures exploring the surrounding environment can be observed; such membrane protrusions are preferentially directed towards nearby cell clusters.

We also investigated in details the dynamic behavior of individual T84 cells within aggregates with varying morphology and size. The aggregates were typically divided into concentric regions, in order to identify differences in the movement of the cells in the inner and outer region of the same colony. We tracked the positions of the cells moving in an almost circular aggregate with an average radius of 84 μm and an aspect ratio (minor axis/major axis ratio) about 0.83. The cluster was divided into 2 regions, the inner one containing all the cells within 46 μm from the cluster center, the external one containing the peripheral cells. In Figure 5.7, the paths of the cells moving in the outer (A and B) and inner (C and D) region are plotted starting from the same initial position (Figure 5.7.A and 5.7.C) or from their real position (Figure 5.7.B and 5.7.D). The trajectories described by the cells in both regions show a circular shape, suggesting that the cells generate a coordinate collective rotation within the aggregate.

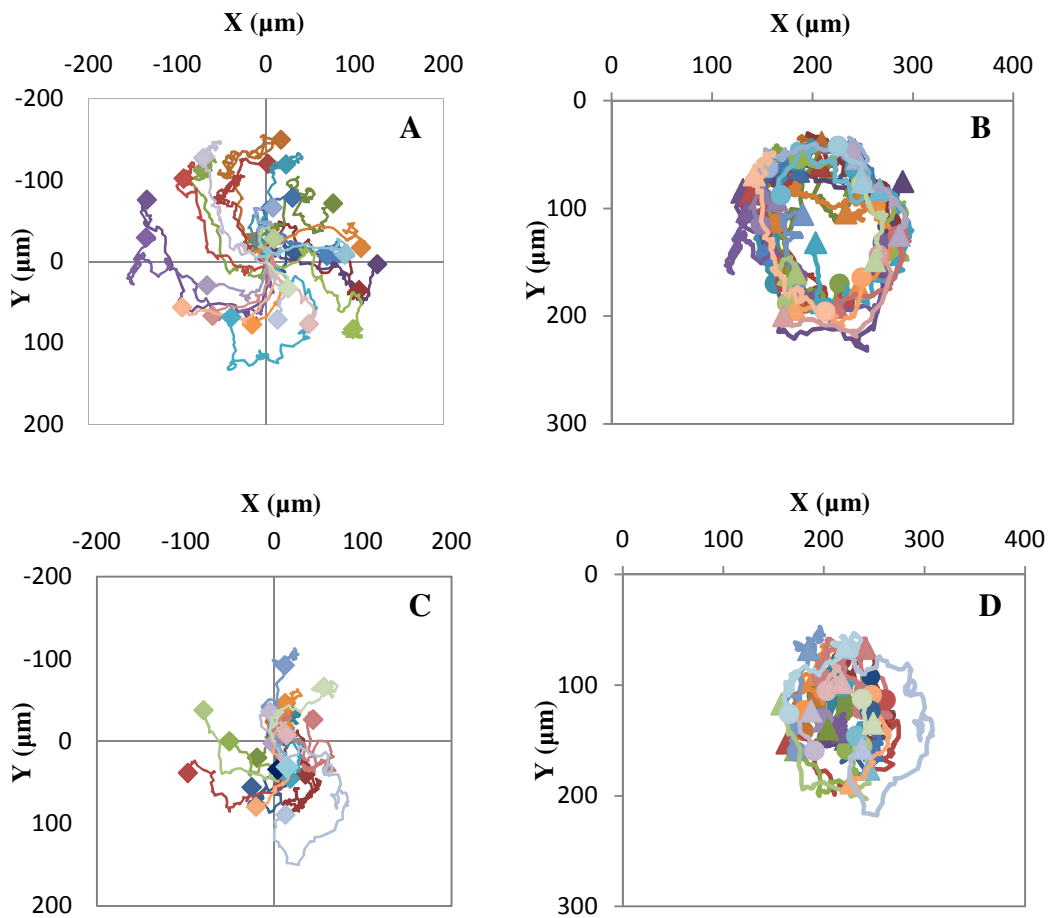


Figure 5.7: Trajectories of the cells moving in the outer (A, B) and inner (C, D) region of a cluster with an average radius of $84 \mu\text{m}$ and an aspect ratio around 0.83.

In order to quantify the movement of the cells in the cluster, we calculated the radial (V_ρ) and angular (V_θ) velocity of the cells moving in the two regions for 12 h. The radial and angular velocity of the cells moving in the outer region are plotted as a function of time in Figure 5.8.A and 5.8.B, respectively. The radial and angular velocity of the cells moving in the core region of the aggregate are reported as a function of time in Figure 5.8.C and 5.8.D, respectively.

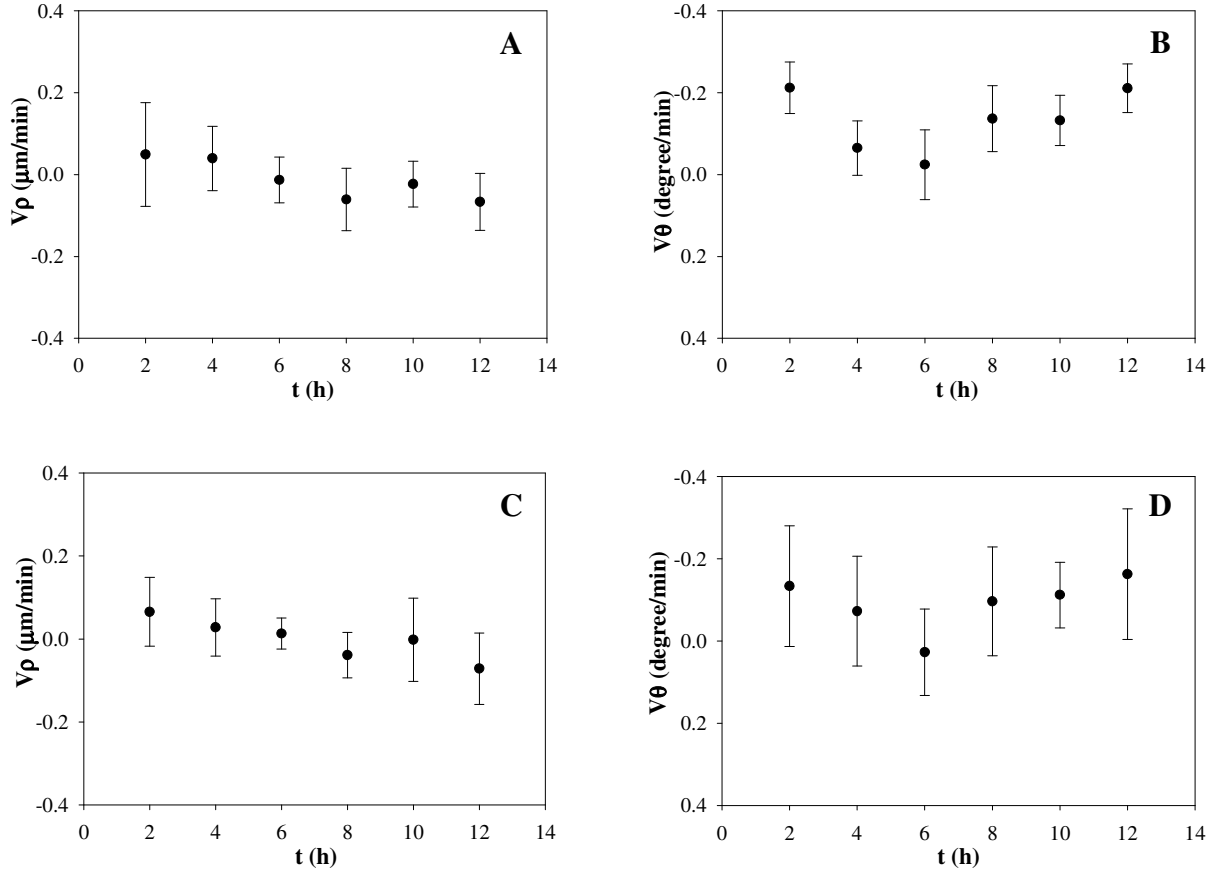


Figure 5.8: Evolution in time of the radial (V_ρ) and angular (V_θ) velocity of the cells moving in the outer (A, B) and inner (C, D) region of a cluster with an average radius of $84 \mu\text{m}$ and an aspect ratio around 0.83. Error bars represent the standard deviation.

Our data suggest that the movement along the radial direction of the cells in the outer as well as in the inner region of the colony is negligible, since the radial velocity is around 0. This means that the cells move within the cluster in a defined circular region. In other words, the cells migrating along the edge of the aggregate do not invade the core region, and vice versa.

The cells moving in the outer region of the colony show higher angular velocity compared to the cells in the aggregate core; moreover, they show a higher coordination in the rotatory movement as suggested by the lower amplitude of the error bars. Anyway, the time evolution of the angular velocity of the cells on the margin and in the core region of the colony exhibit the same trend, suggesting that probably the outer cells tug the inner ones and coordinate their rotatory movement.

Furthermore, we tracked the positions of the cells moving in a colony with an aspect ratio of 0.65, meaning that this cluster show a less circular shape. Also in this case, the cluster was divided into 2 regions, the inner one with an average radius of $38 \mu\text{m}$. In Figure 5.9, the paths

of the cells moving in the outer (A and B) and inner (C and D) region are plotted starting from the same initial position (Figure 5.9.A and 5.9.C) or from their real position (Figure 5.9.B and 5.9.D). In this case, the trajectories described by the cells seem to show a random orientation.

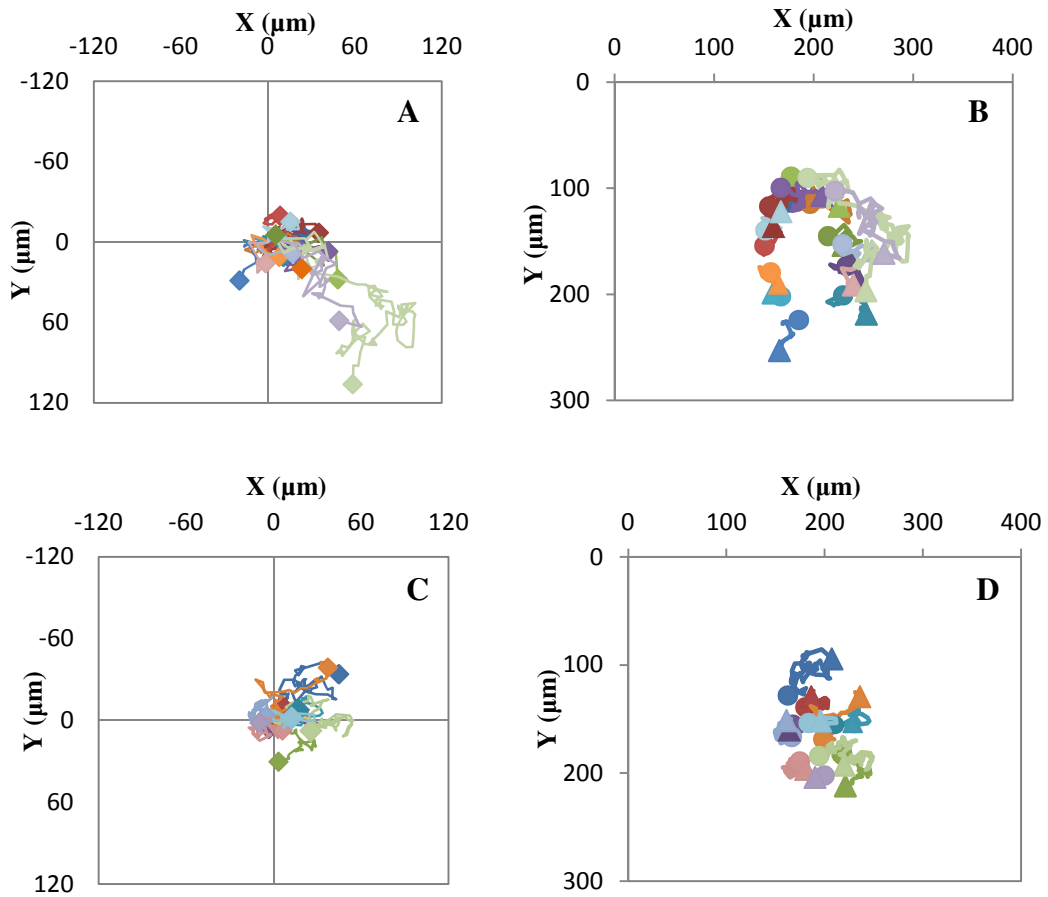


Figure 5.9: Trajectories of the cells moving in the outer (A, B) and inner (C, D) region of a cluster with aspect ratio around 0.65.

The (V_p) and angular (V_θ) velocity of the cells moving in the outer region are plotted as a function of time in Figure 5.10.A and 5.10.B, respectively. The radial and angular velocity of the cells moving in the core region of the aggregate are reported as a function of time in Figure 5.10.C and 5.10.D, respectively.

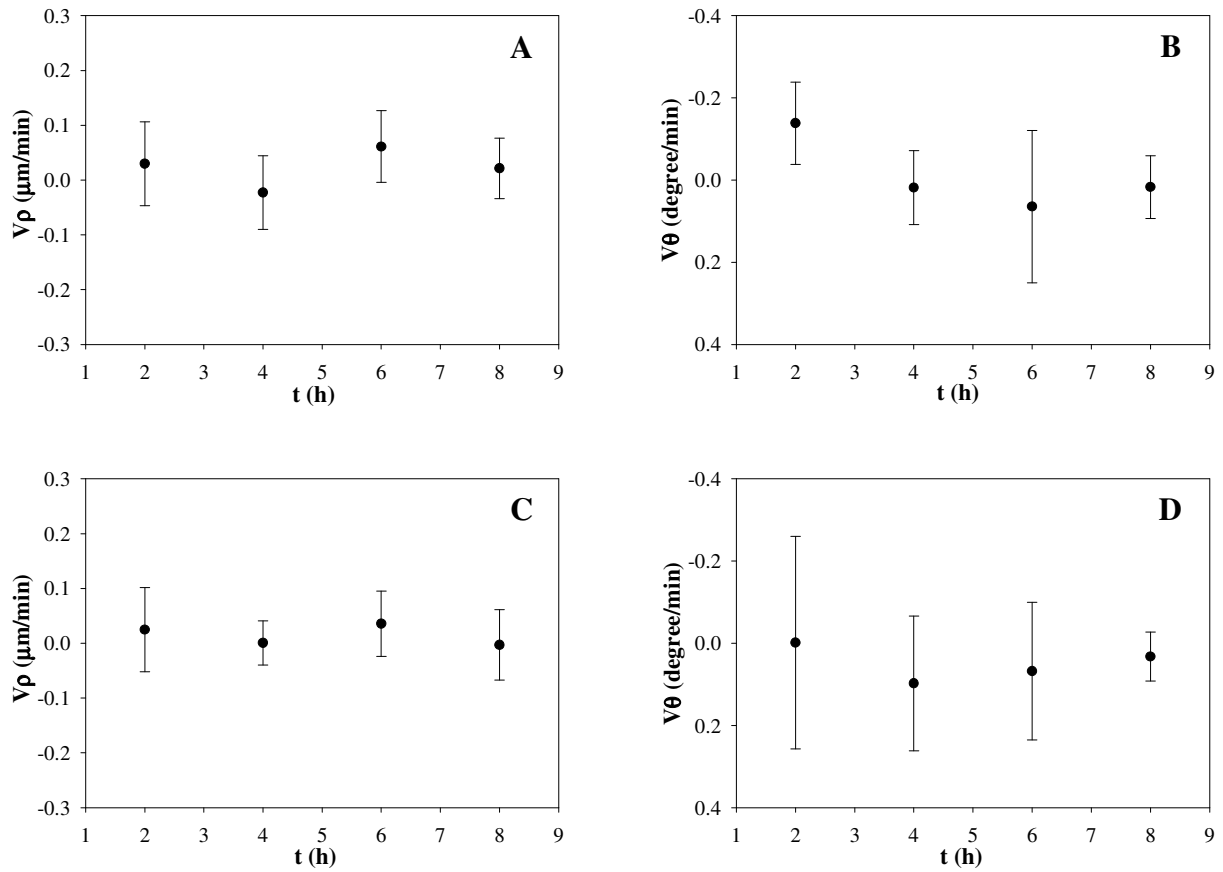


Figure 5.10: Evolution in time of the radial (V_ρ) and angular (V_θ) velocity of the cells moving in the outer (A, B) and inner (C, D) region of a cluster with aspect ratio around 0.65. Error bars represent the standard deviation.

The graphs in Figure 5.10 suggest that there is no synchronized rotation of cells in a cluster which doesn't show a round morphology. This may be probably related to the fact that the aggregate does not have a circular morphology, or cell positions must be tracked for longer time. However, the movement of the cells in both outer and inner region of the colony along the radial direction is negligible, since the radial velocity fluctuates around 0, meaning that the cells move in a confined region within the cluster.

4. Conclusions

In this study, we performed *in vitro* time-lapse microscopy experiments to investigate the dynamics of monolayer formation in T84 intestinal epithelial cells, which show the features of collective cell migration. We analyzed the growth of isolated clusters of T84 cells, the spreading of cell aggregates to form a monolayer and the dynamic behavior of the single cells within the aggregates.

Preliminary observations show that at early times T84 cells are arranged in 2D clusters or islands with different size, depending on the initial cell density. As time goes on, the clusters tend to grow because of cell proliferation mechanism and to fuse together, leading to the formation of larger clusters or eventually of a single cell monolayer spanning the entire available surface.

Our results suggest that the growth of the cell line under investigation is driven by cell proliferation as well as by the expansion of cell area. As a consequence, aggregation events between adjacent clusters seems to not play a central role in monolayer formation, since the growth of individual cell colonies and the spreading of the monolayer follow the same exponential law. Cell cluster aggregation seems to be driven by the cluster growth, whose fusion is due to accidental contact once the free space is reduced. In fact, the clusters show very low motion. However, it's worth mentioning that the extension of lamellipodia and filopodia-like structures exploring the surrounding environment can be observed; such membrane protrusions are preferentially directed towards nearby cell clusters. Further investigations are necessary to elucidate this aspect.

In addition, we analyzed in details the migration of individual T84 cells within aggregates with varying morphology and size. We observed that in colonies showing a round morphology, the cells move in a defined circular region. In fact, the cells migrating along the edge of the aggregate do not invade the core region, and vice versa. We also found a synchronized rotation of cells within the aggregate. The coordination in the rotatory movement seems to be higher for the cells located in the outer regions of the clusters; we can speculate that the outer cells drive and coordinate the movement of the cells located in the core of the aggregates along circular paths. The coordinated rotational movement of the cells in colonies with a round shape has been already shown in previous works [81, 229]. Conversely, we observed a random orientation of cell trajectories in aggregates that do not show a circular morphology. In this case, we didn't find a coordinated and collective rotational movement of the cells. However, the movement of the cells was confined in a defined region within the cluster, as well.

Further investigations will be necessary to confirm these findings and reach a better understanding of the collective dynamic behavior of T84 epithelial cells.

Chapter 6

From single cells to cell aggregates chemotaxis

The experiments described in this chapter were performed at the Institut Curie in Paris, in the framework of the research project “Cell migration and invasion” in the Cell Biology Department directed by Dr. Bruno Goud, under the supervision of Danijela Matic Vignjevic. The experiments were carried out using a chemotaxis chamber projected by Prof. Stefano Guido and Prof. Sergio Caserta, at the University “Federico II” of Naples.

1. Introduction

The ability of the cells to migrate as single units or as multicellular structures (Collective cell migration), is central to tumour invasion and dissemination. In metastatic cancer, tumour cells showing a malignant phenotype escape the primary tumour, and invade adjacent or distant tissues where proliferate forming secondary tumours [10]. In order to reach the blood vessels, cancer cells encounter different ECMs during their course of invasive migration. First, they breach the basement membrane, a thin and dense sheet-like structure composed of a network of collagen IV and laminin [230]. Then, they migrate through the stroma composed of fibrillar collagens, proteoglycans and various glycoproteins [231].

Chemotaxis, i.e. the directional movement of cells along a chemical concentration gradient [14, 15], is crucial in tumour dissemination during progression and metastasis, since it determines that cancer cells explore the surrounding microenvironment in response to external cues. In fact, to successfully metastasize, tumour cells must invade, intravasate, extravasate and grow at a distant site. Chemotaxis is thought to be involved in each of these crucial steps of tumour cell dissemination [13]. The chemotactic behavior of cancer cells and tumour-associated inflammatory and stromal cells is mediated by a complex network of chemokines and growth factors [232].

The chemotactic mechanisms by which invasive tumour cells respond to tissue-derived guidance cues is poorly understood and complicated by the fact that, in order to disseminate, tumour cells can utilize a flexible set of migration modes, frequently referred to as migration plasticity [65, 233]. For such reason, the development of physiologically relevant *in vitro* assays to study chemotaxis in a quantitative way is a topic of growing interest.

Even though the vast majority of *in vitro* studies on cell movement are performed on cells cultured on flat substrates, there is growing evidence that 2D cell cultures fail to reproduce the

architecture of living tissues, and may thus bias the cellular response to external cues or cell-integrated signals [234]. In order to overcome the limitations of 2D cell cultures and avoid systematic animal testing, multicellular spheroids (MCSs), i.e. small spherical clusters of cancer cells, have been proposed as 3D *in vitro* models of avascular solid microtumours [235]. Additionally, MCSs embedded in ECM-like gels have been further used to investigate the mechanisms of cell invasion [236]. These MCS-based assays represent a promising approach in the biomedical research for studying tumour development, given the diffusion limited geometry associated with many solid tumour growths. The formation of a MCS is generally performed using conventional methods, such as the hanging drop method, gyratory rotation, or liquid overlay cultures [237]; the main drawbacks of these techniques are their low yield as well as the difficulty in controlling the size of the cell aggregates. The advent of microscale photolithography has led to automate MCS production using microwells [238], microarrays [239], or microfluidic devices [240]. Recently, a simple and reproducible microfluidic method has been developed to prepare size-controlled spheroids. This technique is based on the encapsulation and growth of cells inside permeable, elastic, hollow microspheres [241].

Here, we tested the chemotactic potential of a tumour cell line, comparing the chemotactic behavior of single cells and spheroids of these cells, in response to concentration gradients of serum and Hepatocyte growth factor (HGF). We used wild-type CT26 mouse colon carcinoma cells as a model system. *In vitro* 3D chemotaxis assays were performed by using a recently developed direct-viewing chamber [129], coupled to a time-lapse video microscopy workstation. In this chamber a chemoattractant concentration gradient in 3D collagen gel samples seeded with cells or cell clusters is generated by diffusion through a porous membrane.

2. Materials and Methods

2.1. Cell cultures and cell spheroids preparation

CT26 mouse colon carcinoma cells (ATCC CRL-2638; American Tissue Culture Collection) were maintained in DMEM (Invitrogen) supplemented with 10% (vol/vol) FBS (Invitrogen) and antibiotics (100 µg/mL streptomycin and 100 U/mL penicillin; Gibco BRL) in a humidified atmosphere containing 5% CO₂ at 37 °C, with medium changed every 2 days.

CT26 spheroids (1.5 x 10⁵ cells for each spheroid) were prepared according to the classical agarose cushion technique [242].

2.2. Chemotaxis chamber

Chemotaxis assays were performed by using a chamber [129, 132] consisting of a single aluminium or steel block glued on top of a microscope slide by using a silicone adhesive. A porous membrane (0.22 μm pore size), sandwiched between two rectangular metal frames, separates two compartments, one for the cell seeded collagen gel (sample well), and the other as a reservoir of the chemoattractant solution (chemoattractant reservoir). During the assay the chemoattractant, loaded in the reservoir, diffuses through the membrane and generates a concentration gradient in the cell seeded collagen gel.

The chemoattractant concentration profile in the collagen gel can be described according to the model of Fickian diffusion in a semi-infinite slab [132]:

$$C(x,t) = \frac{C_0}{2} \left[1 - \operatorname{erf} \left(\frac{y}{\sqrt{4Dt}} \right) \right] \quad (1)$$

where $C(x,t)$ is the chemoattractant concentration as function of the space x and time t , C_0 is the initial concentration in the chemoattractant reservoir, D is the diffusion coefficient of the molecule in the collagen gel.

2.3. Sample preparation

Chemotaxis assays were performed in a three-dimensional gel of 2 mg/mL collagen I solution (BD Biosciences) in 10x PBS and DMEM; 1 M NaOH was added to adjust the pH of the solution (around 7).

For single cells chemotaxis assays, 0.5 % FBS was added to the collagen gel solution; all components were kept on ice during the preparation, except for the cell suspension that was added at the end (1.5×10^5 cells/mL). The solution was placed in the sample well of the chamber and the chamber was incubated at room temperature for 40 min to induce collagen polymerization.

For chemotaxis assays on CT26 spheroids, 170 μL of collagen gel solution not containing spheroids were placed in the sample well of the chamber. After half polymerization of the collagen solution at room temperature for 20 min, 200 μL of collagen gel solution containing about 10 spheroids were added on top. The collagen solution was allowed to polymerize at room temperature for 40 min. At the end of the polymerization process, the spheroids, which fell down, were located at the interface between the two layers of collagen gel.

We added in the chemoattractant reservoir FBS at different concentrations (10% and 100%) or Hepatocyte growth factor (HGF) 10 or 100 ng/mL.

2.4. Imaging by time-lapse microscopy

Time-lapse imaging was performed by using an inverted microscope (Nikon Eclipse Ti, 10×/0.3-N.A. dry objective; Nikon Instruments) equipped with a motorized stage (Märzhäuser) and climate control system (The Brick; Life Imaging Systems). The microscope and the video-camera (CoolSNAP HQ2; Photometrics) were driven by Metamorph software (Molecular Devices). The frequency of acquisition was set to 1 frame every 30 min and the total experiment length was 48.

For single cells experiments, images in the sample well of the chemotaxis chamber were acquired at approximately 2, 4 and 6 mm from the membrane along the y direction and at the center along the x direction. The collagen gel was periodically scanned by optically imaging 15 layers separated by a 16.7 μm distance along the focus (z) direction within the collagen gel. The lowest z layer of the image stack was chosen to be approximately 1 mm from the bottom glass to avoid possible wall effects (such as surface-induced local orientation of collagen fibers).

For experiments on CT26 spheroids, all the aggregates in the sample well of the chemotaxis chamber were imaged periodically scanning 5 layers separated by a 50 μm distance along the focus (z) direction within the collagen gel.

3. Results and Discussion

We investigated the chemotactic potential of CT26 mouse colon carcinoma cells, comparing the chemotactic behavior of single cells and spheroids of these cells in a three-dimensional collagen gel, in response to concentration gradients of serum and Hepatocyte growth factor (HGF) in different concentration. *In vitro* 3D chemotaxis assays were performed by using a recently developed direct-viewing chamber coupled to time-lapse video microscopy technique. Here, some preliminary qualitative results are shown.

In Figure 6.1, we report images acquired within the collagen gel seeded with single cells, corresponding to the last time step ($t = 48$ h). Specifically, Figure 6.1.A and 6.1.B show CT26 cells at 2 mm from the membrane, in the assay in which FBS 100 % and 10 %, respectively, were used as chemoattractant. Figure 6.1.C shows CT26 cells at 2 mm from the membrane, in a control sample, i.e. in absence of chemotactic gradient. For comparison, we also analyzed the movement of the cells in isotropic condition, i.e. in the presence of a uniform concentration of serum (10 %) in the collagen gel (Figure 6.1.D). Visual inspection of time-lapse movies shows that in the control experiments (i.e., in absence of chemoattractant) the

cells exhibit a round morphology and do not move, as expected. In isotropic conditions, as well as in the assays with serum 100 % and 10 % as chemoattractant, the cells show an elongated morphology and are highly motile. Compared to isotropic condition, where there is no preferential directionality in cell movement, in chemotaxis assays most of the cells seem to move with a preferential orientation in the direction of the concentration gradient.

In Figure 6.2, images acquired within the collagen gel seeded with CT26 spheroids, corresponding to 48 h, are shown. Figure 6.2.A and 6.2.B report CT26 spheroids in the chemotaxis assays in which FBS 100 % and 10 %, respectively, were used as chemoattractant. Figure 6.2.C shows CT26 spheroids in a control sample, i.e. in absence of chemoattractant. For comparison, we also analyzed the movement of the cells in isotropic conditions, i.e. in the presence of a uniform concentration of serum (10 %) in the collagen gel (Figure 6.2.D). A visual inspection of time-lapse movies shows that in presence of serum, the spheroids grow becoming bigger, driven by cell proliferation mechanism. In chemotaxis assays in which serum 100 % and 10 % were used as chemoattractant, the cells migrate from the spheroids.

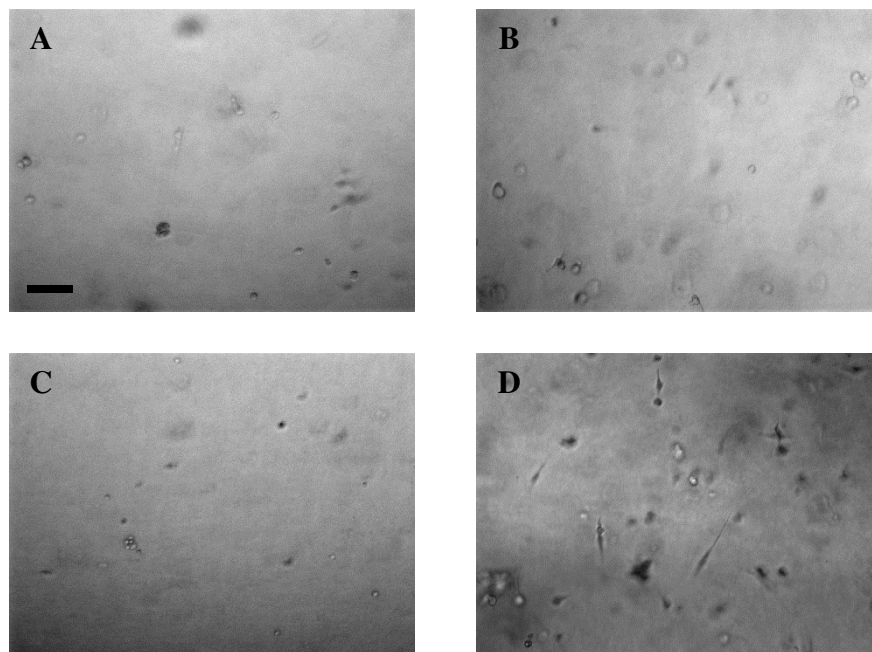


Figure 6.1: Images of CT26 cells acquired at 2 mm from the membrane, at $t=48$ h, in chemotaxis assays in which FBS 100 % (A), 10 % (B) and only culture medium (C) were used in the chemoattractant reservoir, and in isotropic conditions (D). Scale bar = 100 μ m.

However, in the experiments with 10 % serum in the chemoattractant reservoir, the cells appear more elongated and spread out. In addition, in these assays the spheroids seem to grow more compared to the chemotaxis assays with 100 % serum. In both cases, the behavior of the

cells seems to be not chemotactic, since the cells coming out from the spheroids appear uniformly distributed in space and seem to move in a random orientation (i.e., no preferential direction of motion can be distinguished), as in the experiments carried out in isotropic conditions (10% serum), which can be used as a control. Unexpectedly, also in the experiments where no chemoattractant was added, there are few cells showing the tendency to escape the spheroids; however, they do not exhibit significant movement, as they experience no appreciable change in their position in the entire experiment, and show a round morphology (Figure 6.2.C), in comparison with the assays in which the cells sense the serum.

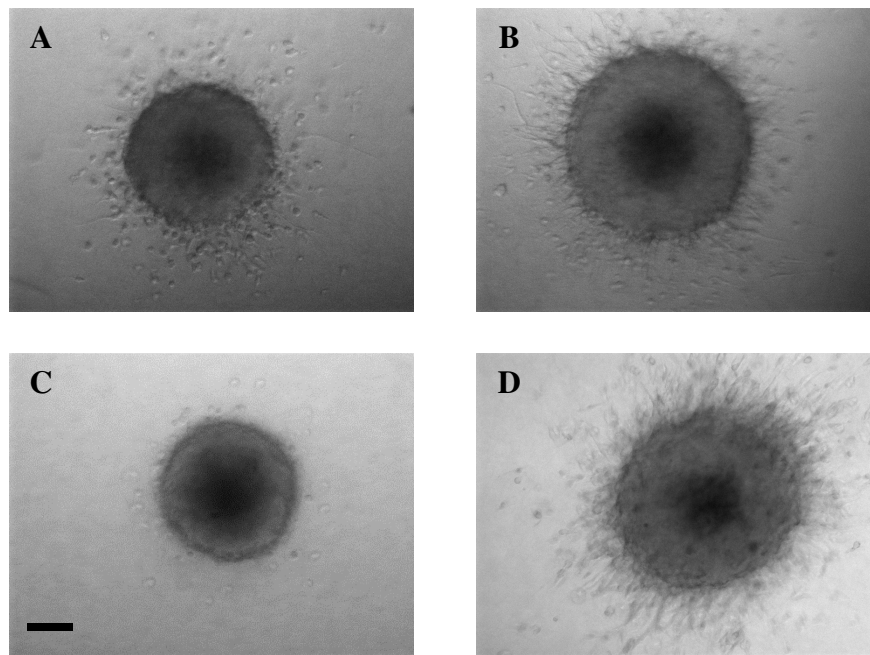


Figure 6.2: Images of CT26 spheroids within the collagen gel, at $t=48$ h, in chemotaxis assays in which FBS 100 % (A), 10 % (B) and only culture medium (C) were used in the chemoattractant reservoir, and in isotropic conditions (D). Scale bar = 100 μ m.

Overall, single cells seem to be sensitive to chemotaxis, whereas the stimulus provided by chemotaxis seem to be a minor effect for cell spheroids. In fact, in the experiments performed on CT26 spheroids, the major effect to serum sensation is the tendency of the cells to migrate from the spheroids in a random orientation, which overcomes their chemotactic behavior. Probably, the cells escape the spheroids because of the stimulus arising from the presence of collagen fibers around the spheroids. Moreover, it is possible that the steepness of the chemoattractant gradient is not strong enough to stimulate cell directional movement.

Image analysis of time-lapse sequences will be performed in order to obtain quantitative information, allowing a direct comparison between the different assays. Cell trajectories will be reconstructed by means of a semi-automated image analysis algorithm and the effect of chemotaxis will be quantitatively characterized in terms of changes in motility parameters, such as the velocity of migration and the cell orientation bias as quantified by the chemotactic index, defined as the ratio between the net movement in the direction of the gradient and the total curvilinear length of cell trajectory [214].

Chapter 7

Conclusions

A wide range of physiological and pathological phenomena, including embryogenesis, tissue repair, immune responses, tumour growth and invasion, are strongly dependent on cell proliferation and migration mechanisms. These processes govern the dynamic evolution of both individual cells and cell aggregates. The framework of cell dynamics has gained impetus in recent years and numerous ongoing research directions have been performed to develop novel *in vitro* assays for studying cell dynamic behavior. However, the current understanding of many mechanisms is still limited and cell dynamic behavior remains a challenging process to study under physiopathologically-relevant conditions *in vitro*.

This thesis work is based on the quantitative investigation of active bio-soft matter dynamics, ranging from single to collective cell dynamic behavior, by using an *in vitro* experimental approach based on live cell imaging, performed by time-lapse microscopy, and image analysis techniques, in order to provide a better understanding of many physiological and pathological processes. Live cell imaging based on *in vitro* time-lapse microscopy is a powerful methodological approach to gain insight into cell dynamics from a quantitative point of view. In fact, time-lapse microscopy allows direct visualization of biological systems during their dynamic evolution. Experiments lasting up to few weeks were performed, while controlling environmental parameters to ensure cell viability throughout the experiments.

Time-lapse microscopy was coupled to several *in vitro* assays, such as single cell random motility assays to gain quantitative information about the movement of individual cells on a planar surface or in a three-dimensional matrix, and wound healing assays to study the spreading of two cell sheets which dynamically evolve one toward the other. Additionally, collective dynamics of cell aggregates in 2D and 3D environment were investigated. We also analyzed the movement of single cells and three-dimensional cell spheroids in presence of a chemotactic stimulus; we performed chemotaxis assays by using a novel methodology for the experimental investigation of drug efficiency *in vitro* based on a chemotaxis chamber in which a concentration gradient in a collagen gel sample seeded with cells was generated by diffusion through a porous membrane.

Furthermore, we performed a direct comparison of two different experimental methods widely used in the literature for the quantification of cell motion: single cell random migration assays and wound healing assays. We found a substantial agreement between independent

quantifications of cell migration based on these assays. Our experimental observations show that the result of one assay can be estimated, at least as order of magnitude, given the result of the other, proving that the two assays are intimately linked with each other for the fibroblast populations we considered. To our knowledge this is the first, quantitative comparison of these two widely used techniques, which are not equivalent from a biological point of view.

Although cell migration assays are a valuable tool to gain insight into cell dynamic behavior, it's really complicated to obtain precise quantitative information on the dynamics of cell systems. We modeled the mechanisms governing single and collective cell dynamic evolution by using mathematical equations based on the transport phenomena approach. In fact, the use of mathematical models based on transport phenomena concepts can simplify the investigation of the dynamic evolution of active bio-soft matter. For example, a phenomenological description of cell migration is given by the Persistent Random Walk model, inspired by Brownian motion, which is associated with two parameters, i.e., the persistence time between significant changes in direction and the cell motility coefficient, analogous of a random walk diffusivity. The spreading of cell sheets in wound healing assays can be mathematically modeled using the Fisher-Kolmogoroff equation [150], which describes cell density evolution in space and time in terms of cell motility, modeled by Fickian diffusion, and proliferation, described by a logistic growth.

Overall, the main goal of this thesis work is to improve the current understanding of the mechanisms driving cell dynamics by using an interdisciplinary approach, based on chemical engineering core disciplines combined with biological, biotechnological and biomedical sciences. This is because understanding cell dynamics as an integrated process requires an appreciation of the chemical and physical mechanisms which almost certainly act in concert to regulate cell dynamic evolution. A rigorous investigation, based on the application of transport phenomena concepts, is essential to measure cell movement and proliferation indices that describe cell dynamics. For this reason, the development of such analyses is nowadays within the core business of Chemical Engineering, which can contribute to the building of mathematical models, based on the transport phenomena approach, useful to describe and predict the mechanisms driving cell dynamics. We believe that our result can be relevant for future experimental and modelling works.

Bibliography

1. Lauffenburger DA, Horwitz AF. Cell migration: A physically integrated molecular process. *Cell*. 1996;84(3):359-69. doi: 10.1016/s0092-8674(00)81280-5. PubMed PMID: WOS:A1996TV70800004.
2. Rørth P. Collective cell migration. *Annu Rev Cell Dev Biol*. 2009;25:407-29. doi: 10.1146/annurev.cellbio.042308.113231. PubMed PMID: 19575657.
3. Friedl P, Locker J, Sahai E, Segall JE. Classifying collective cancer cell invasion. *Nat Cell Biol*. 2012;14(8):777-83. doi: 10.1038/ncb2548. PubMed PMID: 22854810.
4. Khalil AA, Friedl P. Determinants of leader cells in collective cell migration. *Integr Biol (Camb)*. 2010;2(11-12):568-74. doi: 10.1039/c0ib00052c. PubMed PMID: 20886167.
5. Richardson BE, Lehmann R. Mechanisms guiding primordial germ cell migration: strategies from different organisms. *Nature Reviews Molecular Cell Biology*. 2010;11(1):37-49. doi: 10.1038/nrm2815. PubMed PMID: WOS:000272944700011.
6. McDonald B, Pittman K, Menezes GB, Hirota SA, Slaba I, Waterhouse CC, et al. Intravascular danger signals guide neutrophils to sites of sterile inflammation. *Science*. 2010;330(6002):362-6. doi: 10.1126/science.1195491. PubMed PMID: 20947763.
7. Shaw TJ, Martin P. Wound repair at a glance. *Journal of Cell Science*. 2009;122(18):3209-13. doi: 10.1242/jcs.031187. PubMed PMID: WOS:000269521900002.
8. Cristini V, Frieboes HB, Gatenby R, Caserta S, Ferrari M, Sinek J. Morphologic instability and cancer invasion. *Clinical Cancer Research*. 2005;11(19):6772-9. doi: 10.1158/1078-0432.ccr-05-0852. PubMed PMID: WOS:000232238100006.
9. Moserle L, Casanovas O. Anti-angiogenesis and metastasis: a tumour and stromal cell alliance. *Journal of Internal Medicine*. 2013;273(2):128-37. doi: 10.1111/joim.12018. PubMed PMID: WOS:000313869400004.
10. Aceto N, Bardia A, Miyamoto D, Donaldson M, Wittner B, Spencer J, et al. Circulating Tumor Cell Clusters Are Oligoclonal Precursors of Breast Cancer Metastasis. *Cell*. 2014;158(5):1110-22. doi: 10.1016/j.cell.2014.07.013. PubMed PMID: WOS:000340945000016.
11. Langer R. Biomaterials and biomedical engineering. *Chemical Engineering Science*. 1995;50(24):4109-21. doi: 10.1016/0009-2509(95)00226-x. PubMed PMID: WOS:A1995TP49700032.
12. Vital-Lopez FG, Armaou A, Hutnik M, Maranas CD. Modeling the Effect of Chemotaxis on Glioblastoma Tumor Progression. *Aiche Journal*. 2011;57(3):778-92. doi: 10.1002/aic.12296. PubMed PMID: WOS:000287104700019.
13. Roussos ET, Condeelis JS, Patsialou A. Chemotaxis in cancer. *Nature Reviews Cancer*. 2011;11(8):573-87. doi: 10.1038/nrc3078. PubMed PMID: WOS:000292998200011.

14. Franca-Koh J, Devreotes PN. Moving forward: mechanisms of chemoattractant gradient sensing. *Physiology (Bethesda)*. 2004;19:300-8. doi: 10.1152/physiol.00017.2004. PubMed PMID: 15381759.
15. Swaney KF, Huang C-H, Devreotes PN. Eukaryotic Chemotaxis: A Network of Signaling Pathways Controls Motility, Directional Sensing, and Polarity. *Annual Review of Biophysics*, Vol 39. 2010;39:265-89. doi: 10.1146/annurev.biophys.093008.131228. PubMed PMID: WOS:000278959400014.
16. Lauffenburger D. A SIMPLE-MODEL FOR THE EFFECTS OF RECEPTOR-MEDIATED CELL-SUBSTRATUM ADHESION ON CELL-MIGRATION. *Chemical Engineering Science*. 1989;44(9):1903-14. doi: 10.1016/0009-2509(89)85131-0. PubMed PMID: WOS:A1989AY11800016.
17. Veltman D. Actin dynamics: cell migration takes a new turn with arpin. *Curr Biol*. 2014;24(1):R31-3. doi: 10.1016/j.cub.2013.11.022. PubMed PMID: 24405676.
18. Ottino JM. Chemical Engineering in a Complex World: Grand Challenges, Vast Opportunities. *Aiche Journal*. 2011;57(7):1654-68. doi: 10.1002/aic.12686. PubMed PMID: WOS:000291803800001.
19. Love JC. Integrated Process Design for Single-Cell Analytical Technologies. *Aiche Journal*. 2010;56(10):2496-502. doi: 10.1002/aic.12413. PubMed PMID: WOS:000282288400001.
20. THERIOT J, MITCHISON T. ACTIN MICROFILAMENT DYNAMICS IN LOCOMOTING CELLS. *Nature*. 1991;352(6331):126-31. doi: 10.1038/352126a0. PubMed PMID: WOS:A1991FW09700045.
21. Ladoux B, Nicolas A. Physically based principles of cell adhesion mechanosensitivity in tissues. *Rep Prog Phys*. 2012;75(11):116601. doi: 10.1088/0034-4885/75/11/116601. PubMed PMID: 23085962.
22. Sarvestani AS, Jabbari E. Analysis of Cell Locomotion on Ligand Gradient Substrates. *Biotechnology and Bioengineering*. 2009;103(2):424-9. doi: 10.1002/bit.22273. PubMed PMID: WOS:000266078200019.
23. Ridley AJ, Schwartz MA, Burridge K, Firtel RA, Ginsberg MH, Borisy G, et al. Cell migration: Integrating signals from front to back. *Science*. 2003;302(5651):1704-9. doi: 10.1126/science.1092053. PubMed PMID: WOS:000186970100033.
24. Mitchison T, Cramer L. Actin-based cell motility and cell locomotion. *Cell*. 1996;84(3):371-9. doi: 10.1016/S0092-8674(00)81281-7. PubMed PMID: WOS:A1996TV70800005.
25. Sheetz M, Felsenfeld D, Galbraith C, Choquet D, Lackie J, Dunn G, et al. Cell migration as a five-step cycle. *Cell Behaviour: Control and Mechanism of Motility*. 1999;65:233-43. PubMed PMID: WOS:000079153100015.

26. Small J, Rottner K, Kaverina I. Functional design in the actin cytoskeleton. *Current Opinion in Cell Biology*. 1999;11(1):54-60. doi: 10.1016/S0955-0674(99)80007-6. PubMed PMID: WOS:000078614000006.
27. Moissoglu K, Schwarz M. Integrin signalling in directed cell migration. *Biology of the Cell*. 2006;98(9):547-55. doi: 10.1042/BC20060025. PubMed PMID: WOS:000240705800004.
28. Etienne-Manneville S, Hall A. Rho GTPases in cell biology. *Nature*. 2002;420(6916):629-35. doi: 10.1038/nature01148. PubMed PMID: WOS:000179751800036.
29. Erickson J. The C-Terminal Di-Arginine Motif of Cdc42 is Essential for Binding to Phosphatidylinositol 4,5 Bisphosphate-Containing Membranes and Inducing Cellular Transformation. *Biophysical Journal*. 2012;102(3):303A-A. PubMed PMID: WOS:000321561202127.
30. Hall A. Rho GTPases and the actin cytoskeleton. *Science*. 1998;279(5350):509-14. doi: 10.1126/science.279.5350.509. PubMed PMID: WOS:000071616000033.
31. Svitkina T, Verkhovsky A, McQuade K, Borisy G. Analysis of the actin-myosin II system in fish epidermal keratocytes: Mechanism of cell body translocation. *Journal of Cell Biology*. 1997;139(2):397-415. doi: 10.1083/jcb.139.2.397. PubMed PMID: WOS:A1997YC38600009.
32. Borisy G, Svitkina T. Actin machinery: pushing the envelope. *Current Opinion in Cell Biology*. 2000;12(1):104-12. doi: 10.1016/S0955-0674(99)00063-0. PubMed PMID: WOS:000085475200013.
33. Koestler S, Auinger S, Vinzenz M, Rottner K, Small J. Differentially oriented populations of actin filaments generated in lamellipodia collaborate in pushing and pausing at the cell front. *Nature Cell Biology*. 2008;10(3):306-U33. doi: 10.1038/ncb1692. PubMed PMID: WOS:000253778300012.
34. SMALL J, RINNERTHALER G, HINSSEN H. ORGANIZATION OF ACTIN MESHWORKS IN CULTURED-CELLS - THE LEADING-EDGE. *Cold Spring Harbor Symposia on Quantitative Biology*. 1981;46:599-611. PubMed PMID: WOS:A1981NV38800011.
35. Vignjevic D, Kojima S, Svitkina T, Borisy G. Role of fascin in filopodial protrusion. *Journal of Cell Biology*. 2006;174(6):863-75. doi: 10.1083/jcb.200603013. PubMed PMID: WOS:000240697100015.
36. Svitkina T, Bulanova E, Chaga O, Vignjevic D, Kojima S, Vasiliev J, et al. Mechanism of filopodia initiation by reorganization of a dendritic network. *Journal of Cell Biology*. 2003;160(3):409-21. doi: 10.1083/jcb.200210174. PubMed PMID: WOS:000180840800015.
37. Uekita T, Itoh Y, Yana I, Ohno H, Seiki M. Cytoplasmic tail-dependent internalization of membrane-type 1 matrix metalloproteinase is important for its invasion-promoting activity. *Journal of Cell Biology*. 2001;155(7):1345-56. doi: 10.1083/jcb.200108112. PubMed PMID: WOS:000173023500028.
38. Friedl P, Wolf K, Saklatvala J, Nagase H, Salvesen G. Proteolytic and non-proteolytic migration of tumour cells and leucocytes. *Proteases and the Regulation of Biological Processes*. 2003;70:277-85. PubMed PMID: WOS:000186050700023.

39. Wolf K, Wu YI, Liu Y, Geiger J, Tam E, Overall C, et al. Multi-step pericellular proteolysis controls the transition from individual to collective cancer cell invasion. *Nat Cell Biol.* 2007;9(8):893-904. doi: 10.1038/ncb1616. PubMed PMID: 17618273.
40. Friedl P, Wolf K. Proteolytic interstitial cell migration: a five-step process. *Cancer and Metastasis Reviews.* 2009;28(1-2):129-35. doi: 10.1007/s10555-008-9174-3. PubMed PMID: WOS:000264476600011.
41. SANGER J, SANGER J, JOCKUSCH B. DIFFERENCES IN THE STRESS FIBERS BETWEEN FIBROBLASTS AND EPITHELIAL-CELLS. *Journal of Cell Biology.* 1983;96(4):961-9. doi: 10.1083/jcb.96.4.961. PubMed PMID: WOS:A1983QH96000002.
42. Wang J, Lin J. Cell traction force and measurement methods. *Biomechanics and Modeling in Mechanobiology.* 2007;6(6):361-71. doi: 10.1007/s10237-006-0068-4. PubMed PMID: WOS:000250740900001.
43. Balaban N, Schwarz U, Riveline D, Goichberg P, Tzur G, Sabanay I, et al. Force and focal adhesion assembly: a close relationship studied using elastic micropatterned substrates. *Nature Cell Biology.* 2001;3(5):466-72. doi: 10.1038/35074532. PubMed PMID: WOS:000168592500016.
44. Tan J, Tien J, Pirone D, Gray D, Bhadriraju K, Chen C. Cells lying on a bed of microneedles: An approach to isolate mechanical force. *Proceedings of the National Academy of Sciences of the United States of America.* 2003;100(4):1484-9. doi: 10.1073/pnas.0235407100. PubMed PMID: WOS:000181073000009.
45. Zamir E, Geiger B. Molecular complexity and dynamics of cell-matrix adhesions. *Journal of Cell Science.* 2001;114(20):3583-90. PubMed PMID: WOS:000171889300002.
46. WANG N, BUTLER J, INGBER D. MECHANOTRANSDUCTION ACROSS THE CELL-SURFACE AND THROUGH THE CYTOSKELETON. *Science.* 1993;260(5111):1124-7. doi: 10.1126/science.7684161. PubMed PMID: WOS:A1993LC94200029.
47. Ingber D. Mechanosensation through integrins: Cells act locally but think globally. *Proceedings of the National Academy of Sciences of the United States of America.* 2003;100(4):1472-4. doi: 10.1073/pnas.0530201100. PubMed PMID: WOS:000181073000006.
48. McCann C, Kriebel P, Parent C, Losert W. Cell speed, persistence and information transmission during signal relay and collective migration. *Journal of Cell Science.* 2010;123(10):1724-31. doi: 10.1242/jcs.060137. PubMed PMID: WOS:000277357400013.
49. Friedl P, Hegerfeldt Y, Tusch M. Collective cell migration in morphogenesis and cancer. *Int J Dev Biol.* 2004;48(5-6):441-9. doi: 10.1387/ijdb.041821. PubMed PMID: 15349818.
50. Diallo A, Prigent C. The serine/threonine kinases that control cell cycle progression as therapeutic targets. *Bulletin Du Cancer.* 2011;98(11):1335-45. doi: 10.1684/bdc.2011.1467. PubMed PMID: WOS:000297363500010.
51. PARDEE A. A GROWTH-CONTROL EVENT DEFECTIVE IN TUMORS - A CITATION-CLASSIC COMMENTARY ON A RESTRICTION POINT FOR CONTROL OF NORMAL

- ANIMAL-CELL PROLIFERATION BY PARDEE,A.B. *Current Contents/life Sciences*. 1992;(6):11-. PubMed PMID: WOS:A1992HA32900002.
52. Cho R, Campbell M, Winzeler E, Steinmetz L, Conway A, Wodicka L, et al. A genome-wide transcriptional analysis of the mitotic cell cycle. *Molecular Cell*. 1998;2(1):65-73. doi: 10.1016/S1097-2765(00)80114-8. PubMed PMID: WOS:000075174500007.
53. Cicenas J, Kalyan K, Sorokinas A, Jatulyte A, Valiunas D, Kaupinis A, et al. Highlights of the Latest Advances in Research on CDK Inhibitors. *Cancers (Basel)*. 2014;6(4):2224-42. doi: 10.3390/cancers6042224. PubMed PMID: 25349887; PubMed Central PMCID: PMCPMC4276963.
54. HARTWELL L, KASTAN M. CELL-CYCLE CONTROL AND CANCER. *Science*. 1994;266(5192):1821-8. doi: 10.1126/science.7997877. PubMed PMID: WOS:A1994PX38300026.
55. Hall M, Peters G. Genetic alterations of cyclins, cyclin-dependent kinases, and Cdk inhibitors in human cancer. *Advances in Cancer Research*, Vol 68. 1996;68:67-108. doi: 10.1016/S0065-230X(08)60352-8. PubMed PMID: WOS:A1996BF47Q00003.
56. Rørth P. Fellow travellers: emergent properties of collective cell migration. *EMBO Rep*. 2012;13(11):984-91. doi: 10.1038/embor.2012.149. PubMed PMID: 23059978; PubMed Central PMCID: PMCPMC3492716.
57. Iliina O, Friedl P. Mechanisms of collective cell migration at a glance. *J Cell Sci*. 2009;122(Pt 18):3203-8. doi: 10.1242/jcs.036525. PubMed PMID: 19726629.
58. Rørth P. Collective guidance of collective cell migration. *Trends Cell Biol*. 2007;17(12):575-9. doi: 10.1016/j.tcb.2007.09.007. PubMed PMID: 17996447.
59. Vedel S, Tay S, Johnston DM, Bruus H, Quake SR. Migration of cells in a social context. *Proc Natl Acad Sci U S A*. 2013;110(1):129-34. doi: 10.1073/pnas.1204291110. PubMed PMID: 23251032; PubMed Central PMCID: PMCPMC3538227.
60. FRIEDL P, NOBLE P, WALTON P, LAIRD D, CHAUVIN P, TABAH R, et al. MIGRATION OF COORDINATED CELL CLUSTERS IN MESENCHYMAL AND EPITHELIAL CANCER EXPLANTS IN-VITRO. *Cancer Research*. 1995;55(20):4557-60. PubMed PMID: WOS:A1995RZ06900014.
61. Friedl P, Gilmour D. Collective cell migration in morphogenesis, regeneration and cancer. *Nat Rev Mol Cell Biol*. 2009;10(7):445-57. doi: 10.1038/nrm2720. PubMed PMID: 19546857.
62. Chapnick DA, Jacobsen J, Liu X. The development of a novel high throughput computational tool for studying individual and collective cellular migration. *PLoS One*. 2013;8(12):e82444. doi: 10.1371/journal.pone.0082444. PubMed PMID: 24386097; PubMed Central PMCID: PMCPMC3873918.
63. Slater B, Londono C, McGuigan AP. An algorithm to quantify correlated collective cell migration behavior. *Biotechniques*. 2013;54(2):87-92. doi: 10.2144/000113990. PubMed PMID: 23384179.

64. Solnica-Krezel L. Conserved patterns of cell movements during vertebrate gastrulation. *Current Biology*. 2005;15(6):R213-R28. doi: 10.1016/j.cub.2005.03.016. PubMed PMID: WOS:000228208400016.
65. Friedl P, Wolf K. Plasticity of cell migration: a multiscale tuning model. *J Cell Biol*. 2010;188(1):11-9. doi: 10.1083/jcb.200909003. PubMed PMID: 19951899; PubMed Central PMCID: PMCPMC2812848.
66. Lecaudey V, Gilmour D. Organizing moving groups during morphogenesis. *Curr Opin Cell Biol*. 2006;18(1):102-7. doi: 10.1016/j.ceb.2005.12.001. PubMed PMID: 16352429.
67. Graham J, Ayati B. A unified term for directed and undirected motility in collective cell invasion. *Applied Mathematics Letters*. 2012;25(12):2267-71. doi: 10.1016/j.aml.2012.06.015. PubMed PMID: WOS:000309033200049.
68. Li L, Hartley R, Reiss B, Sun Y, Pu J, Wu D, et al. E-cadherin plays an essential role in collective directional migration of large epithelial sheets. *Cell Mol Life Sci*. 2012;69(16):2779-89. doi: 10.1007/s00018-012-0951-3. PubMed PMID: 22410739; PubMed Central PMCID: PMCPMC3459324.
69. Théry M, Racine V, Piel M, Pépin A, Dimitrov A, Chen Y, et al. Anisotropy of cell adhesive microenvironment governs cell internal organization and orientation of polarity. *Proc Natl Acad Sci U S A*. 2006;103(52):19771-6. doi: 10.1073/pnas.0609267103. PubMed PMID: 17179050; PubMed Central PMCID: PMCPMC1750916.
70. Hegerfeldt Y, Tusch M, Bröcker EB, Friedl P. Collective cell movement in primary melanoma explants: plasticity of cell-cell interaction, beta1-integrin function, and migration strategies. *Cancer Res*. 2002;62(7):2125-30. PubMed PMID: 11929834.
71. Ouaknin GY, Bar-Yoseph PZ. Stochastic collective movement of cells and fingering morphology: no maverick cells. *Biophys J*. 2009;97(7):1811-21. doi: 10.1016/j.bpj.2009.05.064. PubMed PMID: 19804711; PubMed Central PMCID: PMCPMC2756401.
72. Friedl P, Maaser K, Klein CE, Niggemann B, Krohne G, Zänker KS. Migration of highly aggressive MV3 melanoma cells in 3-dimensional collagen lattices results in local matrix reorganization and shedding of alpha2 and beta1 integrins and CD44. *Cancer Res*. 1997;57(10):2061-70. PubMed PMID: 9158006.
73. Ladoux B. BIOPHYSICS Cells guided on their journey. *Nature Physics*. 2009;5(6):377-8. doi: 10.1038/nphys1281. PubMed PMID: WOS:000266544800005.
74. Tambe DT, Hardin CC, Angelini TE, Rajendran K, Park CY, Serra-Picamal X, et al. Collective cell guidance by cooperative intercellular forces. *Nature Materials*. 2011;10(6):469-75. doi: 10.1038/nmat3025. PubMed PMID: WOS:000290855100023.
75. Trepat X, Wasserman MR, Angelini TE, Millet E, Weitz DA, Butler JP, et al. Physical forces during collective cell migration. *Nature Physics*. 2009;5(6):426-30. doi: 10.1038/nphys1269. PubMed PMID: WOS:000266544800022.

76. Puliafito A, Hufnagel L, Neveu P, Streichan S, Sigal A, Fygenson DK, et al. Collective and single cell behavior in epithelial contact inhibition. *Proceedings of the National Academy of Sciences of the United States of America*. 2012;109(3):739-44. doi: 10.1073/pnas.1007809109. PubMed PMID: WOS:000299154000025.
77. Szabó B, Szöllösi GJ, Gönci B, Jurányi Z, Selmeczi D, Vicsek T. Phase transition in the collective migration of tissue cells: experiment and model. *Phys Rev E Stat Nonlin Soft Matter Phys*. 2006;74(6 Pt 1):061908. PubMed PMID: 17280097.
78. Angelini TE, Hannezo E, Trepat X, Marquez M, Fredberg JJ, Weitz DA. Glass-like dynamics of collective cell migration. *Proc Natl Acad Sci U S A*. 2011;108(12):4714-9. doi: 10.1073/pnas.1010059108. PubMed PMID: 21321233; PubMed Central PMCID: PMC3064326.
79. Poujade M, Grasland-Mongrain E, Hertzog A, Jouanneau J, Chavrier P, Ladoux B, et al. Collective migration of an epithelial monolayer in response to a model wound. *Proc Natl Acad Sci U S A*. 2007;104(41):15988-93. doi: 10.1073/pnas.0705062104. PubMed PMID: 17905871; PubMed Central PMCID: PMC2042149.
80. Vedula SR, Leong MC, Lai TL, Hersen P, Kabla AJ, Lim CT, et al. Emerging modes of collective cell migration induced by geometrical constraints. *Proc Natl Acad Sci U S A*. 2012;109(32):12974-9. doi: 10.1073/pnas.1119313109. PubMed PMID: 22814373; PubMed Central PMCID: PMC3420172.
81. Doxzen K, Vedula SR, Leong MC, Hirata H, Gov NS, Kabla AJ, et al. Guidance of collective cell migration by substrate geometry. *Integr Biol (Camb)*. 2013;5(8):1026-35. doi: 10.1039/c3ib40054a. PubMed PMID: 23784144.
82. Douezan S, Brochard-Wyart F. Spreading dynamics of cellular aggregates confined to adhesive bands. *European Physical Journal E*. 2012;35(11). doi: 10.1140/epje/i2012-12116-8. PubMed PMID: WOS:000312205800003.
83. Méhes E, Mones E, Németh V, Vicsek T. Collective motion of cells mediates segregation and pattern formation in co-cultures. *PLoS One*. 2012;7(2):e31711. doi: 10.1371/journal.pone.0031711. PubMed PMID: 22359617; PubMed Central PMCID: PMC3280994.
84. Schlett K, Czirók A, Tárnok K, Vicsek T, Madarász E. Dynamics of cell aggregation during in vitro neurogenesis by immortalized neuroectodermal progenitors. *J Neurosci Res*. 2000;60(2):184-94. PubMed PMID: 10740223.
85. Young TH, Hung SH, Hsu JP. Analysis of cell aggregation in the culturing of cerebellar granule neurons. *Chemical Engineering Science*. 2004;59(24):5931-6. doi: 10.1016/j.ces.2004.07.027. PubMed PMID: WOS:000226079100023.
86. Enmon RM, O'Connor KC, Song H, Lacks DJ, Schwartz DK. Aggregation kinetics of well and poorly differentiated human prostate cancer cells. *Biotechnology and Bioengineering*. 2002;80(5):580-8. doi: 10.1002/bit.10394. PubMed PMID: WOS:000178822100012.

87. Fatehi H, Meyer-Hermann M, Figge MT. Modelling cellular aggregation induced by chemotaxis and phototaxis. *Mathematical Medicine and Biology-a Journal of the Ima.* 2010;27(4):373-84. doi: 10.1093/imamm/dqq002. PubMed PMID: WOS:000285194300004.
88. Eyiurekli M, Manley P, Lelkes PI, Breen DE. A computational model of chemotaxis-based cell aggregation. *Biosystems.* 2008;93(3):226-39. doi: 10.1016/j.biosystems.2008.05.005. PubMed PMID: 18602744.
89. Douezan S, Brochard-Wyart F. Active diffusion-limited aggregation of cells. *Soft Matter.* 2012;8(3):784-8. doi: 10.1039/c1sm06399e. PubMed PMID: WOS:000301793700026.
90. Kosztin I, Vunjak-Novakovic G, Forgacs G. Colloquium: Modeling the dynamics of multicellular systems: Application to tissue engineering. *Reviews of Modern Physics.* 2012;84(4):1791-805. doi: 10.1103/RevModPhys.84.1791. PubMed PMID: WOS:000313007800001.
91. Guido S, Simeone M. Binary collision of drops in simple shear flow by computer-assisted video optical microscopy. *Journal of Fluid Mechanics.* 1998;357:1-20. doi: 10.1017/S0022112097007921. PubMed PMID: WOS:000072746400001.
92. Ziebert F, Aranson IS. Effects of adhesion dynamics and substrate compliance on the shape and motility of crawling cells. *PLoS One.* 2013;8(5):e64511. doi: 10.1371/journal.pone.0064511. PubMed PMID: 23741334; PubMed Central PMCID: PMC3669322.
93. Terryn C, Bonnomet A, Cutrona J, Coraux C, Tournier J-M, Nawrocki-Raby B, et al. Video-microscopic imaging of cell spatio-temporal dispersion and migration. *Critical Reviews in Oncology Hematology.* 2009;69(2):144-52. doi: 10.1016/j.critrevonc.2008.06.005. PubMed PMID: WOS:000263013700006.
94. Wong C, Chen AA, Behr B, Shen S. Time-lapse microscopy and image analysis in basic and clinical embryo development research. *Reproductive Biomedicine Online.* 2013;26(2):120-9. doi: 10.1016/j.rbmo.2012.11.003. PubMed PMID: WOS:000314664400003.
95. Debeir O, Megalizzi V, Warzee N, Kiss R, Decaestecker C. Videomicroscopic extraction of specific information on cell proliferation and migration in vitro. *Experimental Cell Research.* 2008;314(16):2985-98. doi: 10.1016/j.yexcr.2008.06.010. PubMed PMID: WOS:000259802600008.
96. Decaestecker C, Debeir O, Van Ham P, Kiss R. Can anti-migratory drugs be screened in vitro? A review of 2D and 3D assays for the quantitative analysis of cell migration. *Med Res Rev.* 2007;27(2):149-76. doi: 10.1002/med.20078. PubMed PMID: 16888756.
97. Hand A, Sun T, Barber D, Hose D, MacNeil S. Automated tracking of migrating cells in phase-contrast video microscopy sequences using image registration. *Journal of Microscopy-Oxford.* 2009;234(1):62-79. doi: 10.1111/j.1365-2818.2009.03144.x. PubMed PMID: WOS:000264373600007.
98. Gail MH, Boone CW. The locomotion of mouse fibroblasts in tissue culture. *Biophysical journal.* 1970;10(10):980-93. PubMed PMID: MEDLINE:5531614.

99. Uhlenbeck GE, Ornstein LS. On the Theory of the Brownian Motion. *Physical Review*. 1930;36(5):823-41. PubMed PMID: 10.1103/PhysRev.36.823.
100. Dickinson RB, Tranquillo RT. Optimal Estimation of Cell-Movement Indexes from the Statistical Analysis of Cell Tracking Data. *Aiche Journal*. 1993;39(12):1995-2010. doi: 10.1002/aic.690391210. PubMed PMID: WOS:A1993MK14000009.
101. Selmeczi D, Li L, Pedersen L, Nrelykke S, Hagedorn P, Mosler S, et al. Cell motility as random motion: A review. *European Physical Journal-Special Topics*. 2008;157:1-15. doi: 10.1140/epjst/e2008-00626-x. PubMed PMID: WOS:000255258800002.
102. Entschladen F, Drell T, Lang K, Masur K, Palm D, Bastian P, et al. Analysis methods of human cell migration. *Experimental Cell Research*. 2005;307(2):418-26. doi: 10.1016/j.yexcr.2005.03.029. PubMed PMID: WOS:000230068800012.
103. Mathias JR, Perrin BJ, Liu TX, Kanki J, Look AT, Huttenlocher A. Resolution of inflammation by retrograde chemotaxis of neutrophils in transgenic zebrafish. *J Leukoc Biol*. 2006;80(6):1281-8. doi: jlb.0506346 [pii] 10.1189/jlb.0506346. PubMed PMID: 16963624.
104. Böttcher R, Niehrs C. Fibroblast growth factor signaling during early vertebrate development. *Endocr Rev*. 2005;26(1):63-77. doi: 26/1/63 [pii] 10.1210/er.2003-0040. PubMed PMID: 15689573.
105. Clark RAF. Wound repair: overview and general considerations. In: Clark RAF, editor. *The Molecular and Cellular Biology of WoundRepair*, 2nd Edition: Springer; 1996. p. 3-35.
106. Martin P, Parkhurst S. Parallels between tissue repair and embryo morphogenesis. *Development*. 2004;131(13):3021-34. doi: 131/13/3021 [pii] 10.1242/dev.01253. PubMed PMID: 15197160.
107. Sasaki A, Firtel R. Regulation of chemotaxis by the orchestrated activation of Ras, PI3K, and TOR. *Eur J Cell Biol*. 2006;85(9-10):873-95. doi: S0171-9335(06)00077-X [pii] 10.1016/j.ejcb.2006.04.007. PubMed PMID: 16740339.
108. Friedl P, Wolf K. Tumour-cell invasion and migration: diversity and escape mechanisms. *Nat Rev Cancer*. 2003;3(5):362-74. doi: nrc1075 [pii] 10.1038/nrc1075. PubMed PMID: 12724734.
109. BOYDEN S. The chemotactic effect of mixtures of antibody and antigen on polymorphonuclear leucocytes. *J Exp Med*. 1962;115:453-66. PubMed PMID: 13872176; PubMed Central PMCID: PMCPMC2137509.
110. Zigmond S, Hirsch J. Leukocyte locomotion and chemotaxis. New methods for evaluation, and demonstration of a cell-derived chemotactic factor. *J Exp Med*. 1973;137(2):387-410. PubMed PMID: 4568301; PubMed Central PMCID: PMCPMC2139498.

111. Nelson RD, Quie PG, Simmons RL. Chemotaxis under agarose: a new and simple method for measuring chemotaxis and spontaneous migration of human polymorphonuclear leukocytes and monocytes. *J Immunol.* 1975;115(6):1650-6. PubMed PMID: 1102606.
112. Bonvin C, Overney J, Shieh AC, Dixon JB, Swartz MA. A multichamber fluidic device for 3D cultures under interstitial flow with live imaging: development, characterization, and applications. *Biotechnol Bioeng.* 2010;105(5):982-91. doi: 10.1002/bit.22608. PubMed PMID: 19953672.
113. Lin F. A MICROFLUIDICS-BASED METHOD FOR ANALYZING LEUKOCYTE MIGRATION TO CHEMOATTRACTANT GRADIENTS. *Methods in Enzymology, Vol 461: Chemokines, Part B. Methods in Enzymology.* 461. San Diego: Elsevier Academic Press Inc; 2009. p. 333-47.
114. Li Jeon N, Baskaran H, Dertinger SKW, Whitesides GM, Van De Water L, Toner M. Neutrophil chemotaxis in linear and complex gradients of interleukin-8 formed in a microfabricated device. *Nat Biotech.* 2002;20(8):826-30.
115. Dertinger SKW, Chiu DT, Jeon NL, Whitesides GM. Generation of Gradients Having Complex Shapes Using Microfluidic Networks. *Analytical Chemistry.* 2001;73(6):1240-6. doi: 10.1021/ac001132d.
116. Sackmann EK, Fulton AL, Beebe DJ. The present and future role of microfluidics in biomedical research. *Nature.* 2014;507(7491):181-9. doi: 10.1038/nature13118. PubMed PMID: 24622198.
117. Shao JB, Wu L, Wu JZ, Zheng YH, Zhao H, Jin QH, et al. Integrated microfluidic chip for endothelial cells culture and analysis exposed to a pulsatile and oscillatory shear stress. *Lab on a Chip.* 2009;9(21):3118-25. doi: 10.1039/b909312e. PubMed PMID: WOS:000270761600014.
118. Haessler U, Kalinin Y, Swartz M, Wu M. An agarose-based microfluidic platform with a gradient buffer for 3D chemotaxis studies. *Biomedical Microdevices.* 2009;11(4):827-35. doi: 10.1007/s10544-009-9299-3. PubMed PMID: WOS:000267886400014.
119. Zigmond SH. Ability of polymorphonuclear leukocytes to orient in gradients of chemotactic factors. *J Cell Biol.* 1977;75(2 Pt 1):606-16. PubMed PMID: 264125; PubMed Central PMCID: PMCPMC2109936.
120. Zicha D, Dunn G, Brown A. A new direct-viewing chemotaxis chamber. *J Cell Sci.* 1991;99 (Pt 4):769-75. PubMed PMID: 1770004.
121. Chaubey S, Ridley AJ, Wells CM. Using the Dunn chemotaxis chamber to analyze primary cell migration in real time. *Methods Mol Biol.* 2011;769:41-51. doi: 10.1007/978-1-61779-207-6_4. PubMed PMID: 21748668.
122. Muinonen-Martin AJ, Veltman DM, Kalna G, Insall RH. An improved chamber for direct visualisation of chemotaxis. *PLoS One.* 2010;5(12):e15309. doi: 10.1371/journal.pone.0015309. PubMed PMID: 21179457; PubMed Central PMCID: PMCPMC3001854.

123. Friedl P, Bröcker EB. Reconstructing leukocyte migration in 3D extracellular matrix by time-lapse videomicroscopy and computer-assisted tracking. *Methods Mol Biol.* 2004;239:77-90. doi: 1-59259-435-2-77 [pii]. PubMed PMID: 14573911.
124. Sixt M, Lämmermann T. In vitro analysis of chemotactic leukocyte migration in 3D environments. *Methods Mol Biol.* 2011;769:149-65. doi: 10.1007/978-1-61779-207-6_11. PubMed PMID: 21748675.
125. Lämmermann T, Bader BL, Monkley SJ, Worbs T, Wedlich-Söldner R, Hirsch K, et al. Rapid leukocyte migration by integrin-independent flowing and squeezing. *Nature.* 2008;453(7191):51-5. doi: nature06887 [pii] 10.1038/nature06887. PubMed PMID: 18451854.
126. Friedl P, Brocker EB. The biology of cell locomotion within three-dimensional extracellular matrix. *Cellular and Molecular Life Sciences.* 2000;57(1):41-64. doi: 10.1007/s000180050498. PubMed PMID: WOS:000085572900005.
127. Cukierman E, Pankov R, Yamada KM. Cell interactions with three-dimensional matrices. *Current Opinion in Cell Biology.* 2002;14(5):633-9. doi: 10.1016/s0955-0674(02)00364-2. PubMed PMID: WOS:000177837900017.
128. Di Costanzo A, Troiano A, di Martino O, Cacace A, Natale CF, Ventre M, et al. The p63 Protein Isoform Delta Np63 alpha Modulates Y-box Binding Protein 1 in Its Subcellular Distribution and Regulation of Cell Survival and Motility Genes. *Journal of Biological Chemistry.* 2012;287(36):30170-80. doi: 10.1074/jbc.M112.349951. PubMed PMID: WOS:000308579800012.
129. Vasaturo A, Caserta S, Russo I, Preziosi V, Ciacci C, Guido S. A novel chemotaxis assay in 3-D collagen gels by time-lapse microscopy. *PLoS One.* 2012;7(12):e52251. doi: 10.1371/journal.pone.0052251. PubMed PMID: 23284956; PubMed Central PMCID: PMC3526591.
130. Moghe PV, Nelson RD, Tranquillo RT. CYTOKINE-STIMULATED CHEMOTAXIS OF HUMAN NEUTROPHILS IN A 3-D CONJOINED FIBRIN GEL ASSAY. *Journal of Immunological Methods.* 1995;180(2):193-211. PubMed PMID: ISI:A1995QQ91000005.
131. Knapp DM, Helou EF, Tranquillo RT. A fibrin or collagen gel assay for tissue cell chemotaxis: Assessment of fibroblast chemotaxis to GRGDSP. *Experimental Cell Research.* 1999;247(2):543-53. PubMed PMID: ISI:000079087300025.
132. Caserta S, Campello S, Tomaiuolo G, Sabetta L, Guido S. A methodology to study chemotaxis in 3-D collagen gels. *Aiche Journal.* 2013. doi: 10.1002/aic.14164.
133. Kramer N, Walzl A, Unger C, Rosner M, Krupitza G, Hengstschlaeger M, et al. In vitro cell migration and invasion assays. *Mutation Research-Reviews in Mutation Research.* 2013;752(1):10-24. doi: 10.1016/j.mrrev.2012.08.001. PubMed PMID: WOS:000315072800003.

134. Bindschadler M, McGrath JL. Sheet migration by wounded monolayers as an emergent property of single-cell dynamics. *Journal of Cell Science*. 2007;120(5):876-84. doi: 10.1242/jcs.03395. PubMed PMID: WOS:000244384300017.
135. Rodriguez LG, Wu X, Guan JL. Wound-healing assay. *Methods Mol Biol*. 2005;294:23-9. PubMed PMID: 15576902.
136. Tremel A, Cai A, Tirtaatmadja N, Hughes BD, Stevens GW, Landman KA, et al. Cell migration and proliferation during monolayer formation and wound healing. *Chemical Engineering Science*. 2009;64(2):247-53. doi: 10.1016/j.ces.2008.10.008. PubMed PMID: WOS:000262802800007.
137. Bikfalvi A, Klein S, Pintucci G, Rifkin D. Biological roles of fibroblast growth factor-2. *Endocrine Reviews*. 1997;18(1):26-45. doi: 10.1210/er.18.1.26. PubMed PMID: WOS:A1997WG33000003.
138. Kouhara H, Hadari Y, SpivakKroizman T, Schilling J, BarSagi D, Lax I, et al. A lipid-anchored Grb2-binding protein that links FGF-receptor activation to the Ras/MAPK signaling pathway. *Cell*. 1997;89(5):693-702. doi: 10.1016/S0092-8674(00)80252-4. PubMed PMID: WOS:A1997XB92500006.
139. Kanazawa S, Fujiwara T, Matsuzaki S, Shingaki K, Taniguchi M, Miyata S, et al. bFGF regulates PI3-kinase-Rac1-JNK pathway and promotes fibroblast migration in wound healing. *PLoS One*. 2010;5(8):e12228. doi: 10.1371/journal.pone.0012228. PubMed PMID: 20808927; PubMed Central PMCID: PMC2923192.
140. Liang C-C, Park AY, Guan J-L. In vitro scratch assay: a convenient and inexpensive method for analysis of cell migration in vitro. *Nature Protocols*. 2007;2(2):329-33. doi: 10.1038/nprot.2007.30. PubMed PMID: WOS:000253138100013.
141. Vitorino P, Meyer T. Modular control of endothelial sheet migration. *Genes Dev*. 2008;22(23):3268-81. doi: 10.1101/gad.1725808. PubMed PMID: 19056882; PubMed Central PMCID: PMC2600767.
142. Nikolić DL, Boettiger AN, Bar-Sagi D, Carbeck JD, Shvartsman SY. Role of boundary conditions in an experimental model of epithelial wound healing. *Am J Physiol Cell Physiol*. 2006;291(1):C68-75. doi: 10.1152/ajpcell.00411.2005. PubMed PMID: 16495370.
143. Todaro GJ, Lazar GK, Green H. The initiation of cell division in a contact-inhibited mammalian cell line. *J Cell Physiol*. 1965;66(3):325-33. PubMed PMID: 5884360.
144. Murrell M, Kamm R, Matsudaira P. Tension, free space, and cell damage in a microfluidic wound healing assay. *PLoS One*. 2011;6(9):e24283. doi: 10.1371/journal.pone.0024283. PubMed PMID: 21915305; PubMed Central PMCID: PMC3167843.
145. Sepúlveda N, Petitjean L, Cochet O, Grasland-Mongrain E, Silberzan P, Hakim V. Collective cell motion in an epithelial sheet can be quantitatively described by a stochastic interacting particle

- model. *PLoS Comput Biol.* 2013;9(3):e1002944. doi: 10.1371/journal.pcbi.1002944. PubMed PMID: 23505356; PubMed Central PMCID: PMC3591275.
146. Matsubayashi Y, Ebisuya M, Honjoh S, Nishida E. ERK activation propagates in epithelial cell sheets and regulates their migration during wound healing. *Curr Biol.* 2004;14(8):731-5. doi: 10.1016/j.cub.2004.03.060. PubMed PMID: 15084290.
147. Jacinto A, Martinez-Arias A, Martin P. Mechanisms of epithelial fusion and repair. *Nat Cell Biol.* 2001;3(5):E117-23. doi: 10.1038/35074643. PubMed PMID: 11331897.
148. Block ER, Matela AR, SundarRaj N, Iszkula ER, Klarlund JK. Wounding induces motility in sheets of corneal epithelial cells through loss of spatial constraints: role of heparin-binding epidermal growth factor-like growth factor signaling. *J Biol Chem.* 2004;279(23):24307-12. doi: 10.1074/jbc.M401058200. PubMed PMID: 15039441.
149. Nikolic D, Boettiger A, Bar-Sagi D, Carbeck J, Shvartsman S. Role of boundary conditions in an experimental model of epithelial wound healing. *American Journal of Physiology-Cell Physiology.* 2006;291(1):C68-C75. doi: 10.1152/ajpcell.00411.2005. PubMed PMID: WOS:000238287500009.
150. Fisher RA. THE WAVE OF ADVANCE OF ADVANTAGEOUS GENES. *Annals of Eugenics.* 1937;7(4):355-69.
151. Simpson M, Merrifield A, Landman K, Hughes B. Simulating invasion with cellular automata: Connecting cell-scale and population-scale properties. *Physical Review E.* 2007;76(2). doi: 10.1103/PhysRevE.76.021918. PubMed PMID: WOS:000249154600082.
152. Maini PK, McElwain DLS, Leavesley D. Travelling waves in a wound healing assay. *Applied Mathematics Letters.* 2004;17(5):575-80. doi: 10.1016/j.aml.2003.01.011. PubMed PMID: WOS:000221547800013.
153. Arnold J, Adam J. A simplified model of wound healing - II: The critical size defect in two dimensions. *Mathematical and Computer Modelling.* 1999;30(11-12):47-60. doi: 10.1016/S0895-7177(99)00197-1. PubMed PMID: WOS:000084310400005.
154. Maini PK, McElwain DLS, Leavesley DI. Traveling wave model to interpret a wound-healing cell migration assay for human peritoneal mesothelial cells. *Tissue Engineering.* 2004;10(3-4):475-82. doi: 10.1089/107632704323061834. PubMed PMID: WOS:000221105000017.
155. Cai AQ, Landman KA, Hughes BD. Multi-scale modeling of a wound-healing cell migration assay. *J Theor Biol.* 2007;245(3):576-94. doi: 10.1016/j.jtbi.2006.10.024. PubMed PMID: 17188306.
156. Johnston S, Simpson M, McElwain D. How much information can be obtained from tracking the position of the leading edge in a scratch assay? *Journal of the Royal Society Interface.* 2014;11(97). doi: 10.1098/rsif.2014.0325. PubMed PMID: WOS:000338436200010.
157. SHATKIN A, REICH E, TATUM E, FRANKLIN R. EFFECT OF MITOMYCIN C ON MAMMALIAN CELLS IN CULTURE. *Biochimica Et Biophysica Acta.* 1962;55(3):277-&. PubMed PMID: WOS:A19626777A00023.

158. Sengers BG, Please CP, Oreffo RO. Experimental characterization and computational modelling of two-dimensional cell spreading for skeletal regeneration. *J R Soc Interface*. 2007;4(17):1107-17. doi: 10.1098/rsif.2007.0233. PubMed PMID: 17472907; PubMed Central PMCID: PMCPMC2396206.
159. Sengers BG, Please CP, Taylor M, Oreffo RO. Experimental-computational evaluation of human bone marrow stromal cell spreading on trabecular bone structures. *Ann Biomed Eng*. 2009;37(6):1165-76. doi: 10.1007/s10439-009-9676-3. PubMed PMID: 19296221.
160. Sherratt JA, Murray JD. Models of epidermal wound healing. *Proc Biol Sci*. 1990;241(1300):29-36. doi: 10.1098/rspb.1990.0061. PubMed PMID: 1978332.
161. Takamizawa K, Niu S, Matsuda T. Mathematical simulation of unidirectional tissue formation: In vitro transanastomotic endothelialization model. *Journal of Biomaterials Science-Polymer Edition*. 1996;8(4):323-34. PubMed PMID: WOS:A1996WF91900007.
162. Savla U, Olson L, Waters C. Mathematical modeling of airway epithelial wound closure during cyclic mechanical strain. *Journal of Applied Physiology*. 2004;96(2):566-74. doi: 10.1152/jappphysiol.00510.2003. PubMed PMID: WOS:000187888400022.
163. Dale PD, Maini PK, Sherratt JA. Mathematical modeling of corneal epithelial wound healing. *Math Biosci*. 1994;124(2):127-47. PubMed PMID: 7833592.
164. Simpson M, Treloar K, Binder B, Haridas P, Manton K, Leavesley D, et al. Quantifying the roles of cell motility and cell proliferation in a circular barrier assay. *Journal of the Royal Society Interface*. 2013;10(82). doi: 10.1098/rsif.2013.0007. PubMed PMID: WOS:000316415600013.
165. Cai AQ, Landman KA, Hughes BD. Modelling directional guidance and motility regulation in cell migration. *Bull Math Biol*. 2006;68(1):25-52. doi: 10.1007/s11538-005-9028-x. PubMed PMID: 16794920.
166. Zahm JM, Kaplan H, Hérard AL, Doriot F, Pierrot D, Somelette P, et al. Cell migration and proliferation during the in vitro wound repair of the respiratory epithelium. *Cell Motil Cytoskeleton*. 1997;37(1):33-43. doi: 10.1002/(SICI)1097-0169(1997)37:1<33::AID-CM4>3.0.CO;2-I. PubMed PMID: 9142437.
167. Lucena S, Sanchez EE, Perez JC. Anti-metastatic activity of the recombinant disintegrin, r-mojastin 1, from the Mohave rattlesnake. *Toxicon*. 2011;57(5):794-802. doi: 10.1016/j.toxicon.2011.02.014. PubMed PMID: 21334359; PubMed Central PMCID: PMCPMC3293478.
168. Andújar I, Ríos JL, Giner RM, Recio MC. Shikonin promotes intestinal wound healing in vitro via induction of TGF- β release in IEC-18 cells. *Eur J Pharm Sci*. 2013;49(4):637-41. doi: 10.1016/j.ejps.2013.05.018. PubMed PMID: 23727294.
169. Tsai M, Huang H, Hsu J, Lai Y, Hsiao Y, Lu F, et al. Topical N-Acetylcysteine Accelerates Wound Healing in Vitro and in Vivo via the PKC/Stat3 Pathway. *International Journal of Molecular Sciences*. 2014;15(5):7563-78. doi: 10.3390/ijms15057563. PubMed PMID: WOS:000336841800031.

170. Zhang H, Han Y, Tao J, Liu S, Yan C, Li S. Cellular repressor of E1A-stimulated genes regulates vascular endothelial cell migration by The ILK/AKT/mTOR/VEGF(165) signaling pathway. *Experimental Cell Research*. 2011;317(20):2904-13. doi: 10.1016/j.yexcr.2011.08.012. PubMed PMID: WOS:000297450900010.
171. Yue P, Leung E, Mak N, Wong R. A Simplified Method for Quantifying Cell Migration/Wound Healing in 96-Well Plates. *Journal of Biomolecular Screening*. 2010;15(4):427-33. doi: 10.1177/1087057110361772. PubMed PMID: WOS:000276248200009.
172. Sumagin R, Robin AZ, Nusrat A, Parkos CA. Activation of PKC β II by PMA facilitates enhanced epithelial wound repair through increased cell spreading and migration. *PLoS One*. 2013;8(2):e55775. doi: 10.1371/journal.pone.0055775. PubMed PMID: 23409039; PubMed Central PMCID: PMC3569445.
173. Silano M, Vincentini O, Luciani A, Felli C, Caserta S, Esposito S, et al. Early tissue transglutaminase-mediated response underlies K562(S)-cell gliadin-dependent agglutination. *Pediatric Research*. 2012;71(5):532-8. doi: 10.1038/pr.2012.4. PubMed PMID: WOS:000303373300002.
174. Rosello C, Ballet P, Planus E, Tracqui P. Model driven quantification of individual and collective cell migration. *Acta Biotheor*. 2004;52(4):343-63. doi: 10.1023/B:ACBI.0000046602.58202.5e. PubMed PMID: 15520538.
175. Buonomo R, Giacco F, Vasaturo A, Caserta S, Guido S, Pagliara V, et al. PED/PEA-15 controls fibroblast motility and wound closure by ERK1/2-dependent mechanisms. *Journal of Cellular Physiology*. 2012;227(5):2106-16. doi: 10.1002/jcp.22944. PubMed PMID: WOS:000299373900036.
176. Grasso S, Hernandez J, Chifflet S. Roles of wound geometry, wound size, and extracellular matrix in the healing response of bovine corneal endothelial cells in culture. *American Journal of Physiology-Cell Physiology*. 2007;293(4):C1327-C37. doi: 10.1152/ajpcell.00001.2007. PubMed PMID: WOS:000250052400015.
177. Riahi R, Yang Y, Zhang D, Wong P. Advances in Wound-Healing Assays for Probing Collective Cell Migration. *Jala*. 2012;17(1):59-65. doi: 10.1177/2211068211426550. PubMed PMID: WOS:000304773900008.
178. Anon E, Serra-Picamal X, Hersen P, Gauthier NC, Sheetz MP, Trepat X, et al. Cell crawling mediates collective cell migration to close undamaged epithelial gaps. *Proc Natl Acad Sci U S A*. 2012;109(27):10891-6. doi: 10.1073/pnas.1117814109. PubMed PMID: 22711834; PubMed Central PMCID: PMC3390890.
179. Zhang M, Li H, Ma H, Qin J. A simple microfluidic strategy for cell migration assay in an in vitro wound-healing model. *Wound Repair and Regeneration*. 2013;21(6):897-903. doi: 10.1111/wrr.12106. PubMed PMID: WOS:000326327100162.
180. Cochet-Escartin O, Ranft J, Silberzan P, Marcq P. Border forces and friction control epithelial closure dynamics. *Biophys J*. 2014;106(1):65-73. doi: 10.1016/j.bpj.2013.11.015. PubMed PMID: 24411238; PubMed Central PMCID: PMC3907253.

181. CHOU L, FIRTH J, UITTO V, BRUNETTE D. SUBSTRATUM SURFACE-TOPOGRAPHY ALTERS CELL-SHAPE AND REGULATES FIBRONECTIN MESSENGER-RNA LEVEL, MESSENGER-RNA STABILITY, SECRETION AND ASSEMBLY IN HUMAN FIBROBLASTS. *Journal of Cell Science*. 1995;108:1563-73. PubMed PMID: WOS:A1995QV62600023.
182. Ranucci C, Moghe P. Substrate microtopography can enhance cell adhesive and migratory responsiveness to matrix ligand density. *Journal of Biomedical Materials Research*. 2001;54(2):149-61. doi: 10.1002/1097-4636(200102)54:2<149::AID-JBM1>3.0.CO;2-O. PubMed PMID: WOS:000165602500001.
183. Doran MR, Mills RJ, Parker AJ, Landman KA, Cooper-White JJ. A cell migration device that maintains a defined surface with no cellular damage during wound edge generation. *Lab Chip*. 2009;9(16):2364-9. doi: 10.1039/b900791a. PubMed PMID: 19636468.
184. BURK R. FACTOR FROM A TRANSFORMED CELL LINE THAT AFFECTS CELL MIGRATION. *Proceedings of the National Academy of Sciences of the United States of America*. 1973;70(2):369-72. doi: 10.1073/pnas.70.2.369. PubMed PMID: WOS:A1973O785500021.
185. Fronza M, Heinzmann B, Hamburger M, Laufer S, Merfort I. Determination of the wound healing effect of Calendula extracts using the scratch assay with 3T3 fibroblasts. *Journal of Ethnopharmacology*. 2009;126(3):463-7. doi: 10.1016/j.jep.2009.09.014. PubMed PMID: WOS:000273157900014.
186. Simpson K, Selfors L, Bui J, Reynolds A, Leake D, Khvorova A, et al. Identification of genes that regulate epithelial cell migration using an siRNA screening approach. *Nature Cell Biology*. 2008;10(9):1027-38. doi: 10.1038/ncb1762. PubMed PMID: WOS:000258910400008.
187. Kam Y, Guess C, Estrada L, Weidow B, Quaranta V. A novel circular invasion assay mimics in vivo invasive behavior of cancer cell lines and distinguishes single-cell motility in vitro. *Bmc Cancer*. 2008;8. doi: 10.1186/1471-2407-8-198. PubMed PMID: WOS:000258101400001.
188. Fong E, Tzllil S, Tirrell D. Boundary crossing in epithelial wound healing. *Proceedings of the National Academy of Sciences of the United States of America*. 2010;107(45):19302-7. doi: 10.1073/pnas.1008291107. PubMed PMID: WOS:000283997800034.
189. Lee J, Wang Y, Ren F, Lele T. Stamp Wound Assay for Studying Coupled Cell Migration and Cell Debris Clearance. *Langmuir*. 2010;26(22):16672-6. doi: 10.1021/la103542y. PubMed PMID: WOS:000283837800011.
190. Lan R, Geng H, Hwang Y, Mishra P, Skloss W, Sprague E, et al. A novel wounding device suitable for quantitative biochemical analysis of wound healing and regeneration of cultured epithelium. *Wound Repair and Regeneration*. 2010;18(2):159-67. doi: 10.1111/j.1524-475X.2010.00576.x. PubMed PMID: WOS:000275760600005.
191. PRATT B, HARRIS A, MORROW J, MADRI J. MECHANISMS OF CYTOSKELETAL REGULATION - MODULATION OF AORTIC ENDOTHELIAL-CELL SPECTRIN BY THE

- EXTRACELLULAR-MATRIX. *American Journal of Pathology*. 1984;117(3):349-54. PubMed PMID: WOS:A1984TW40300002.
192. van Horssen R, ten Hagen T. Crossing Barriers: The New Dimension of 2D Cell Migration Assays. *Journal of Cellular Physiology*. 2011;226(1):288-90. doi: 10.1002/jcp.22330. PubMed PMID: WOS:000284212100034.
193. van Horssen R, Galjart N, Rens J, Eggermont A, ten Hagen T. Differential effects of matrix and growth factors on endothelial and fibroblast motility: Application of a modified cell migration assay. *Journal of Cellular Biochemistry*. 2006;99(6):1536-52. doi: 10.1002/jcb.20994. PubMed PMID: WOS:000242122500007.
194. FISCHER E, STINGL A, KIRKPATRICK C. MIGRATION ASSAY FOR ENDOTHELIAL-CELLS IN MULTIWELLS - APPLICATION TO STUDIES ON THE EFFECT OF OPIOIDS. *Journal of Immunological Methods*. 1990;128(2):235-9. doi: 10.1016/0022-1759(90)90215-H. PubMed PMID: WOS:A1990CZ76500011.
195. Kaji H, Yokoi T, Kawashima T, Nishizawa M. Controlled cocultures of HeLa cells and human umbilical vein endothelial cells on detachable substrates. *Lab on a Chip*. 2009;9(3):427-32. doi: 10.1039/b812510d. PubMed PMID: WOS:000262649600008.
196. VARANI J, ORR W, WARD P. COMPARISON OF MIGRATION PATTERNS OF NORMAL AND MALIGNANT CELLS IN 2 ASSAY SYSTEMS. *American Journal of Pathology*. 1978;90(1):159-71. PubMed PMID: WOS:A1978EG74400011.
197. Legrand C, Gilles C, Zahm J, Polette M, Buisson A, Kaplan H, et al. Airway epithelial cell migration dynamics: MMP-9 role in cell-extracellular matrix remodeling. *Journal of Cell Biology*. 1999;146(2):517-29. doi: 10.1083/jcb.146.2.517. PubMed PMID: WOS:000081725700021.
198. Nie F, Yamada M, Kobayashi J, Yamato M, Kikuchi A, Okano T. On-chip cell migration assay using microfluidic channels. *Biomaterials*. 2007;28(27):4017-22. doi: 10.1016/j.biomaterials.2007.05.037. PubMed PMID: WOS:000248898000014.
199. Lo C, Keese C, Giaever I. Impedance analysis of MDCK cells measured by electric cell-substrate impedance sensing. *Biophysical Journal*. 1995;69(6):2800-7. PubMed PMID: WOS:A1995TV01800061.
200. Keese C, Wegener J, Walker S, Giaever L. Electrical wound-healing assay for cells in vitro. *Proceedings of the National Academy of Sciences of the United States of America*. 2004;101(6):1554-9. doi: 10.1073/pnas.0307588100|10.1073/pnas.030758810. PubMed PMID: WOS:000188921200025.
201. Noiri E, Hu Y, Bahou W, Keese C, Giaever I, Goligorsky M. Permissive role of nitric oxide in endothelin-induced migration of endothelial cells. *Journal of Biological Chemistry*. 1997;272(3):1747-52. PubMed PMID: WOS:A1997WD05800054.
202. Kiehart D, Galbraith C, Edwards K, Rickoll W, Montague R. Multiple forces contribute to cell sheet morphogenesis for dorsal closure in *Drosophila*. *Journal of Cell Biology*. 2000;149(2):471-90. doi: 10.1083/jcb.149.2.471. PubMed PMID: WOS:000086598600021.

203. Zordan M, Mill C, Riese D, Leary J. A High Throughput, Interactive Imaging, Bright-Field Wound Healing Assay. *Cytometry Part a*. 2011;79A(3):227-32. doi: 10.1002/cyto.a.21029. PubMed PMID: WOS:000288091000007.
204. Boyden S. The chemotactic effect of mixtures of antibody and antigen on polymorphonuclear leucocytes. *The Journal of experimental medicine*. 1962;115:453-66. doi: 10.1084/jem.115.3.453. PubMed PMID: MEDLINE:13872176.
205. Ottino J. Chemical Engineering in a Complex World: Grand Challenges, Vast Opportunities. *Aiche Journal*. 2011;57(7):1654-68. doi: 10.1002/aic.12686. PubMed PMID: WOS:000291803800001.
206. Preziosi V, Perazzo A, Caserta S, Tomaiuolo G, Guido S. Phase inversion emulsification. *Chemical Engineering Transactions*. 2013;32:1585-90. doi: 10.33032/CET1332265.
207. Caserta S, Preziosi V, Pommella A, Guido S. Non-newtonian liquid-liquid fluids in kenics static mixers. *Chemical Engineering Transactions*. 2013;32:1477-82. doi: 10.33032/CET1332247.
208. Caserta S, Guido S. Vorticity Banding in Biphasic Polymer Blends. *Langmuir*. 2012;28(47):16254-62. doi: 10.1021/la303232w. PubMed PMID: WOS:000312515200003.
209. Benassi MS, Pazzaglia L, Chiechi A, Alberghini M, Conti A, Cattaruzza S, et al. NG2 expression predicts the metastasis formation in soft-tissue sarcoma patients.
210. Berger W, Setinek U, Mohr T, Kindas-Mügge I, Vetterlein M, Dekan G, et al. Evidence for a role of FGF-2 and FGF receptors in the proliferation of non-small cell lung cancer cells.
211. Horwitz R, Webb D. Cell migration. *Current Biology*. 2003;13(19):R756-R9. doi: 10.1016/j.cub.2003.09.014. PubMed PMID: WOS:000185723700007.
212. Chieng-Yane P, Bocquet A, Létienné R, Bourbon T, Sablayrolles S, Perez M, et al. Protease-activated receptor-1 antagonist F 16618 reduces arterial restenosis by down-regulation of tumor necrosis factor α and matrix metalloproteinase 7 expression, migration, and proliferation of vascular smooth muscle cells. *J Pharmacol Exp Ther*. 2011;336(3):643-51. doi: 10.1124/jpet.110.175182. PubMed PMID: 21139058.
213. Yarrow J, Perlman Z, Westwood N, Mitchison T. A high-throughput cell migration assay using scratch wound healing, a comparison of image-based readout methods. *Bmc Biotechnology*. 2004;4. doi: 10.1186/1472-6750-4-21. PubMed PMID: WOS:000224203600001.
214. Ascione F, Caserta S, Perris R, Guido S. Investigation of Cell Dynamics in vitro by Time Lapse Microscopy and Image Analysis. *CHEMICAL ENGINEERING TRANSACTIONS*. 2014;38:517-22. doi: 10.3303/CET1438087.
215. Ubelmann F, Chamailard M, El-Marjou F, Simon A, Netter J, Vignjevic D, et al. Enterocyte loss of polarity and gut wound healing rely upon the F-actin-severing function of villin. *Proceedings of the National Academy of Sciences of the United States of America*. 2013;110(15):E1380-E9. doi: 10.1073/pnas.1218446110. PubMed PMID: WOS:000317948000008.

216. Condorelli G, Vigliotta G, Cafieri A, Trencia A, Beguinot F. PED/PEA-15 gene controls glucose transport and is overexpressed in type 2 diabetes mellitus. *Diabetologia*. 1998;41:A32-A. PubMed PMID: WOS:000075353800124.
217. Valentino R, Lupoli GA, Raciti GA, Oriente F, Farinaro E, Della Valle E, et al. The PEA15 gene is overexpressed and related to insulin resistance in healthy first-degree relatives of patients with type 2 diabetes. *Diabetologia*. 2006;49(12):3058-66. doi: 10.1007/s00125-006-0455-5. PubMed PMID: WOS:000241948200030.
218. Vigliotta G, Miele C, Santopietro S, Portella G, Perfetti A, Maitan MA, et al. Overexpression of the ped/pea-15 gene causes diabetes by impairing glucose-stimulated insulin secretion in addition to insulin action. *Molecular and Cellular Biology*. 2004;24(11):5005-15. doi: 10.1128/mcb.24.11.5005-5015.2004. PubMed PMID: WOS:000221536600035.
219. Dickinson RB, Guido S, Tranquillo RT. BIASED CELL-MIGRATION OF FIBROBLASTS EXHIBITING CONTACT GUIDANCE IN ORIENTED COLLAGEN GELS. *Annals of Biomedical Engineering*. 1994;22(4):342-56. doi: 10.1007/bf02368241. PubMed PMID: WOS:A1994PC15100002.
220. Matthes T, Gruler H. ANALYSIS OF CELL LOCOMOTION - CONTACT GUIDANCE OF HUMAN POLYMORPHONUCLEAR LEUKOCYTES. *European Biophysics Journal with Biophysics Letters*. 1988;15(6):343-57. PubMed PMID: WOS:A1988M734900004.
221. PARKHURST M, SALTZMAN W. QUANTIFICATION OF HUMAN NEUTROPHIL MOTILITY IN 3-DIMENSIONAL COLLAGEN GELS - EFFECT OF COLLAGEN CONCENTRATION. *Biophysical Journal*. 1992;61(2):306-15. PubMed PMID: WOS:A1992HC77800003.
222. Ashby W, Zijlstra A. Established and novel methods of interrogating two-dimensional cell migration. *Integrative Biology*. 2012;4(11):1338-50. doi: 10.1039/c2ib20154b. PubMed PMID: WOS:000311069200002.
223. Decaestecker C, Debeir O, Van Ham P, Kiss R. Can anti-migratory drugs be screened in vitro? A review of 2D and 3D assays for the quantitative analysis of cell migration.
224. Hunt K, Wingate H, Yokota T, Liu Y, Mills G, Zhang F, et al. Elafin, an inhibitor of elastase, is a prognostic indicator in breast cancer. *Breast Cancer Research*. 2013;15(1). doi: 10.1186/bcr3374. PubMed PMID: WOS:000320158100012.
225. Jonas A, De Luca A, Pesce G, Rusciano G, Sasso A, Caserta S, et al. Diffusive Mixing of Polymers Investigated by Raman Microspectroscopy and Microrheology. *Langmuir*. 2010;26(17):14223-30. doi: 10.1021/la101498h. PubMed PMID: WOS:000281354000070.
226. SCHREIER T, DEGEN E, BASCHONG W. FIBROBLAST MIGRATION AND PROLIFERATION DURING IN-VITRO WOUND-HEALING - A QUANTITATIVE COMPARISON BETWEEN VARIOUS GROWTH-FACTORS AND A LOW-MOLECULAR-WEIGHT BLOOD DIALYSATE USED IN THE CLINIC TO NORMALIZE IMPAIRED WOUND-

- HEALING. *Research in Experimental Medicine*. 1993;193(4):195-205. doi: 10.1007/BF02576227. PubMed PMID: WOS:A1993LU28500001.
227. Pommella A, Caserta S, Guida V, Guido S. Shear-induced deformation of surfactant multilamellar vesicles. *Phys Rev Lett*. 2012;108(13):138301. PubMed PMID: 22540731.
228. Nusrat A, Delp C, Madara JL. Intestinal epithelial restitution. Characterization of a cell culture model and mapping of cytoskeletal elements in migrating cells. *J Clin Invest*. 1992;89(5):1501-11. doi: 10.1172/JCI115741. PubMed PMID: 1569187; PubMed Central PMCID: PMC443021.
229. Malet-Engra G, Yu W, Oldani A, Rey-Barroso J, Gov NS, Scita G, et al. Collective cell motility promotes chemotactic prowess and resistance to chemorepulsion. *Curr Biol*. 2015;25(2):242-50. doi: 10.1016/j.cub.2014.11.030. PubMed PMID: 25578904.
230. Yurchenco P. Basement Membranes: Cell Scaffoldings and Signaling Platforms. *Cold Spring Harbor Perspectives in Biology*. 2011;3(2). doi: 10.1101/cshperspect.a004911. PubMed PMID: WOS:000286810200010.
231. Naba A, Clauser K, Hoersch S, Liu H, Carr S, Hynes R. The Matrisome: In Silico Definition and In Vivo Characterization by Proteomics of Normal and Tumor Extracellular Matrices. *Molecular & Cellular Proteomics*. 2012;11(4). doi: 10.1074/mcp.M111.014647. PubMed PMID: WOS:000302786500016.
232. Balkwill F. Cancer and the chemokine network. *Nature Reviews Cancer*. 2004;4(7):540-50. doi: 10.1038/nrc1388. PubMed PMID: WOS:000222435500014.
233. Friedl P, Alexander S. Cancer invasion and the microenvironment: plasticity and reciprocity. *Cell*. 2011;147(5):992-1009. doi: 10.1016/j.cell.2011.11.016. PubMed PMID: 22118458.
234. Cukierman E, Pankov R, Stevens D, Yamada K. Taking cell-matrix adhesions to the third dimension. *Science*. 2001;294(5547):1708-12. doi: 10.1126/science.1064829. PubMed PMID: WOS:000172307400042.
235. SUTHERLAND R. CELL AND ENVIRONMENT INTERACTIONS IN TUMOR MICROREGIONS - THE MULTICELL SPHEROID MODEL. *Science*. 1988;240(4849):177-84. doi: 10.1126/science.2451290. PubMed PMID: WOS:A1988M822900027.
236. Lee G, Kenny P, Lee E, Bissell M. Three-dimensional culture models of normal and malignant breast epithelial cells. *Nature Methods*. 2007;4(4):359-65. doi: 10.1038/nmeth1015|10.1038/NMETH1015. PubMed PMID: WOS:000245584900018.
237. Bin Kim J, Stein R, O'Hare M. Three-dimensional in vitro tissue culture models of breast cancer - a review. *Breast Cancer Research and Treatment*. 2004;85(3):281-91. PubMed PMID: WOS:000221057500011.
238. Lee K, No D, Kim S, Ryoo J, Wong S, Lee S. Diffusion-mediated in situ alginate encapsulation of cell spheroids using microscale concave well and nanoporous membrane. *Lab on a Chip*. 2011;11(6):1168-73. doi: 10.1039/c0lc00540a. PubMed PMID: WOS:000287867100028.

239. Lee M, Kumar R, Sukumaran S, Hogg M, Clark D, Dordick J. Three-dimensional cellular microarray for high-throughput toxicology assays. *Proceedings of the National Academy of Sciences of the United States of America*. 2008;105(1):59-63. doi: 10.1073/pnas.0708756105. PubMed PMID: WOS:000252435300015.
240. Kim C, Chung S, Kim Y, Lee K, Lee S, Oh K, et al. Generation of core-shell microcapsules with three-dimensional focusing device for efficient formation of cell spheroid. *Lab on a Chip*. 2011;11(2):246-52. doi: 10.1039/c0lc00036a. PubMed PMID: WOS:000285514700008.
241. Alessandri K, Sarangi B, Gurchenkov V, Sinha B, Kiessling T, Fetler L, et al. Cellular capsules as a tool for multicellular spheroid production and for investigating the mechanics of tumor progression in vitro. *Proceedings of the National Academy of Sciences of the United States of America*. 2013;110(37):14843-8. doi: 10.1073/pnas.1309482110. PubMed PMID: WOS:000324125100021.
242. Sutherland RM. Cell and environment interactions in tumor microregions: the multicell spheroid model. *Science*. 1988;240(4849):177-84. PubMed PMID: 2451290.

Appendix

1. Publications

- F. Ascione, S. Caserta, R. Perris, S. Guido, “Investigation of Cell Dynamics in vitro by Time Lapse Microscopy and Image Analysis”. CHEMICAL ENGINEERING TRANSACTIONS. 2014;38:517-22. doi: 10.3303/CET1438087.
- F. Ascione, A. Vasaturo, S. Caserta, V. D'Esposito, P. Formisano, S. Guido, “Comparison between fibroblast wound healing and cell random migration assays in vitro”. Submitted (PLoS One).

2. Conferences

- S. Caserta, V. Preziosi, **F. Ascione**, G. Tomaiuolo, S. Guido, “*Cell migration in vitro by time-lapse microscopy*”, MCM, 4-9 September 2011, Urbino (Italy).
- S. Caserta, **F. Ascione**, S. Guido, “*Rheo-Optical Characterization of Dairy Beverages Stability*”, ICR 2012, 5-10 Agosto 2012, Lisbona (Portugal).
- S. Caserta, **F. Ascione**, S. Guido, “*Analisi della Migrazione e Proliferazione Cellulare Mediante Microscopia Time Lapse in Vitro*”, Convegno GRICU 2012, 16-19 September 2012, Montesilvano (PE) (Italy).
- **F. Ascione**, S. Caserta, P. Formisano, S. Guido, “*Investigation of cell dynamics by in vitro Time Lapse Microscopy*”, ABCD Congress 2013, 12-14 September 2013, Ravenna (Italy).
- A. Carciati, R. Liuzzi, **F. Ascione**, S. Caserta, S. Guido, “*In vitro Interactions Between Microstructured Fluids and Tissue Equivalents*”, Cosminnov, 8-9 October 2013, Orleans (France).
- **F. Ascione**, S. Caserta, P. Formisano, S. Guido, “*Cell migration assays by in vitro Time Lapse Microscopy*”, Invadosomes 2013, 13-17 October 2013, Nijmegen (Netherlands).
- **F. Ascione**, S. Caserta, S. Guido, “*The wound healing assay revisited: a transport phenomena approach based on time-lapse microscopy and image analysis*”, SCDRM 2014, 6-7 June 2014, Salerno (Italy).
- **F. Ascione**, S. Caserta, R. Perris, S. Guido, “*Investigation of Cell Dynamics in vitro by Time Lapse Microscopy and Image Analysis*”, IBIC 2014, 8-11 June 2014, Roma (Italy).

- R. Liuzzi, A. Carciati, **F. Ascione**, S. Caserta, S. Guido, “*Flusso di Fluidi Microstrutturati in Tessuti Biologici: Applicazioni Farmaceutiche e Cosmetiche*”, SIR 2014, 7-10 September 2014, Brescia (Italy).
- **F. Ascione**, S. Caserta, S. Guido, “*Quantitative in vitro investigation of cell migration on 2D and 3D substrata by Time Lapse Microscopy*”, Italian Soft Days, 7-10 September 2014, Roma (Italy).
- R. Liuzzi, A. Carciati, **F. Ascione**, A. Magliocca, L. Guadagno, S. Caserta, P. Abete, S. Guido, “*Interactions Between Microstructured Fluids and Stratum Corneum: Pharmaceutical and Cosmetic Applications*”, Stratum Corneum 2014, 17-19 September 2014, Cardiff (UK).
- **F. Ascione**, S. Caserta, S. Guido, “*From Droplets to Cells: Dynamic Evolution of Active Interfaces*”, Smart and Green Interfaces Conference 2015, 30 March-1 April 2015, Belgrade (Serbia).
- R. Liuzzi, A. Carciati, **F. Ascione**, A. Magliocca, L. Guadagno, S. Caserta, P. Abete, S. Guido, “*Interactions Between Micro-structured Fluids and Stratum Corneum: Pharmaceutical and Cosmetic Applications*”, Smart and Green Interfaces Conference 2015, 30 March-1 April 2015, Belgrade (Serbia).